UNIVERSITY OF CAPE TOWN

DEPARTMENT OF PHYSICS

PROMPT NEUTRONS FROM FISSION OF ^{252}Cf AND ^{235}U

J.S. PRINGLE

Thesis submitted for the degree of
Doctor of Philosophy
in the Faculty of Science

August 1977

A B S T R A C T

Measurements have been made of the n-n angular correlation for neutrons emitted in spontaneous fission of ^{252}Cf and thermal-neutron-induced fission of ^{235}U. The dependence of the angular correlation on the neutron detection threshold energy was investigated. These measurements and other experimental data on the fission spectrum and the neutron angular distribution are compared with Monte Carlo calculations based on the evaporation model. It is apparent that a model assuming isotropic evaporation of all neutrons from the moving fragments cannot adequately explain the observed distributions. No evidence was found favouring the emission of a fraction of the neutrons isotropically at scission, or during the fragment acceleration period. Discrepancies are observed which suggest that the emission of neutrons with energies $\lesssim 2$ MeV is enhanced at small angles to the fission axis. It is suggested that the discrepancies could be attributed to polar neutron emission during scission, analogous to the recently observed enhanced polar emission of charged particles in ternary fission. Higher energy neutrons ($2 \lesssim E_n \lesssim 6$ MeV) appear to be emitted with a reduced yield, and distributed more isotropically in the laboratory frame than is expected for an evaporation model.

ACKNOWLEDGEMENTS

I express my appreciation and gratitude to:

Professor F.D. Brooks, who supervised and guided me through this work;

Mr. C.B. Franklyn, Dr. C. Hofmeyr and Dr. D.W. Mingay of the Atomic Energy Board, Pelindaba, who collected the data of run series F, and for their time and help during two preliminary experimental runs on ^{235}U;

The Atomic Energy Board for funding and providing facilities at Pelindaba to carry out measurements on ^{235}U;

The Council for Scientific and Industrial Research for their generous financial assistance;

The International Atomic Energy Agency, Vienna for the loan of the ^{252}Cf source;

Professor I.J. van Heerden for the use of experimental facilities at the Southern Universities Nuclear Institute;

Alun and Megan Stevens, who kept an open house for me in Pretoria during runs at Pelindaba, for their generous hospitality;

My parents for their support of my studies;

Mrs. M.I. Cousins for typing the manuscript, and Mr. P Groenewald for help with some of the diagrams in Chapter Four.

C O N T E N T S

CHAPTER ONE

INTRODUCTION

The primary products formed in the fission process are highly excited, deformed, neutron-rich heavy nuclei. Thus the investigation of the physics of fission can provide information on the nuclear structure and de-excitation of deformed nuclei far from the line of stability.

Shortly after the experimental verification of the phenomenon of fission came the development of the liquid drop model (LDM), which successfully explained many of the experimental observations. The theoretical treatments by Bohr and Wheeler (Bo39), and Hill and Wheeler (Hi53) show an accurate early interpretation of the physics of the process, despite the relatively limited experimental data available at that time. Indeed, Milton (Mi69) has referred to Hill and Wheeler's paper as *"the Old Testament itself, wherein, suitably interpreted, almost anything can be found!"*

A. Bohr (Bo56) introduced the concept of a "cold" deformed transition nucleas at the saddle point, and suggested that the features of low energy fission could be understood in terms of the quantum states of the transition nucleus. Undoubtedly the major advances in the theoretical understanding of fission in the past decade have resulted from the work of Strutinsky (St67,St68) on the inclusion of shell effects in spherical and deformed nuclei. Double-humped fission barriers predicted as a result of this work successfully explained the existence of spontaneously fissioning isomers, and resonances in the sub-threshold fission cross-sections of several actinide nuclei. Recent experimental evidence has suggested that the fission barrier for some light actinides (Ra-Th) is actually triple-humped (Ga76a).

Commercial and military applications of nuclear fission have spurred experimental investigations of innumerable aspects of the phenomenon. Yet, remarkably, some areas are almost totally unexplored, for example measurements of the angular correlation of fission neutrons, which form the basis of the present work. Other aspects, as basic as the angular distribution of neutron emission, have been the subject of few, relatively old investigations. A body of largely contradictory evidence on "scission neutrons" has brought no new understanding of their emission since they were first proposed 15 years ago. In other areas, such as the measurement of prompt neutron multiplicity as a function of fragment mass, experimental progress has accompanied theoretical understanding. Measurements of this distribution have identified fine structures which are in excellent agreement with structures expected to result from odd-even fragment charge effects (Wa77).

The many reviews by Whitehouse (Wh52), Halpern (Ha59), Hyde (Hy64), Fraser and Milton (Fr66), Nix (Ni72a), Michaudon (Mi73), Vandenbosch and Huizenga (Va73), Hoffman and Hoffman (Ho74), Specht (Sp74a) and Grant (Gr76) have charted out the development of experimental techniques and measurements, and theoretical understanding of this complex process. The proceedings of three IAEA conferences on the physics and chemistry of fission, held in 1965, 1969 and 1973, provide a wealth of additional information. Halpern (Ha71) has reviewed the literature on ternary fission, a rare process in which fission is accompanied by the emission of light charged particles. Ternary fission is of much interest because it provides information on the scission parameters and has implications for scission neutron emission.

The present investigation has sought to provide new information on the emission of prompt neutrons in fission by way of measurements of the neutron-neutron angular correlation.

1.1 FISSION MODELS

The liquid drop model (LDM) is a phenomenological classical description of the average properties of the nucleus which has had much success in describing the general features of the fission barrier. The model has been used extensively in the investigation of low-energy fission. The LDM nucleus is represented by a nonviscous, incompressible, charged liquid possessing surface tension. Early calculations, in which nuclear shell effects were ignored, predicted that nuclei were held together by a single fission barrier which resulted from a slight excess of the attractive short-range nuclear force (= surface tension) over the repulsive Coulomb interaction between nucleons. Barrier heights for actinide nuclei were found to be of the order of 5-6 MeV. Deviations of nuclear masses from smooth liquid drop predictions, the presence of resonance structure in subthreshold fission cross-sections, and the existence of fission isomers all pointed to the need to incorporate the effects of shells, even in deformed nuclei. Sophisticated fission barrier calculations by Strutinsky (St67,St68) showed that the presence of shells at different deformations in deformed nuclei, as well as in spherical nuclei, is important for the stability of particular nuclear shapes. According to the Strutinsky "prescription" the nuclear potential energy surface is obtained by adding a fluctuating potential energy representing shell and pairing corrections to the smooth liquid drop potential. Shell corrections to the liquid drop potential energy surface have indicated the existence of a secondary minimum at a deformation approximately twice as large as the ground state deformation. In order for the compound nucleus ^{236}U to fission, it must traverse two saddle points separated by a secondary potential minimum which is about 2.5 MeV higher in energy than the ground state minimum (Ni72a). Low energy fission may be induced by incident radiation eg $^{235}U(n_{th},f)$ or, in the case of spontaneous fission, it proceeds via barrier penetration, eg $^{252}Cf(sf)$.

The two main stages in the fission process are the approach to the saddle point configuration (the "transition nucleus") and the descent from the saddle to the point of scission, where the nascent fragments are formed ie the nucleus divides into two parts. Thus a fissioning nucleus evolves from its initial spherical or slightly deformed ground state configuration, through highly deformed saddle and scission shapes, to separated and subsequently spherical fragments at infinity. Although various treatments give qualitative agreement with some of the observed distributions of fragment mass, kinetic energy, etc., in fission, the fundamental question of when in the process the distributions are determined (ie at the saddle point, at the scission point, or somewhere in between) remains unanswered.

An alternative theory to the dynamical LDM is the statistical theory proposed by Fong (Fo56). According to this theory, the descent from saddle to scission points is a slow process during which thermodynamic equilibrium is maintained. If this is true, all fission phenomena are determined by the level densities of the fragments when statistical equilibrium is last established at the instant of scission. One of the successes of Fong's theory is that it predicts the observed preference for asymmetric mass division in low energy fission (Fo74). However there are many objections to the statistical theory. It takes no account of the quantum states of the transition nucleus at the saddle point, is very sensitive to input parameters (such as the level density distribution), and it cannot account for the observed emission rates of charged particles in ternary fission (Ha71). Recently observed odd-even fine structure in fragment mass yields has provided evidence that statistical thermodynamic equilibrium does not exist at scission (Di73). This observation implies that the fundamental assumption of the statistical theory is incorrect.

In low-energy fission, the transition nucleus at the saddle point can be considered to be "cold", due to its excitation energy having been converted into potential energy of deformation. A. Bohr (Bo56) suggested that the spectrum of transition states of the deformed nucleus should resemble the levels of the nucleus in its ground state configuration. Further, Bohr proposed that the detailed behaviour of the fission fragments is likely to be correlated with the properties of the saddle point quantum states _ie_ the transition states are regarded as the exit channels for the fission reaction. Only a few relatively widely spaced levels are available to the transition nucleus and the spins and parities of these levels probably have a marked effect on the fission mode. The Bohr channel theory had much success in explaining the observed fragment anisotropy (relative to the incident beam) in threshold photofission (Bo56). The strong energy dependence of the angular distributions at energies near the fission barrier appears to be related to the double-humped nature of the barrier, and the relative heights of the two humps (Bj69). At higher excitations more exit channels become available to the transition nucleus, and anisotropy effects are washed out.

The fragment mass distributions from low-energy fission of actinide nuclei are strongly asymmetric (see Figure 1.1). This feature, although still not satisfactorily explained, appears to be the result of shell effects either in the transition nucleus or in the primary fragments (Ke68,Ma74). Resistance to breaking doubly magic shells Z = 50, N = 82 (A = 132) and Z = 28, N = 50 (A = 78) favours asymmetric fission modes. Development of shell structure in the nascent fragments during fission results in a nearly constant heavy fragment mass A ≃ 138 in spontaneous and low energy fission of the U-Cf nucleides (Mo71,Wi76).

The influence of nuclear shells also introduces structure into the prompt neutron yield distribution. The sawtooth variation in the average neutron yield as a function of

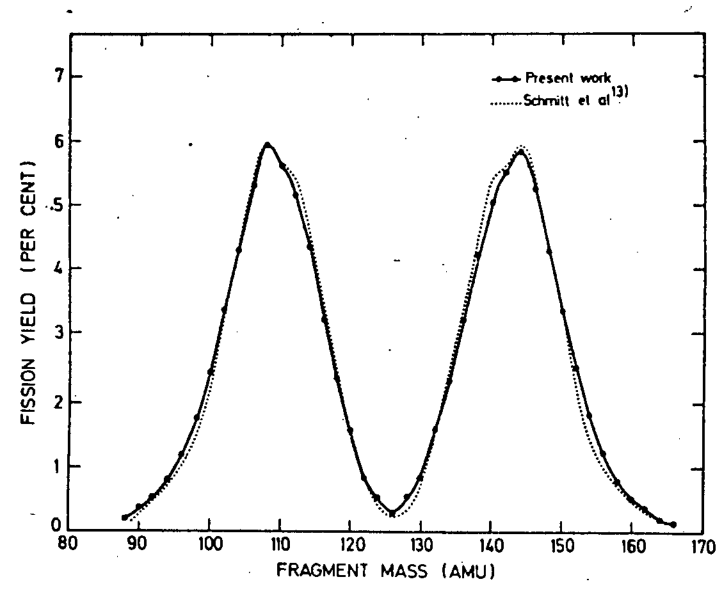

Figure 1.1 The pre-neutron emission fragment mass distribution for spontaneous fission of ^{252}Cf, showing measurements by Walsh and Boldeman (Wa77), and Schmitt *et al* (Sc66). (Figure from Wa77).

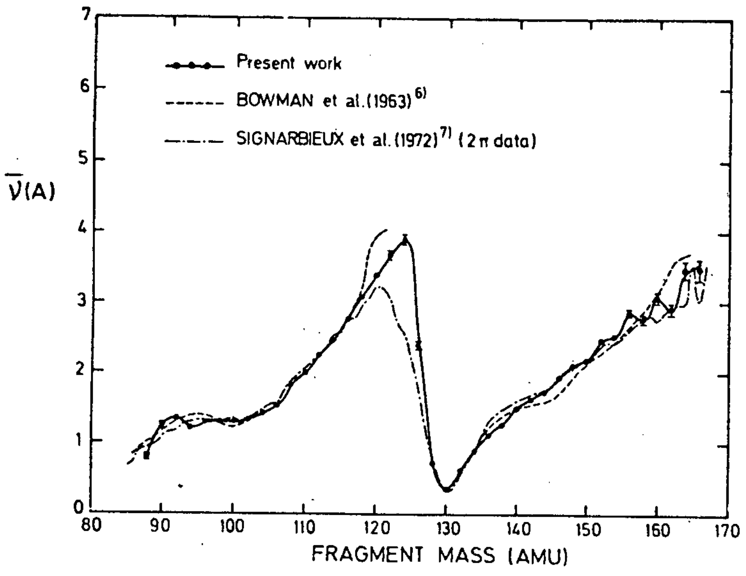

Figure 1.2 The measured average neutron yield distribution for fragments from spontaneous fission of ^{252}Cf. (Figure from Wa77.)

fragment mass (see Figure 1.2) is believed to result from the different "stiffnesses" towards deformation of the nascent fragments. Nuclei near closed shells possess extra rigidity against deformation whereas midshell nuclei are more susceptible towards deformation. Consequently, near the scission point, nascent fragments in the region of closed shell nuclei tend to retain their spherical shape, whereas fragments in the region of midshell nuclei tend to become deformed. The energy which subsequently appears as excitation (resulting in particle emission) is that which is bound up in deformation at the scission point.

Both the fragment mass yield (Re73,Wo76a) and sawtooth neutron yield (Wa77) distributions display fine structures which reflect the influence of nucleon pairing correlations during fission. The structure observed in mass yields (for fragments in specific kinetic energy intervals) from thermal neutron induced fission of ^{235}U has a periodicity of approximately 5 amu, with preferential formation of fragments with even proton numbers (Wo76a). The masses of the most stable nuclei for neighbouring even-Z nuclei differ by $\sim$5 amu (Re73). Measurements (from Wo76a) exhibiting this fine structure are shown in Figure 1.3. The fragment mass yield fine structure results from the pairing energy depressing the kinetic energy surface for odd-mass fragments below that for even-even fragments (Th64). The formation of even-even fragments is strongly favoured at low excitation or high kinetic energies, since less excitation energy is available for breaking nucleon pairs in this case.

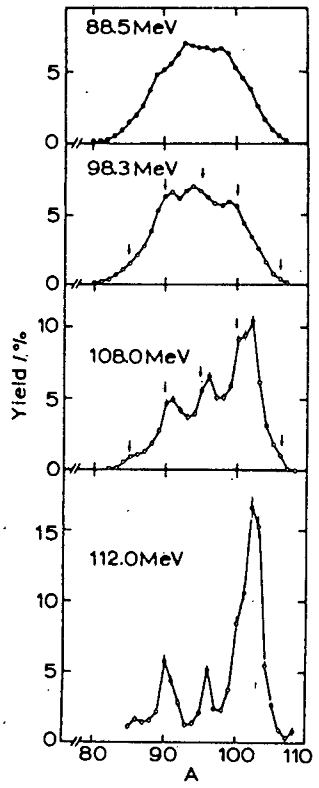

Figure 1.3 Measurements, for different fragment kinetic energy intervals, of the mass distributions for light fragments from thermal neutron induced fission of ^{235}U. The arrows, which are seen to correspond with the observed fine structure, indicate fragment masses where the average proton number is close to an even value. (Figure from Wo76a.)

Walsh and Boldeman (Wa77) have reported the existence of fine structure in the sawtooth neutron yield distribution for $^{252}Cf(sf)$. The position and periodicity of this structure corresponds precisely with that of the fine structure observed in the mass yield distribution. The energetically favoured fission into two even-even fragments releases about 2.7 MeV more energy than odd-odd fission, and this additional energy manifests itself in a slight excess in the average neutron emission from even-Z fragments. Figure 1.4 shows this structure, which is largest in heavy fragments with mass $\gtrsim$150 amu.

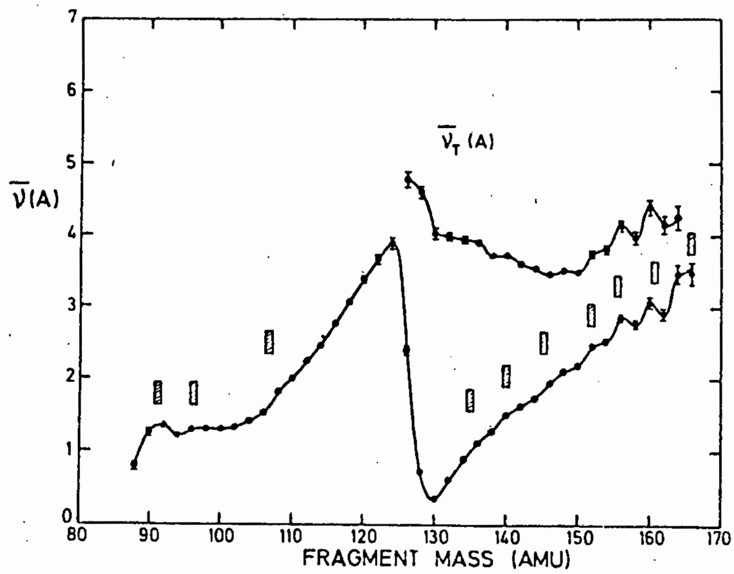

Figure 1.4 Fine structure in the neutron yield distribution for ^{252}Cf (sf). The shaded vertical bars show the average masses of evenly charged fragments. The upper curve shows the average total neutron emission per fission as a function of the heavy fragment mass. (Figure from Wa77.)

The main features of the fragment mass distribution appear to be determined before the nucleus begins its descent from the second saddle point towards scission (Ni72a). This view is consistent with Bohr's channel theory (Bo56) of fission. Other features of fission, such as fragment kinetic energies, angular momenta, and neutron yields, are critically dependent on the fragment deformations at the scission point, and it is likely that they are determined at this stage of the fission process.

A better understanding of the mass and energy distributions in fission awaits the full dynamical treatment, including nuclear viscosity effects, of the formation of the nascent fragments.

1.2 THE FISSION PROCESS

Theoretical calculations of the time taken by the ^{236}U nucleus to pass from saddle to scission give values of $\sim 3\times 10^{-21}$s (Gr76). At scission the deformed nucleus divides and collapses into two separate fragments. The separated fragments are rapidly accelerated by the Coulomb interaction to reach ∿99% of their final velocities in about 4×10^{-20}s (Sk73). Their lines of flight define the fission axis.

Particle emission in fission can be divided into three main stages: (i) scission particles emitted at the scission point (ii) prompt radiations emitted by the separated fragments and (iii) delayed radiation emitted from the fission products in the time range from 10^{-3} to 10^{+2}s after scission. The present work is concerned with particle emission during the first two stages.

SCISSION PARTICLES

Light charged particles emitted in the rare ternary fission modes appear to be released at, or near, the point of scission. Alpha particles are by far the most abundant third particles emitted in ternary fission. Alpha-particle-accompanied fission occurs with a frequency of about 1 in 330 spontaneous fissions of ^{252}Cf (Ra68), and about 1 in 615 for $^{235}U(n_{th},f)$ (Wa75). Many other isotopes of H, He, Li, Be, B, C and O have been observed in ternary fission, with yields several orders of magnitude lower than that of ^{4}He (Ha71). Trajectory calculations and measurements of the angular and energy distributions of the charged particles show that the bulk are emitted in the region between the nascent fragments at the time of scission. Thus they are vectors of information on the scission conditions. It is found that ternary fission has all the essential characteristics of binary fission, except those having to do with energetics (Ha71). Information gained on the scission stage from studies of ternary fission is therefore of relevance to the understanding of the more common binary mode.

The yields of ternary third particles appear to be correlated with the estimated "energy cost" for their release. The excitation energy required for charged particle emission is the sum of the particle binding energy, the increase in Coulomb potential energy in the ternary configuration, and the initial kinetic energy of the particle. For alpha particle emission the energy cost is about 22 MeV (Ha71). The relative frequency of alpha-accompanied-fission clearly disfavours the statistical theory of fission. In order to account for the observed emission rates, a nonstatistical energy distribution is required so that large fractions of the fragment potential energy stored in distortion can be given over to the charged particles as the fragments collapse. A slow adiabatic approach to scission and a slow deformation collapse would result in a charged particle emission rate orders of magnitude smaller than that observed (Ha71).

Of relevance to the present project is the possible existence of a scission neutron component. Since there is no Coulomb barrier, the energy cost for neutron emission is about 7 MeV, composed of the binding energy ($\sim$5 MeV) and the initial kinetic energy ($\sim$2 MeV). It seems likely that at the scission stage some neutrons may be excited to unbound single particle states, with the possibility of prompt neutron decay. Although there is some evidence for neutron emission at scission, much controversy surrounds their existence. Scission neutrons are dealt with in more detail in Chapter 2.

PROMPT RADIATIONS

The total excitation energy of the fragments from spontaneous fission of ^{252}Cf is of the order of 40 MeV (Gr76). The fragments de-excite by prompt emission of neutron and γ-rays. About 6% of the gamma transitions are internally converted in the K shell, leading to the emission of conversion electrons and K X-rays (Na71).

Prompt emission of 3-4 neutrons (for ^{252}Cf) occurs during the time interval from $\sim 10^{-21}$ to 4×10^{-14}s after scission (Fr52). This process removes ∿25-32 MeV of the fragment excitation energy. To a first approximation, most neutrons appear to be evaporated isotropically from the fully accelerated fragments (Bo62a). Extensive measurements of the neutron emission characteristics have appeared in the literature, and these are reviewed in Chapter 2.

Cascade emission of about 8 prompt γ-rays from the fragments of ^{252}Cf spontaneous fission occurs mainly during the time interval from 10^{-14} to 10^{-7}s (Ho74). The γ-ray emission dissipates about 7 MeV of the fragment excitation energy (Ho74). It is interesting to examine the time distribution of the average energy and multiplicity of the prompt γ-rays from ^{252}Cf spontaneous fission. Within 10^{-12}s of scission, 30% of the γ-rays are emitted, forming 62% of the total γ-ray energy emission. In the time interval 10^{-12} to 10^{-10}s, 51% of the γ-rays and 32% of the γ-energy is emitted. The remaining 19% of the γ-rays and 6% of the γ-energy is emitted between 10^{-10} and $\sim 10^{-7}$s (Sk75). Thus the earliest γ-rays have a much larger average energy than those emitted later in the fission process. It is possible that some γ-rays are emitted before neutron emission is completed, but measurements at times $<10^{-14}$s are beyond the range of present experimental capabilities.

The total prompt γ-ray energy release in fission is approximately twice as large as expected on the assumption that γ-emission occurs only after further neutron emission becomes energetically impossible (Ni72b). That γ-emission competes with neutron emission is apparent from the observed sawtooth mass dependence of the average γ-multiplicity (Jo69, Pℓ72). If neutron emission preceded all γ-emission and continued until energetically prohibited, then the γ-multiplicity curve would display little or no mass dependence. Measurements of the angular distribution of fission γ-rays show that they are emitted preferentially in the direction of the fission axis (Wo76b). These observations, and the fact that the γ-spectra show an abundance of low energy transitions, indicate that fission fragments are formed with large angular momenta (Ma65). In nuclei possessing high angular momenta, γ-ray emission competes strongly with neutron emission (Sp66).

Savel'ev *et al* (Sa76) have evaluated the effects of γ-neutron competition in fission fragment de-excitation. They suggested that the spectrum of "last" neutrons emitted by the fragments may deviate from the normal evaporation distribution as a result of the level structure in the final nucleus. It is unlikely that this structure will be observed, in view of the large range of fragment masses and the spread in initial states populated in each fragment.

FRAGMENT ANGULAR MOMENTUM

Fragment angular momentum appears to result mainly from the vibrational bending modes of the distorted nucleus at the scission point, with a smaller contribution arising from subsequent Coulomb repulsion between the non-coaxial neck stumps of the fragments (Zi74,Wo76b). The fragments are pictured as tumbling apart along the fission axis, with angular momenta aligned (antiparallel) and directed perpendicular to the fission axis (Wi72,Wo76b). The fragment angular momenta exhibit a sawtooth dependence on mass (see Figure 1.5), similar to that observed for the average neutron yield. Thus, on average, the lightest fragments in both light and heavy fragment groups have the smallest angular momentum, and the heavy fragments in each group have the largest angular momentum. For $^{235}U(n_{th},f)$, average fragment angular momenta vary from $\sim 1\hbar$ to $\sim 12\hbar$, while in spontaneous fission of ^{252}Cf, the average angular momenta range from $\sim 6\hbar$ to $\sim 14\hbar$ (Zi74,Di76).

In fissions involving highly-asymmetric or near-symmetric mass division there is a large difference in the angular momenta of the complementary fragments. Since the initial ^{252}Cf nucleus has ground state spin zero, this implies that for conservation of the total angular momentum of the fission-

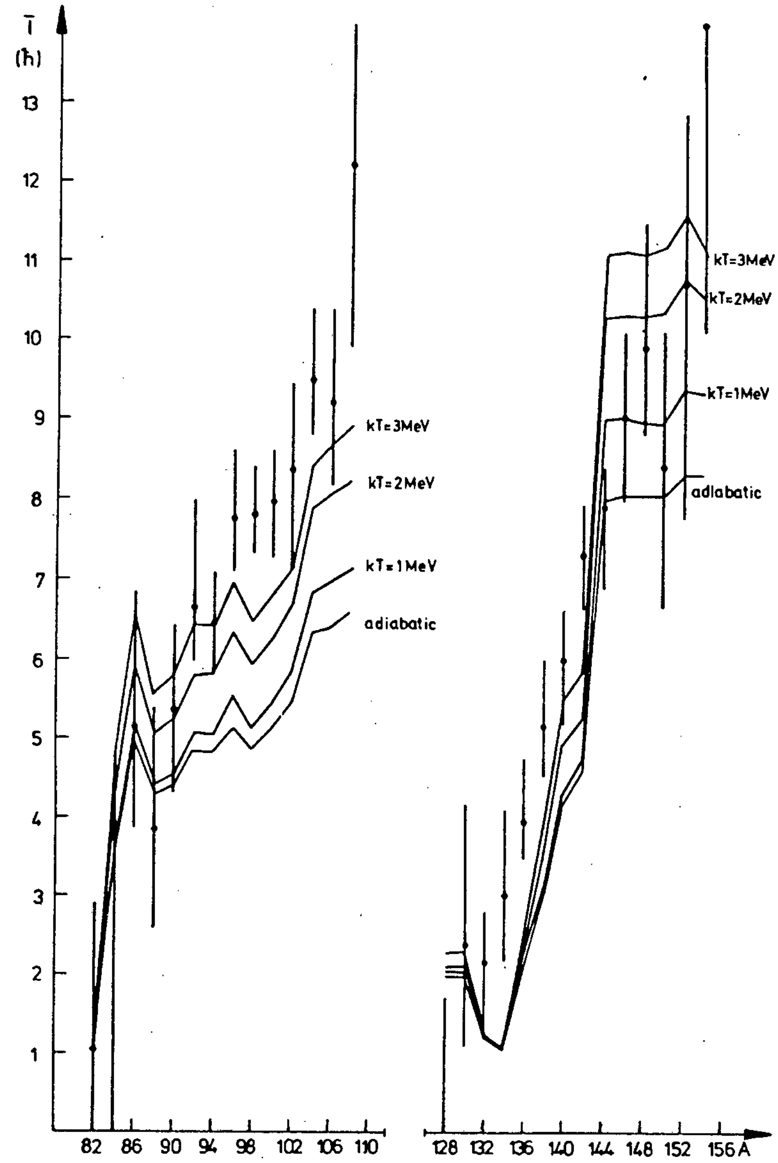

Figure 1.5 The measured mass dependence of the average angular momenta of fragments from $^{235}U(n_{th},f)$. Curves show model predictions. (Figure from Zi74.)

ing system the separated fragments must have some relative orbital angular momentum.

The main implications of the large fragment angular momenta are the existence of an angular momentum barrier for neutron emission, and the possibility that γ-emission may occur before prompt neutron emission is completed. Both neutron and γ-emission depend on the density and energy range of final states in the fragments. Below the yrast line (the locus of lowest energy levels for particular angular momenta -

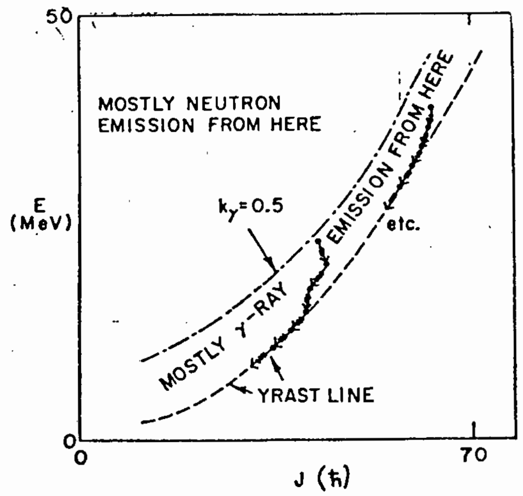

Figure 1.6 Schematic illustration of the yrast line and examples of possible de-excitation paths for fragments with different combinations of excitation energy and angular momentum. Below the line marked k_j = 0.5 the probability of γ-emission is greater than 50%. (Figure from Gr67.)

see Figure 1.6) no levels exist for that angular momentum, and neutron emission cannot occur. Neutron emission decreases the fragment excitation energy but does not substantially change the initial angular momentum (Jo64). Thus the fragment excitation energy drops to the region near the yrast levels and neutron emission is hindered by the low density of final states at that angular momentum. Gamma decay competes favourably with neutron emission below energies of about one neutron binding energy above the yrast line (see Figure 1.6). When the fragment energy reaches the yrast line the de-excitation process continues by a low-energy γ-cascade from one yrast level to the next. (Gamma emission can proceed since no binding energy is involved.) Yrast levels and γ-neutron competition are discussed in detail by Sperber (Sp66), Grover and Gilat (Gr67), Thomas and Grover (Th67), and Thomas (Th68).

An effect which is of possible importance to the present project is the anisotropy which results from the angular momentum dependence of the level density of the residual fragment nucleus (Er58). The low number of available states in a residual fragment possessing large angular momentum favours emission of neutrons with orbital angular momentum parallel to the fragment angular momentum. Preferential equatorial emission achieves a large reduction in the fragment angular momentum, and the residual level density is maximised. The extent of this anisotropy is one of the topics discussed in Chapter 2, which deals with the properties of prompt neutrons emitted in fission.

CHAPTER TWO

PROMPT FISSION NEUTRONS

Measurements on prompt fission neutrons can provide information on the mechanism of their emission, and on the deformation of the distorted fragments at scission. Their value as a tool to study the fission process has led to a proliferation of experimental measurements on many aspects of neutron emission. Terrell (Te65) reviewed the status of knowledge on fission neutrons in 1965, and Nifenecker *et al* (Ni74) have reviewed some recent detailed measurements on neutron and gamma emission in fission. A survey of the literature on fission neutron angular and energy distributions, their angular correlation, and the controversial scission neutron component is presented in this chapter. The effects of fragment angular momentum on neutron emission are discussed. The survey illustrates the discrepancies which need to be resolved because of their important implications concerning models of the fission process.

2.1 THE FISSION SPECTRUM

The spectra of neutrons from fission of ^{235}U induced by neutrons with energies below 150 keV and from spontaneous fission of ^{252}Cf were adopted as international standards at a consultants' meeting on fission spectra (IAEA, Vienna, August 1971).

For $^{235}U(n_{th},f)$ most measurements cover the limited spectral range from 0.5 to 7 MeV, with only one recent measurement (We72) extending below 0.3 MeV. The most recent measurements for ^{235}U are for fission induced by intermediate energy (keV) neutrons ((Jo77) at 530 keV, and (Is73) at 400 keV). Smith (Sm71) measured the spectrum for fission of ^{235}U induced by 35 keV neutrons, but the measurements are restricted to the range ∿0.5 to ∿6.0 MeV. Measurements for thermal neutron fission of ^{235}U covering the energy range ∿0.1 to 10 MeV were reported by Werle and Bluhm (We72). It is in the low energy region that measurements are subject to the largest errors, as a result of the low spectral intensity at this energy, uncertainty of the detector efficiency, and by virtue of the presence of scattered neutrons and the incident low energy neutron beam needed to induce fission in ^{235}U. Even above 4 MeV there are few measurements and relatively large uncertainties.

In contrast to the situation for ^{235}U, measurements of the fission spectrum for ^{252}Cf are not complicated by the presence of an incident beam of low energy neutrons and gammas. At least four detailed measurements of the ^{252}Cf fission neutron spectrum have been reported recently, two of them (Me67,Je72) extending down to 0.002 and 0.003 MeV. Measurements by Green *et al* (Gr73) and Meadows (Me67) extend up to 13 MeV and 15 MeV respectively. Kotel'nikova *et al* (Ko76) have measured the ^{252}Cf spectrum over the energy range 0.5 to 7 MeV.

On the basis of these measurements it is apparent that the gross form of the fission spectrum is reasonably well represented by both the Watt (Wa52) and Maxwellian (Te59) distributions. These distributions have the following forms:

<u>Watt</u>: $N(E) = A \exp(-bE) \sinh\sqrt{cE}$

where A is a normalizing constant, and b and c are parameters defining the shape of the distribution.

<u>Maxwellian</u>: $N(E) = B\sqrt{E} \exp(-E/T_m)$

where B is a normalizing constant and T_m is related to the average neutron energy ($\overline{E}$) by the equation $T_m = \frac{2}{3}\overline{E}$.

Terrell (Te59) has shown that the assumption of Weisskopf (We37) evaporation spectra over a range of nuclear temperatures for neutrons in the centre of mass frame leads to a Maxwellian distribution in the laboratory system. The Weisskopf spectrum has the form:

$$N(E_{cm}) = (E_{cm}/T^2) \exp(-E_{cm}/T)$$

where T corresponds to the nuclear temperature of the fragment and is related to the mean centre of mass energy ($\overline{E}_{cm}$) by $T = \frac{1}{2}\overline{E}_{cm}$. (It should be noted that T_m in the Maxwellian distribution is not the nuclear temperature.)

While the Watt and Maxwellian distributions are broadly representative of the experimental measurements, there are systematic deviations. Measurements of the ^{252}Cf fission spectrum show that the yield of low energy neutrons ($E_n \lesssim 0.5$ MeV) exceeds the predictions of both distributions (Me67,Je72,Gr73). In addition, the measurements of Green *et al* (Gr73) indicate an excess yield of high energy neutrons (2 MeV $\lesssim E_n \lesssim$ 8 MeV). These deviations from the Maxwellian

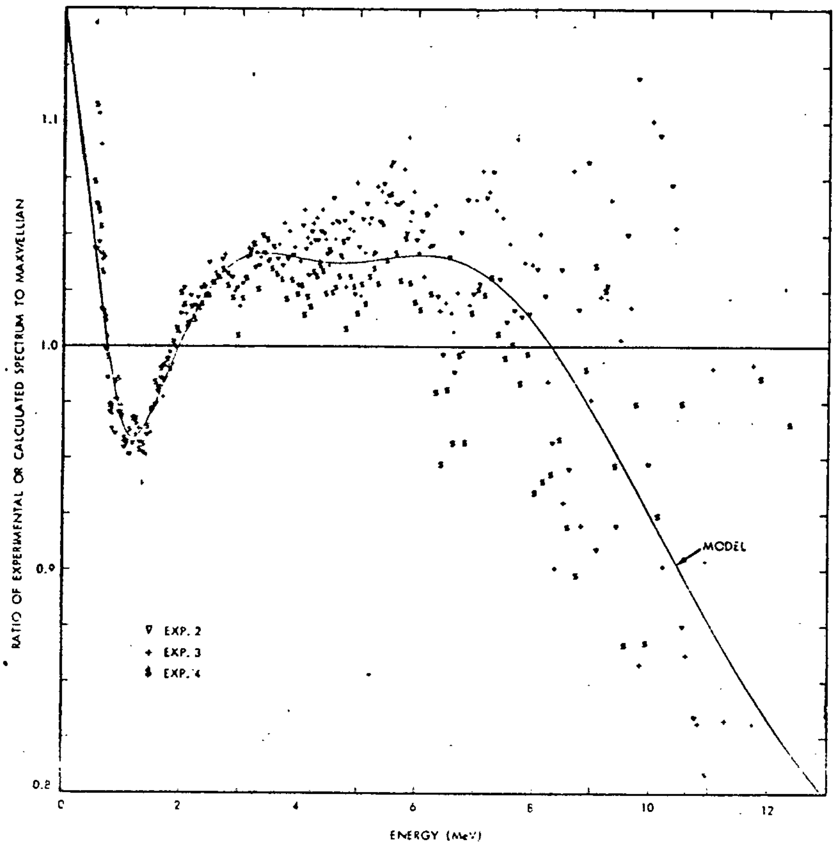

Figure 2.1 A measurement of the ^{252}Cf fission spectrum. Points represent ratios of the experimental values to a fitted Maxwellian. The curve shows the prediction of a model developed to fit the data. (Figure from Gr73.)

distribution are shown in Figure 2.1 Measurements by Werle and Bluhm (We72) for thermal neutron fission of ^{235}U show excess yields below ∿0.8 MeV and from ∿2 to ∿7 MeV, and a deficient yield in the range 1-2 MeV compared with a least squares fitted Maxwellian distribution. Further measurements are needed for this nucleide, especially in the low and high energy regions of the spectrum.

The discrepancies between measured and predicted yields suggest that neutrons may be emitted anisotropically from the fission fragments. Terrell (Te59) showed that the main effect of anisotropy of the form $1 + b\ \mathrm{Cos}^2\theta$ (ie preferential emission along the fission axis) is to increase the yields of neutrons with energies below ∿0.7 MeV and above ∿3.3 MeV. Excess yields observed in early experimental data suggested the presence of such anisotropy, but Terrell (Te59) considered that in view of the many approximations in the evaporation model, evidence based on the spectrum alone was inconclusive.

Evaporation model calculations by Green *et al* (Gr73) showed that the ^{252}Cf fission spectrum could be fitted by assuming that fragment neutrons were emitted according to a $1+b\ Cos^2\theta$ distribution in the centre of mass ($b \simeq 1.5$). Similar calculations by Meadows (Me67), which included an anisotropy even more sharply peaked along the fission axis ($1+b\ Cos^{16}\theta$), achieved a better fit to the observed spectrum than was predicted by the assumption of pure evaporation spectra in the moving fragment frames. However, a good fit was also achieved by the assumption of a small (∿3%) low energy component of neutron emission isotropic in the laboratory frame with an evaporation spectrum at a temperature of ∿0.2 MeV.

FINE STRUCTURE

Fine structure in the ^{252}Cf fission spectrum was reported by Nefedov *et al* (Ne72) and Averchenkov *et al* (Av72). The structure was interpreted as evidence for "delayed" neutron emission* occurring about 10^{-9} to 10^{-8}s after scission. The total yield of "delayed" neutrons during the time 2 to 30 ns was estimated to be 3-3.5% of the neutrons emitted per fission. Averchenkov *et al* (Av72) considered that these neutrons were emitted from the fragments after they were stopped in the target backing. Competition between γ-ray and neutron emission from fragments with high angular momentum was regarded

*Emission was regarded as "delayed" relative to prompt emission which occurs during the time range $\sim 10^{-21}$ to 4×10^{-14}s. True delayed neutrons are emitted from $\sim 10^{-1}$ to 10^{2}s after scission.

as the reason for the long time delay before emission.

Further experimental searches for these "delayed" neutron groups in the ^{252}Cf fission spectrum have given negative results (Dy74,Sc75,Bℓ76). The most recent measurements, by Piksajkin *et al* (Pi77), covered the time range 0.5 ns to 1.5 μs and the energy range 0.01 MeV to 1 MeV. From these measurements the upper limit of "delayed" neutron emission was estimated to be 0.1% of the total fission neutron yield. Fine structure has not been observed in other detailed measurements (eg Me67), and it seems likely that it is the result of instrumental effects or scattering processes.

2.2 ANGULAR DISTRIBUTION

From the preceding section it is clear that a knowledge of the angular distribution of emitted neutrons over a wide range of energies is basic to the interpretation of measurements of the fission spectrum. The angular distribution of prompt neutrons relative to the direction of motion of the fragments has been measured for thermal neutron fission of ^{233}U (Fr52), ^{235}U (Fr52,Ra61,Ka63,Sk63), ^{239}Pu (Fr52), and for spontaneous fission of ^{252}Cf (Bo62a). The conclusions drawn from these measurements play an important role in the interpretation of the fission process.

Pioneering work by Wilson (Wi47) and Fraser (Fr52) gave results consistent with the view that neutrons are emitted isotropically in the fully accelerated fragment frames. However, in their classic theoretical treatment, Hill and Wheeler (Hi53) suggested that in the centre of mass frame, preferential neutron emission directed parallel to the fission axis was to be expected. Although acknowledging that the fission spectrum is broadly consistent with isotropic emission, Hill and Wheeler considered that *"there is little doubt that a substantial preference for emission parallel and antiparallel to the line of fragment motion is also compatible with the observed distribution in energy."* This anisotropy was expected to result from the rapid retraction along the fission axis of the fragment neck stumps.

Ramanna *et al* (Ra61) measured the neutron angular distribution as a function of energy for thermal neutron induced fission of ^{235}U. They obtained weak evidence for anisotropy of the form $1+b\ Cos^2\theta$ where $b > 0$ (ie preferential axial emission) for neutrons with centre of mass energies greater than 1 MeV. Neutrons with emission energies < 1 MeV appeared to be emitted isotropically.

Further detailed energy and angular distribution measurements for neutron from $^{235}U(n_{th},f)$ were reported by Skarsvåg and Bergheim (Sk63) and Kapoor *et al* (Ka63). These analyses supported the assumption that most neutrons are emitted isotropically during the evaporation decay of the moving and highly-excited fission fragments. A small fraction of the neutrons appeared to be emitted isotropically in the laboratory frame. Although allowed for in their evaporation models, the measurements indicated little or no anisotropy of the form $1+b\ Cos^2\theta$ (ie $b \simeq 0$).

Similar measurements on ^{252}Cf by Bowman *et al* (Bo62a, Bo63) were in broad agreement with the findings for ^{235}U (see Figures 2.2 and 2.3), with the exception of an anomalously

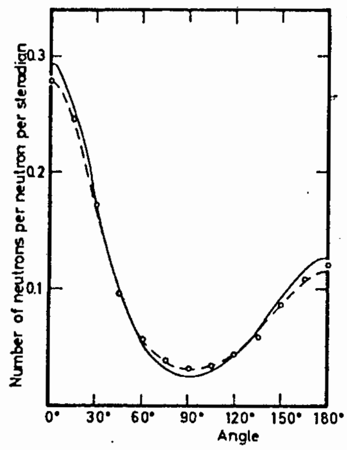

Figure 2.2 The angular distribution (points) of neutrons in the energy range 0.39 to 11.34 MeV emitted in thermal neutron fission of ^{235}U. The emission angle is measured relative to the direction of motion of the light fragment. Curves represent fits to the data. (Figure from Sk63.)

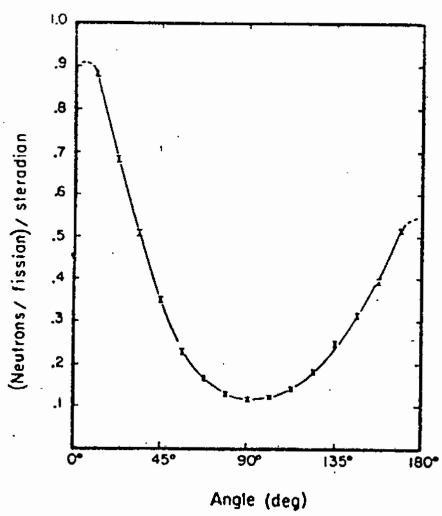

Figure 2.3 The measured angular distribution of neutrons (with energies >0.55 MeV) from spontaneous fission of ^{252}Cf. (Figure from Bo62a.)

high number of neutrons emitted at 11.25^{0} and 168.75^{0} relative to the fission axis. No measurements were made at 0^{0} or 180^{0}. Bowman *et al* suggested that the small-angle anomaly may have been partly the result of instrumental effects, but they did not rule out the possibility of an emission mechanism producing an excess of neutrons collimated within a cone of about 15^{0} relative to the fission axis.

With the exception of data by Piekarz *et al* (Pi70a), who measured the neutron angular distribution for ^{252}Cf (sf) without identifying light or heavy fragments, no recent angular distribution measurements for low energy fission have been reported. Many analyses of fission neutron experiments have continued to assume an idealised evaporation process in which emission occurs isotropically from fully accelerated fragments. This assumption is based largely on the work of Bowman *et al* (Bo62a,Bo63) and Skarsvåg and Bergheim (Sk63). Recently however, Skarsvåg (Sk73) reanalysed the original data of Skarsvåg and Bergheim (Sk63) and Bowman *et al* (Bo62a) and concluded that emission in the centre of mass frame is anisotropic, with peaking along the fission axis. Green *et al* (Gr73) have reached similar conclusions (calling for even stronger anisotropy) from a simultaneous analysis of the ^{252}Cf fission spectrum and the angular distribution data of Bowman *et al* (Bo62a).

Some early angular distribution measurements (Bo62a,Sk63) suggested that a small percentage of neutrons ("scission neutrons") are emitted isotropically in the laboratory frame. Numerous investigations have since been undertaken to determine the extent and nature of this component.

2.3 SCISSION NEUTRONS

The possibility that neutrons may be emitted from the fissioning nucleus at the instant of scission was investigated by Fuller (Fu62). By treating the violent snapping of the neck joining the two fission fragments at the scission point as a nonadiabatic distortion of the nuclear potential, Fuller calculated the energy transfer to the nucleons in the nucleus and gave estimates of scission neutron emission. The nucleus was treated as a square well potential containing a Fermi sea

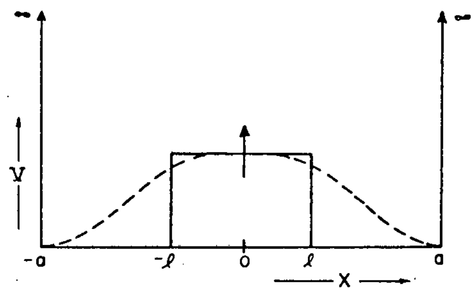

Figure 2.4 Fuller's "volcano" mechanism for division of the nucleus into two fragments. The nucleus is pictured as a square well potential of width 2a, and it is divided by inverted square well (solid) or rounded (dashed) "vólcanos" rising in time. (Figure from Fu62.)

of nucleons, and scission was modelled as the eruption of an inverted potential ("volcano") which divided the original square-well into two idealized fission fragments. The division of the square-well nucleus into two fragments is shown in Figure 2.4. A rise time of the "volcano" of 2.5×10^{-22} s corresponded to the emission of about 1% of the neutrons in the nucleus. For ^{252}Cf, this is equivalent to the emission of 1.5 scission neutrons <u>ie</u> ∿40% of the neutron yield per fission. The energy of the scission neutrons was estimated to be 5-6 MeV. The number and energy of scission particles were found to be very sensitive to the rise-time used, and to the shape of the erupting scission potential. However, Fuller concluded that <u>some</u> neutrons (and possibly heavier particles) are emitted by this mechanism at the time of scission.

Boneh and Fraenkel (Bo74a) calculated the single-particle excitations in the nucleus resulting from a rapid nonadiabatic transition from the saddle point to scission. In fission of ^{237}Np, the calculated scission neutron yield for a transition time of 3.0×10^{-21}s (the approximate time scale predicted by the LDM) was 0,06 neutrons per fission. The yield was found to be extremely sensitive to the transition time, increasing by a factor of $\sim$7 for a transition time of 1.5×10^{-21}s.

Bowman *et al* (Bo62a,Bo63) supplied the first experimental evidence of the existence of scission neutrons emitted in spontaneous fission of ^{252}Cf. Their measurements of neutron spectra at different angles to the fission axis were compared with the predictions of an analytical model which used average values, independent of the fragment mass ratio, for the velocities, nuclear temperatures and neutron yields of the fission fragments. They concluded from their observations that an isotropic scission component contributed a maximum of 10% of the total neutron emission.

Skarsvåg and Bergheim (Sk63) applied a similar analysis to their measurements of the angular and energy distribution of prompt neutrons from $^{235}U(n_{th},f)$. They concluded that about 15% of the neutrons were emitted during the fission process itself (ie scission neutrons), with an evaporation energy spectrum. The remaining 85% of the neutrons were considered to be evaporated isotropically with a Maxwellian energy distribution from the moving fragments.

Further measurements on neutrons from thermal neutron induced fission of ^{235}U were made by Kapoor *et al* (Ka63) and Milton and Fraser (Mi65). Kapoor *et al* estimated that $\sim$10% of the prompt fission neutrons belonged to a scission component represented by an evaporation spectrum with average energy 3.2 MeV. They suggested that a transfer of excitation energy to the nucleons occurred after the fissioning nucleus crossed the saddle point, and that the excited nucleus was likely to evaporate a small fraction of prompt neutrons between the saddle point and scission.

Milton and Fraser's preliminary analysis (Mi65,Fr66) of their measurements also supported the existence of an isotropic scission component (∿20%) for $^{235}U(n_{th},f)$. Milton and Fraser estimated a 27% scission neutron component in thermal neutron fission of ^{239}Pu, and they found that this component was equally distributed over all mass divisions and fragment excitation energies.

Work following these initial experimental investigations has led to contradictory results, both supporting and rejecting the hypothesis of scission neutron emission. Sargent *et al* (Sa65) measured the angular and energy distributions of prompt neutrons from threshold photofission of ^{232}Th. An analysis of their results similar to that carried out by Bowman *et al* (Bo62a,Bo63) on ^{252}Cf gave no conclusive evidence of an isotropic scission component. Their estimate for the scission yield was 7 $\pm$ 9% of the neutrons per fission.

In a review, Terrell (Te65) concluded that there was no convincing experimental evidence that a fraction of the neutrons was emitted at scission from a stationary source. He suggested that the evidence showed a slight anisotropy favouring neutron emission along the fission axis.

Cheifetz and Fraenkel (Ch68) measured the number and energy distribution of prompt neutrons from fission of ^{238}U

induced by 12 MeV protons. They estimated that 0.62 ± 0.25 prefission neutrons were emitted per fission event. (Pre-fission neutrons include scission neutrons and spallation neutrons, which are evaporated from the compound nucleus in competition with fission.) On the basis of fission-spallation measurements for ^{239}Np, 0.25 - 0.42 spallation neutrons are expected before fission (Ch68). Thus the scission component, estimated by subtracting the spallation contribution, is 0.2 - 0.4 neutrons per fission. In a calibration run using a ^{252}Cf source, Cheifetz and Fraenkel found that 0.25 ± 0.20 neutrons were emitted isotropically in the laboratory system.

Further proton-induced fission experiments by Cheifetz *et al* (Ch70) gave a 10 - 20% scission neutron yield from the reaction ^{238}U + 155 MeV p.

On the basis of detailed neutron cascade calculations, Kluge (Kℓ71) questioned the existence of scission neutrons. Kluge considered the evidence for scission neutrons of Bowman *et al* (Bo62a,Bo63) to be the combined result of uncertainties in the calculated efficiencies of their neutron detectors, in the determination of the gamma background, and the inadequate separation of neutrons emitted from different members of each fission fragment pair.

Skarsvåg (Sk73) reanalysed the data of Skarsvåg and Bergheim (Sk63) and Bowman *et al* (Bo62a,Bo63) within the framework of an equilibrium statistical model. This re-evaluation indicated that some neutron evaporation could occur during the acceleration period of the fragments (see also Pik-Pichak (Pi70b)), resulting in a less anisotropic angular distribution in the laboratory frame. Earlier suggestions (Sk63) of the existence of a 15% scission neutron component were withdrawn. However, an independent calculation of neutron emission during fragment acceleration (Ch70) has given an estimate that less than 5% of the neutrons are emitted during this stage.

Despite these developments, recent experimental work has again supported the scission neutron hypothesis. Multiparameter measurements of neutron energy and angular distributions as a function of fragment kinetic energies were carried out for ^{252}Cf by Blinov *et al* (Bℓ73). Their analysis showed that for neutrons emitted in the direction of the fission axis there was a reasonable fit between evaporation model predictions and measured neutron spectra as a function of total fragment kinetic energy. However, at 90^0 to the fission axis, their measurements indicated an excess emission from fragments with high kinetic energy. They concluded that a kinetic energy-dependent scission component contributed 20-25% of the neutron emission. (The absolute yield was dependent on the angular distribution assumed for this component.) Concerning the emission mechanism, Blinov *et al* rejected emission during fragment acceleration (Sk73) or during the saddle-to-scission transition (Ka63,Bo74a) on the basis of the observed fragment kinetic energy dependence of the deviations. Instead they attributed the deviations from the evaporation model to neutron emission during an abrupt, nonadiabatic change in nuclear potential at scission (ie the mechanism proposed by Fuller (Fu62)).

Time-of-flight measurements of the ^{252}Cf spectrum were reported by Green *et al* (Gr73), who included the angular distribution data of Bowman *et al* in their analysis. They concluded that about 25% of the neutrons originated from a stationary source (ie scission), that this component was *emitted preferentially at right angles to the fission axis,* and that the neutron emission from the fragments was highly anisotropic in the fragment frames, with emission preferred along the fission axis. The extent of the anisotropy of fragment neutrons was an order of magnitude larger than is expected (Ch70,Ga74) to result from the fragment angular momentum.

Gavron and Fraenkel (Ga74) made detailed measurements for ^{252}Cf (sf) of the average number $\bar{\nu}(A,E_k)$ of neutrons emitted from fragments of mass A and total fragment kinetic energy E_k, as well as the variance and covariance of the neutron distributions from complementary fragment pairs. In their analysis they allowed for an 11 ± 13% scission neutron component, based on the results of Bowman *et al* (Bo62a) and unpublished work by Mayek (M.Sc. thesis, Weizmann Institute of Science, 1973). They assumed that not more than one scission neutron was emitted per fission, and that scission neutron and fragment neutron emission are anticorrelated ie if one scission neutron is emitted then the fragments emit one neutron fewer. Additional *ad hoc* assumptions were made of angular isotropy and a Maxwellian energy distribution with mean energy 1.5 MeV. Agreement between their experimental determination of the variance of the total number of neutrons emitted per fission and previous measurements was found to be improved by inclusion of a scission component of this nature.

A different approach to the measurement of the scission neutron component has been followed by Nair *et al* (Na74,Na75, Na76). The method takes advantage of the strongly anisotropic fission fragment angular distributions (relative to the incident beam) in certain neutron-induced and photofission reactions. Nair *et al* have measured the fission neutron angular distribution resulting from fast-neutron-induced fission of ^{238}U and threshold photofission of ^{232}Th and ^{238}U. A basic assumption in their analysis is that the scission component is isotropic, while neutrons emitted by the fragments are expected to have a strongly anisotropic angular distribution related to the fragment anisotropy. From a comparison of their observed angular distributions (at neutron energies $\gtrsim$1.5 MeV) and those expected for emission solely from the fully accelerated fragments, Nair *et al* have derived scission components of 11 - 13%. Relatively large uncertainties (of the order of 40 - 80%) are associated with these measurements.

Another experimental investigation of the scission component in ^{252}Cf spontaneous fission is currently being undertaken at Saclay (Lu76), and the results may help to elucidate discrepancies between earlier data.

The various experimental estimates of the scission neutron component are summarized in Table 2.1.

It is clear that our knowledge of the fraction of scission neutrons, their angular distributions, and energy spectra has progressed little in the 15 years since they were first postulated. In fact, even their existence has not really been unambiguously demonstrated. Possibly the most convincing evidence (Bo62a,Bo63) is based on an analysis in terms of a model

TABLE 2.1 Estimates of the scission neutron component in various fission reactions

Fission reaction	Scission component (%)	Average laboratory energy (MeV)	Assumed angular distribution	References
^{232}Th (γ,f)	7 ± 9	2.5	isotropic	Sa65
^{232}Th (γ,f)	13 ± 5	-	isotropic	Na76
$^{235}U + n_{th}$	∿10	3.2	isotropic	Ka63
$^{235}U + n_{th}$	15 ± 2	1.8	isotropic	Sk63
$^{235}U + n_{th}$	0	reanalysis of	Sk63	Sk73
$^{235}U + n_{th}$	19-22	1.9 - 2.1	isotropic	Mi65
^{238}U + 2 MeV n	13 ± 11	1.8	isotropic	Na75
^{238}U (γ,f)	11 ± 6	-	isotropic	Na76
^{238}U + 12 MeV p	5 - 10	-	isotropic	Ch68
^{238}U + 155 MeV p	10 - 20	-	isotropic	Ch70
$^{239}Pu + n_{th}$	∿27	2.0	isotropic	Mi65
^{252}Cf (sf)	∿10	2.6	isotropic	Bo62a
^{252}Cf (sf)	0	reanalysis of	Bo62a	Sk73
^{252}Cf (sf)	7 ± 5	-	isotropic	Ch68
^{252}Cf (sf)	25 ± 1	2.8	preferentially at 90° to fission axis	Gr73
^{252}Cf (sf)	20 - 25	2.4	isotropic	Bℓ73
^{252}Cf (sf)	11 ± 13	1.5	isotropic	Ga74

which takes no account of the strong dependence of neutron emission characteristics on the fragment masses. An analysis deriving from the present work and based on a more realistic Monte Carlo model (Pr75) has demonstrated the importance of these effects, and lays open to question the conclusions of Bowman *et al* concerning scission neutrons.

However, despite the lack of definitive experimental evidence for their existence, it seems highly plausible that a scission neutron component is emitted in the fission process. The reasons for this opinion are twofold. Firstly, theoretical work (Fu62,Bo74a) on the excitation of individual nucleons during the transition from the saddle point to scission suggests that some neutrons are emitted at this stage of the fission process. Secondly, the detailed experimental investigations of the yields of charged particles accompanying ternary fission (eg Co67,Wh67) provide strong circumstantial evidence that neutrons are emitted during scission.

Measurements of the angular and energy distributions of these charged particles have shown that they are emitted in the region between the fission fragments at the time of scission (Ha71). Feather (Fe69) pointed out that the emission of scission neutrons was analogous to charged-particle accompanied fission, since the time and position of particle emission appeared to be the same in both cases. Whetstone and Thomas (Wh67) showed that the absolute yields of ^{1}H, ^{2}H, ^{3}H, ^{3}He, ^{4}He, ^{6}He, and ^{8}He were approximately dependent on the energy cost (E_C) required for their emission according to $\exp(-E_C/T)$, where T corresponds to the nuclear temperature. The energy cost for emitting charged particles is $E_C = B + \Delta V + K$ where B is the particle binding energy, ΔV the increase in Coulomb energy in the scission configuration, and K is the initial kinetic energy of the particle (Ha71). For neutrons, $\Delta V = 0$ and $E_R \simeq 7$ MeV compared with about 22 MeV for α particles.

Recently Val'skii (Va76) fitted the logarithms of the yields of H, He, Li, Be, B, C, N and O nuclei emitted in thermal fission of ^{235}U by the energy cost for emitting the nuclei, and extrapolated to estimate the yield of scission neutrons as 1.1 per fission. This corresponds to approximately 45% of the prompt neutron yield. However, the uncertainties associated with the measured charged particle yields are relatively large, and the scission neutron estimate is correspondingly unreliable.

Feather's opinion (Fe69), expressed in 1969, that the very existence of scission neutrons *"still poses a serious challenge to the experimenter"* remains true today. Experimentalists are hampered by the indistinguishability of scission neutrons and those emitted from the fission fragments.

2.4 EFFECTS OF FRAGMENT ANGULAR MOMENTUM

The relatively large angular momenta of the fission fragments should enhance the component of p-wave neutrons emitted during de-excitation, resulting in an anisotropic neutron angular distribution. Emission of neutrons with orbital angular momentum parallel to the fragment angular momentum is favoured, since this achieves maximum reduction of the fragment angular momentum and thereby maximises the level density of the residual nucleus (Bo62b). Thus neutron emission is expected to occur preferentially in the equatorial plane ($\Psi = 90^{\circ}$; see Figure 2.5) of the fragments. Experimental observations suggest that the fragment angular momenta are initially aligned perpendicular to the fission axis (Wo76b), and neutron emission should therefore be peaked in the plane containing this axis.

A classical model is considered here as the basis for

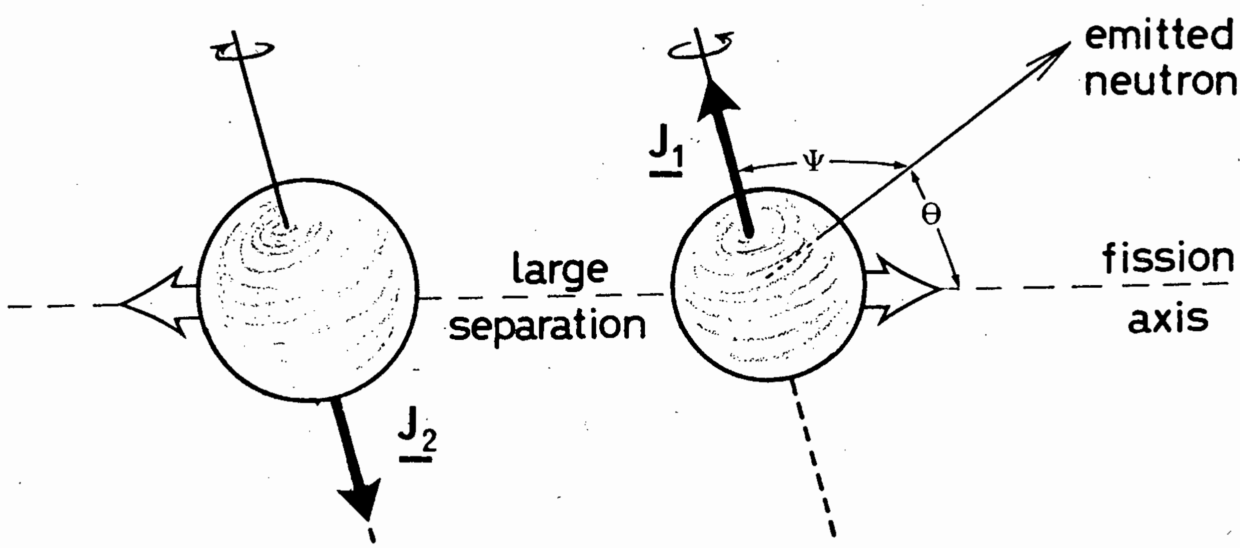

Figure 2.5 Relative orientations of the fission axis, an emitted neutron, and the angular momenta $\underline{J_1}$ and $\underline{J_2}$ of the fission fragments.

evaluating neutron emission from the rotating fragments. Ericson and Strutinsky (Er58,Er59), and Bodansky (Bo62b) have derived the classical neutron angular distribution and demonstrated the equivalence of the corresponding quantal expression in the limit of high angular momentum. The neutron angular distribution relative to the fragment angular momentum axis may be described (Bo62b) in terms of

$$W(\Psi) \simeq 1 + b \, \mathrm{Sin}^2\Psi \qquad 2.4.1$$

where b is the anisotropy parameter. (b = 0 for isotropic emission.) The above expression for $W(\Psi)$ is valid when $b \ll 1$; this is found to be the case for fission fragments. The anisotropy parameter is defined by the relation (Bo62b)

$$b = \frac{m\omega^2 R^2}{2T} \qquad 2.4.2$$

where m = the neutron rest mass
ω = the angular velocity of the fission fragment
R = the interaction radius, here taken to be the fission fragment nuclear radius
T = the average fragment temperature.

The magnitude of b is estimated below for average fragments from ^{252}Cf (sf).

The average angular velocity $\omega = \frac{\bar{J}}{I}$, where $\bar{J}$ is the average fragment angular momentum and I is the moment of inertia. Average fragments from ^{252}Cf (sf) have $\bar{J} \sim 10\hbar$ (Di76). The angular momentum is not substantially reduced during the neutron decay cascade (Bo62b). Assuming an average fragment temperature of 0.65 MeV (Ga74) and the spherical rigid body moment of inertia ($\frac{2}{5}$ mAR^2), the angular distribution is approximately given by

$W(\Psi) \simeq 1 + 0.04\ \mathrm{Sin}^2\Psi$, indicating a small anisotropy.

On averaging over a large number of fissions (and thus over all possible orientations of the fragment angular momentum axis in the plane perpendicular to the fission axis), the neutron angular distribution is expected to be forward-backward peaked along the fission axis ($\theta = 0^{\circ}$) (Er58). The angular distribution relative to the fission axis is described (Er58) by

$$V(\theta) \simeq 1 + \tfrac{1}{2}b\ \mathrm{Cos}^2\theta \qquad 2.4.3$$

Evaluation of the anisotropy parameter b depends in a very sensitive way on assumptions regarding the values of R and I. Possible reduction of the moment of inertia from the rigid body value should be considered.

For large angular momenta ($J \simeq 30 - 40\ \hbar$) and high excitation energies, nuclear moments of inertia tend to rigid body values (Gr67). Effective moments of inertia of nuclei with $J < 20\ \hbar$ are smaller than the rigid body value (Gr67). Grover (Gr67) has calculated the ratio of effective- to rigid-body moments of inertia as a function of nuclear angular momentum. For $J = 10\ \hbar$, the nuclei ^{111}In, ^{138}Xe, and ^{152}Dy (typical fission fragments) have effective moments of inertia of 40 - 60% of the rigid body value. Skarsvåg (Sk73) estimated that fission fragment moments of inertia are reduced to 20 - 60% of the rigid body value. This reduction has a strong effect on the anisotropy parameter, since $b \propto I^{-2}$. A reduction to 45% of the rigid body value increases b by a factor of five. Thus $W(\Psi) \simeq 1 + 0.2 \, \mathrm{Sin}^2\Psi$ may be a more realistic estimate of the angular distribution.

The above estimate of the anisotropy parameter b is an average value for average fragments from spontaneous fission of ^{252}Cf. However, b is actually a function of the mass division in the individual fission, since the temperature and angular momentum of the fragment are dependent on its mass. The fragment angular momentum distribution has a sawtooth appearance, for ^{252}Cf (sf) varying from $\sim 7\hbar$ for fragment masses 96 and 132 amu to $\sim 14\hbar$ for fragment masses 120 and 156 amu (Di76). The nuclear temperature distribution is nearly symmetric about symmetric mass division, and increases from $\sim$0.65 MeV for highly asymmetric fission to $\sim$0.85 MeV in symmetric fission (Ga74).

Figure 2.6 shows the calculated mass dependence of the anisotropy parameter for neutrons emitted in spontaneous fission of ^{252}Cf and thermal neutron induced fission of ^{235}U. The calculated anisotropy of the neutron angular distribution displays a sawtooth mass dependence, and is substantially larger for light fragment neutrons than for those emitted from the heavy fragment. It is important to note that the largest anisotropy occurs in those fragments which emit the largest number of neutrons. This effect may have important consequences for the neutron-neutron angular correlation.

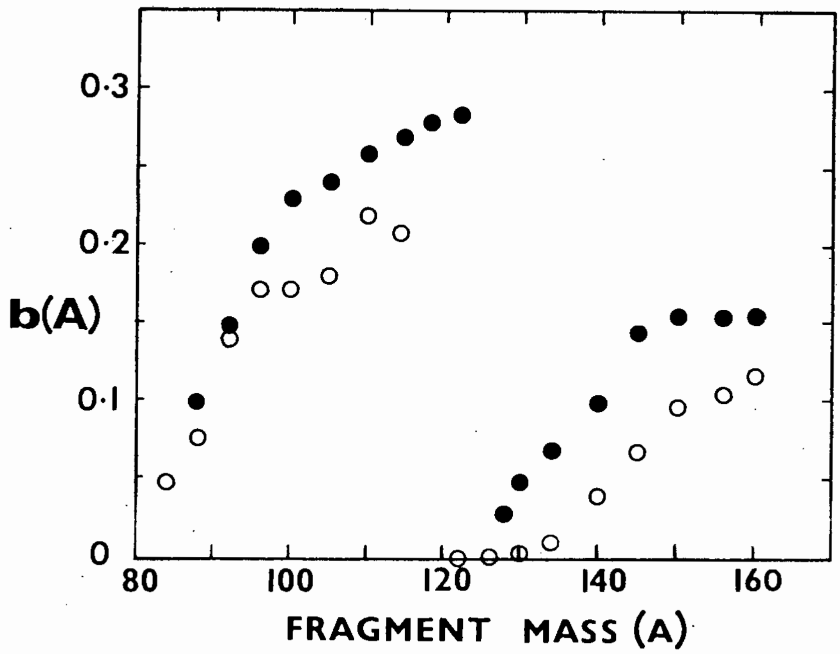

Figure 2.6 The anisotropy parameter (b) as a function of fragment mass for fission of ^{252}Cf (solid circles) and ^{235}U (open circles). Nuclear temperatures were taken from Kℓ69 and Ga74, and fragment angular momenta from Zi74 and Di76. Effective moments of inertia were assumed to be 50% of the rigid body value.

2.5 ANGULAR CORRELATION

The interpretation of fission experiments often relies on the basic assumption of isotropic neutron emission in the fragment centre of mass eg pre-neutron emission fragment mass determinations are dependent on the assumption that fragment velocities are, on average, unaltered by isotropic neutron emission. Experimental observations of the neutron angular distribution (see Section 2.2) support this assumption for a large fraction of neutron emission. Implicit in the assumption of isotropy is the important associated assumption that there is no angular correlation between neutrons emitted in the same fission. However, the observation that neutron emission appears to be isotropic when averaged over a large number of fissions does not necessarily imply that there is no neutron-neutron angular correlation in individual fissions.

Prior to the present study, the only measurement of the fission neutron angular correlation appears to have been that reported by De Benedetti *et al* in 1948 (De48). De Benedetti *et al* used proportional counters to measure the angular dependence of the coincidence rate between neutrons emitted in thermal neutron induced fission of ^{235}U (without any knowledge of the fragment directions). Figure 2.7 shows their experimental arrangement, consisting of two neutron detectors and a ^{235}U source mounted in a plane perpendicular to an incident beam of thermal neutrons. Measurements were made at angles of 30^0, 60^0, 90^0, 135^0 and 180^0 between the detectors in the presence of a random coincidence background which was 3 to 5 times the true rate. Their measurements of the neutron-neutron

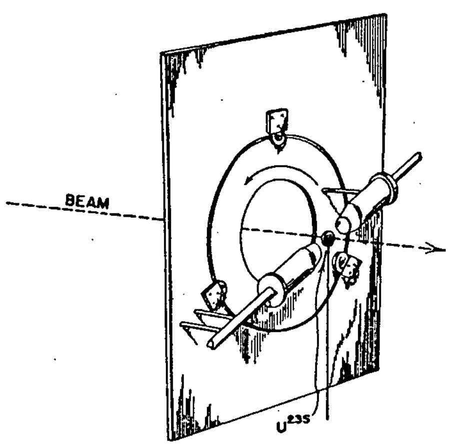

Figure 2.7 Illustration of the apparatus used by De Benedetti *et al* for angular correlation measurements. The ^{235}U sample was mounted in a thin brass ring between the two proportional counters. The beam diameter was about 5 cm. (Figure from De48.)

angular correlation are shown in Figure 2.8. On the assumption that neutrons are emitted from moving fragments, De Benedetti *et al* concluded that neutrons are preferentially emitted by

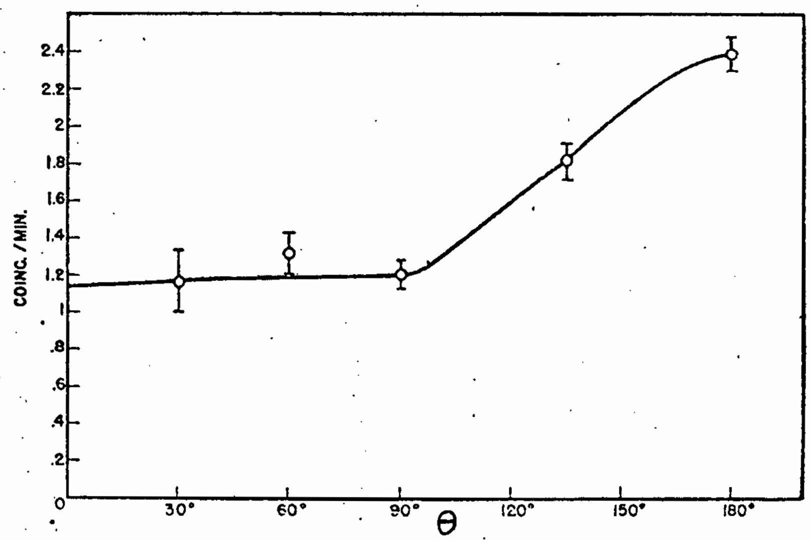

Figure 2.8 The measured angular distribution of coincidences between pairs of fission neutrons from $^{235}U(n_{th},f)$. The datum at 30^{0} was corrected for coincidences resulting from scattering. (Figure from De48.)

opposite fragments. The measurements suggested that twice as many neutron pairs are emitted from opposite fragments as from the same fragment.

Gavron and Fraenkel (Ga74) noted that neutron angular correlations could have important effects on their measurements of the variance and covariance of the neutron distributions from fission fragments of ^{252}Cf (sf). They considered that the angular correlation induced by the high angular momentum of the fragments was insignificant.

Recent calculations by Gavron (Ga76b) have shown that, as a result of fragment spin, the directional correlation between neutrons in the centre of mass frame is narrower (ie favouring smaller relative angles of emission) than that of two neutrons emitted randomly from a spinless fragment. The enhanced small-angle correlation results from the anisotropy of emission from a spinning nucleus, as discussed in Section 2.4. Gavron calculated that the anisotropy in the centre of mass system was of the order of 10%.

2.6 MOTIVATION AND APPROACH

The preceding sections have served to illustrate the incomplete state of our present knowledge on fission neutron emission. The possible existence of scission neutrons has not been convincingly demonstrated (or disproven), largely due to the inherent experimental difficulties in identifying such a component. Even the emission of neutrons from the fragments has not been exhaustively investigated. Although it is generally assumed that this emission occurs isotropically, there are indications from measurements described earlier in this chapter that this may not be the case. Fission neutron anisotropy in the centre of mass frame is suggested by spectral measurements which show excess low- and high-energy yields; by some angular distribution measurements (eg small-angle deviations in Bo62a); and by virtue of the high angular momenta of fission fragments.

An observable relating to the neutron emission process which has been largely neglected until now is the neutron-neutron angular correlation. The sensitivity of the correlation to the neutron emission characteristics means that measurements of this distribution are potentially able to provide new information on the nature and extent of the scission component. If the angular emission from the fragments is indeed anisotropic, then this feature should also be apparent from the observed n-n angular correlation. Thus measurements of the angular correlation provide an additional method of testing models of the fission process, and thereby gaining insight into the mechanism of de-excitation of the fission fragments.

The angular correlation experiments are basically straightforward, requiring measurement of the neutron-neutron coincidence rate as a function of angle between emitted neutrons. The experiments may be performed using strong, thick sources since the fission fragments are not detected. Measurements are automatically averaged over all orientations of the fission axis, and also over a wide range of fragment mass ratios, excitations, angular momenta etc. One is therefore faced with the difficulty of interpreting the results, and understanding their relevance to models of neutron emission. In the past, fission experiments have generally been interpreted in terms of analytical models (eg Bo62a), but these have serious shortcomings, which are outlined in Chapter 3. To avoid these limitations, Monte Carlo calculations were performed in order to simulate the present experiments and previous measurements (Bo62a,Sk63,We72,Gr73) of the neutron spectrum and angular distribution. These calculations were used to relate the measurements to various neutron emission models.

Thus, this work developed along two lines; on the one hand, experiments to measure the n-n angular correlation (and its energy dependence) for fission of ^{252}Cf and ^{235}U, and on the other hand, Monte Carlo modelling of the fission process and simulation of various fission experiments. The Monte Carlo calculation uses, as input, several of the measurements of various fission observables which have been discussed in Chapters 1 and 2. In the next chapter we first discuss the limitations of previous analytical methods, and then proceed with a description of the present Monte Carlo approach.

CHAPTER THREE

COMPUTER SIMULATION OF FISSION

3.1 METHODS

Fission is a complex process involving many variables. In order to interpret the results of fission experiments, measurements are usually compared with the prediction of the liquid drop model obtained from the solution of analytical equations. These analytical formulae must necessarily approximate by using average values, independent of the fragment mass ratio, for the velocities, temperatures, and neutron yields of the fission fragments.

Bowman *et al* (Bo62a) reported detailed measurements of the energy and angular distributions of neutrons relative to the directions of fragments from spontaneous fission of ^{252}Cf. They analysed their results for consistency with the hypothesis of isotropic emission from fully accelerated fragments. Their method assumed that the neutron distributions could be represented by superpositions of evaporation spectra, each spectrum being characterised by its temperature, and a relative weight. Allowance was made for anisotropy in the centre of mass neutron angular distributions. Using the evaporation temperatures, spectrum weights, anisotropy parameter, and average neutron yields from light and heavy fragments as adjustable parameters, least squares fits were made to the data. The best fits were achieved using three evaporation components at different temperatures.

Considering that the method took no account of the mass dependence of the fission neutron characteristics, the fits achieved were remarkably good.

A similar analysis (using mass-independent quantities) performed by Skarsvåg and Bergheim (Sk63) also gave good agreement between evaporation model predictions and measurements of neutron energy and angular distributions for $^{235}U(n_{th},f)$. A recent reanalysis of these data (Sk73) again assumed neutron emission parameters averaged over all fission modes.

Green *et al* (Gr73) analysed neutron spectrum measurements simultaneously with angular distribution data (Bo62a) using a three-temperature per fragment evaporation model. Their conclusions concerning the angular anisotropies of neutrons from the fragments and a stationary source differed markedly from those of Bowman *et al* (Bo62a).

Figure 3.1 illustrates the strong mass dependence of the neutron emission characteristics in fission of ^{235}U and ^{252}Cf. Clearly, model predictions used for the interpretation of fission experiments should take account of this dependence. An exact analytical treatment becomes virtually impossible under these conditions.

The Monte Carlo (random sampling) method offers a simple and promising alternative approach, since the method can, in principle, simulate any process that is physically understood. The Monte Carlo approach to the present problem consists of the formulation of a game of chance which strives to imitate the fission process. In the case of fission of ^{252}Cf and ^{235}U,

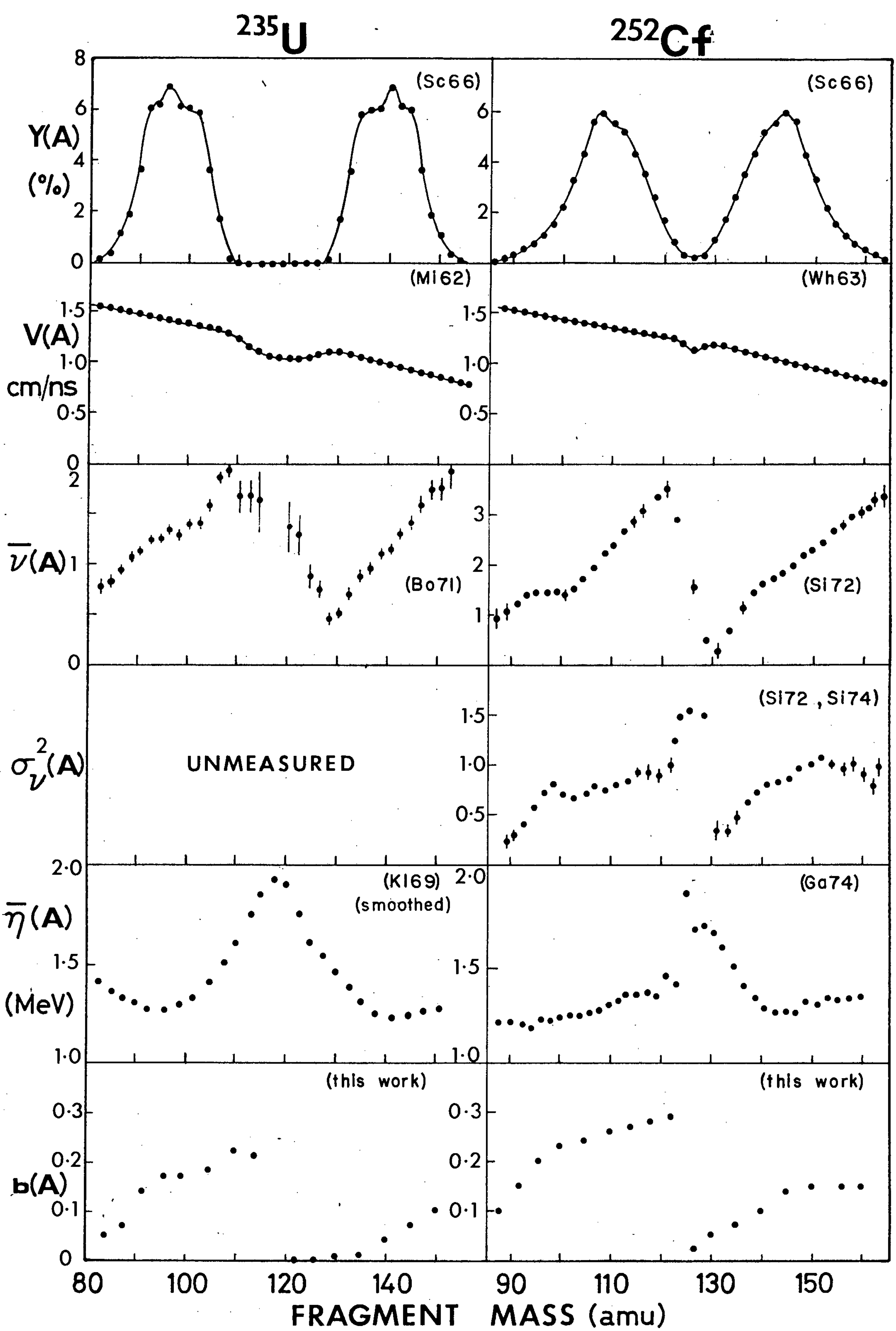

Figure 3.1 The fragment mass dependence of the average values of : pre-neutron emission mass yield Y, fragment velocity V, neutron yield ν, variance of the neutron yield σ_{ν}^{2}, centre of mass neutron energy η, and anisotropy parameter b for $^{235}U(n_{th},f)$ and ^{252}Cf (sf). References are shown in brackets.

good experimental data are available for many of the distributions of the fission variables. Random numbers are used to sample from these distributions, and in this way individual fission histories are generated. The fact that Monte Carlo calculations are closely analogous to physical processes means that, in this instance, the formulation of the computer programme is a simple extension of understanding of the physics of fission. Another major advantage of this method is that the complexity of the calculation is only marginally increased by adding to the number of variables. This means that only relatively minor programme modifications are needed in order to test the effects of different neutron emission models.

The Monte Carlo calculation is divided into two rather distinct parts:

(i) Step-by-step simulation of a fission event, in which the behaviour of a fissioning nucleus and subsequent fission fragments is randomly selected from existing possibilities. Prompt neutron yields, energies and trajectories are decided in a selection process in which choices are weighted according to the experimentally measured probabilities of their occurrence. It is at this stage that various models of the fission process are introduced - for example, the emission of a scission neutron component of specified magnitude and angular distribution. The fission parameters chosen in this part of the calculation are stored and used as input data for the second stage, in which fission experiments are simulated.

(ii) Fission experiments are simulated by imposing the appropriate boundary conditions eg the detector biases and efficiency functions. Measurements of observables such as the neutron-neutron angular correlation, or the neutron angular distribution, are simulated by determining the probabilities of detection of the fission neutrons in detectors having the properties of those used in the actual experiments. Statistical weights are assigned to the neutrons depending on their detection probabilities, and the total detected weights at the end of the calculation provide the Monte Carlo predictions.

The division of the calculation into two parts means that the simulation of different fission experiments involving different boundary conditions can be performed using the same set of fission histories. This leads to computing economy and also increases the accuracy of the calculations, since irrelevant statistical fluctuations in different sets of fission histories are eliminated. In general the statistical error in the Monte Carlo calculation depends on the number of independent histories examined, and it can therefore be reduced by generating more fissions.

Pseudo-random numbers, uniformly distributed on the interval [0,1] were used to sample from measured probability distributions by means of the rejection technique developed by von Neumann (Ca59).

3.2 SIMULATION OF THE FISSION PROCESS

The composite Figure 3.1 virtually represents a flow-chart of the Monte Carlo programme. The main steps in the simulation of each fission event proceeded in the order of the distributions shown in that Figure, starting with the choice of the fragment mass ratio. Only binary fissions were considered, since the proportion of ternary fissions is only about 0.30% for ^{252}Cf (sf) (Ra68), and 0.16% for ^{235}U(n_{th},f) (Wa75).

The computer programmes used to simulate fission of ^{235}U and ^{252}Cf were very similar, the main differences being the experimental distributions used as input. In each run the Monte Carlo programme was normally made to simulate 4×10^4 fissions. The CPU time required for these runs varied from $\sim$10-20 minutes, depending on the nucleide (ie on $\bar{\nu}$) and on the complexity of the model. The generation of fission events proceeded as follows.

(i) FRAGMENT MASSES

Fragment masses in each fission of ^{252}Cf or ^{235}U were chosen randomly from the distributions reported by Schmitt *et al* (Sc66). Allowed fragment masses were limited to the range 80-156 amu for ^{235}U, and the range 80-172 amu for ^{252}Cf. Yields of fragments with masses outside these ranges are $\lesssim$ 0.1% and experimental data on neutron emission parameters are generally unavailable.

(ii) FRAGMENT VELOCITIES

The fully accelerated velocities of the fission fragments were determined from the data of Milton and Fraser (Mi62) (for ^{235}U) and Whetstone (Wh63)(for ^{252}Cf). Fragment velocities were taken to be fixed for any particular fragment mass, since the magnitudes of the variances in fragment velocities are such that they introduce a spread of only 2-4% in the final neutron velocities.

(iii) NEUTRON YIELDS

For each fragment from fission of ^{252}Cf, the average neutron yield $\bar{\nu}$ and the variance σ_ν^2 were determined from the data of Signarbieux *et al* (Si72,Si74). The actual number of neutrons emitted by each fragment was chosen by random sampling from a Gaussian $(\bar{\nu},\sigma_\nu^2)$ distribution. The neutron yields per fragment selected in this manner were converted to the nearest integral value over an allowed range of 0-10 neutrons per fragment. In those cases where the chosen value of ν fell outside the allowed range, another neutron yield was selected by further random sampling.

Measurements of the neutron variance distribution $\sigma_\nu^2(A)$ for ^{252}Cf fission have also been reported by Gavron and Fraenkel (Ga71,Ga74). The choice of the measurements by Signarbieux *et al* in preference to those of Gavron and Fraenkel as input for the Monte Carlo programme was made on the basis of: (a) the more accurate large volume liquid scintillator tank method used by Signarbieux *et al*, and (b) the 25% discrepancy between Gavron and Fraenkel's measurement (Ga74) of the variance in the total number of neutrons emitted per fission and the value of 1.56 which has been measured to within 3% precision by a number of research groups (Ri72, Si74,Bo74b). Gavron and Fraenkel considered that this discrepancy was indicative of the order of magnitude of systematic errors in their results.

For fission of ^{235}U, an average neutron yield distribution $\bar{\nu}(A)$ based on the measurements of Maslin *et al* (Ma67) and Boldeman *et al* (Bo71) was used as input. The choice of fragment neutron yields is complicated by the lack of reported measurements of the yield variance $\sigma_\nu^2(A)$. However it seems reasonable to assume that the distribution $\sigma_\nu^2(A)$ is similar in the fission of both ^{235}U and ^{252}Cf, since all other observables in the two fission reactions display the same trends. As a first approximation it was assumed that the distribution $\sigma_\nu^2(A)$ for ^{235}U could be represented by the measured (Si72) variance distribution for ^{252}Cf, suitably adjusted to cover the mass range 80-156 amu. As for ^{252}Cf, neutron yields per fragment were chosen by random sampling from Gaussian $(\bar{\nu},\sigma_\nu^2)$ distribution.

An alternative approach (C. Franklyn, private communication) is to assume a binomial distribution for the neutron yield per fragment. Using this distribution, the upper limit on the neutron yield (ν_{max}) is an adjustable parameter which effectively modifies the variance of the yield distribution. For the binomial distribution, the mean $\overline{X} = np$ and the variance $\sigma_X^2 = npq$

where n is the number of Bernoulli trials

(= ν_{max}, the maximum neutron yield)

p is the probability of success in a given trial (= probability per trial of emitting a neutron)

and $q = 1-p$ (= probability per trial of not emitting a neutron).

The suitability of the binomial distribution may be investigated as follows. The distribution of the mean $\overline{X}(A)$ is known from measurements of the yield distribution $\overline{\nu}(A)$ for fission of ^{252}Cf. Thus the mass dependence of the (binomial) variance $\sigma_X^2(A)$ may be determined for any assumed value of ν_{max}. It is found that for realistic values of ν_{max} the corresponding variances differ (often considerably) from those measured (Si72,Si74) for ^{252}Cf. For this reason, neutron yields from $^{235}U(n_{th},f)$ were instead chosen by sampling Gaussian $(\overline{\nu},\sigma_\nu^2)$ distributions using a variance distribution $\sigma_\nu^2(A)$ obtained from measurements (Si72) on ^{252}Cf.

However the possibility of using a binomial distribution for sampling neutron yields is worthy of further investigation. It is important to note that the n-n angular correlation predicted by the simulation model is sensitive to the assumed form of $\sigma_\nu^2(A)$.

(iv) SCISSION NEUTRONS

The possibility of emission of neutrons at the scission stage is incorporated at this point of the Monte Carlo the mean $\overline{X} = np$ and the variance $\sigma_X^2 = npq$

where n is the number of Bernoulli trials

(= ν_{max}, the maximum neutron yield)

p is the probability of success in a given trial (= probability per trial of emitting a neutron)

and q = 1-p (= probability per trial of not emitting a neutron).

The suitability of the binomial distribution may be investigated as follows. The distribution of the mean $\overline{X}(A)$ is known from measurements of the yield distribution $\overline{\nu}(A)$ for fission of ^{252}Cf. Thus the mass dependence of the (binomial) variance $\sigma_X^2(A)$ may be determined for any assumed value of ν_{max}. It is found that for realistic values of ν_{max} the corresponding variances differ (often considerably) from those measured (Si72,Si74) for ^{252}Cf. For this reason, neutron yields from $^{235}U(n_{th},f)$ were instead chosen by sampling Gaussian $(\overline{\nu},\sigma_\nu^2)$ distributions using a variance distribution $\sigma_\nu^2(A)$ obtained from measurements (Si72) on ^{252}Cf.

However the possibility of using a binomial distribution for sampling neutron yields is worthy of further investigation. It is important to note that the n-n angular correlation predicted by the simulation model is sensitive to the assumed form of $\sigma_\nu^2(A)$.

(iv) SCISSION NEUTRONS

The possibility of emission of neutrons at the scission stage is incorporated at this point of the Monte Carlo programme. The neutron yield measurements (Si72, Ma67,Bo71) used as input did not distinguish a scission neutron component from the neutrons emitted by the fragments. It was assumed that in these experiments, the scission neutrons were associated with the fragments in the same proportion as the relative fragment neutron yields. In the simulation model a fraction of the fragment neutrons, randomly chosen, was designated as scission neutrons. The scission fraction was an adjustable parameter specified as input.

(v) NEUTRON EMISSION ENERGIES

Neutron emission energies (E) in the centre of mass frame were sampled from evaporation spectra of the Weisskopf form (We37) given by:

$$N(E) = (E/T^2)\ \exp(-E/T)$$

where T is the nuclear temperature (in MeV) of the fragment emitting the neutron. In the case of fragment neutrons, the evaporation temperature T as a function of fragment mass was determined from the data of Bowman *et al* (Bo63) and Gavron and Fraenkel (Ga74) (for ^{252}Cf), and Kluge and Lajtai (Kℓ69) (for ^{235}U). The energies of scission neutrons in the laboratory frame were also sampled from a Weisskopf evaporation spectrum. In this case the nuclear temperature (T_S) used was a parameter of the model used in the simulation.

In accordance with the findings of Gavron and Fraenkel

(Ga74), it was assumed that the emission energies of neutrons in an evaporation cascade from the fragments are uncorrelated.

(vi) ANGULAR DISTRIBUTION

Isotropic emission

The directions (θ,ϕ) of emission of the fragment neutrons in their parent fragment frames, or of the scission neutrons in the laboratory frame, were chosen by sampling θ from a Sin θ distribution and ϕ from a uniform distribution on $[-\Pi,\Pi]$. Here θ is the angle between the directions of the neutron and its associated fragment (see Figure 2.5 on p 2.20), and has the range $[0,\Pi]$. The angle ϕ is the azimuth defined with respect to an arbitrary axis in a plane perpendicular to the fission axis.

Anisotropic emission

The choice of neutron emission angles is modified when the effects of fragment angular momentum are taken into account. In this case emission is anisotropic, and of the form

$W(\Psi) = 1 + b\ \mathrm{Sin}^2\Psi$ where b is the anisotropy parameter.

The directions (Ψ,δ) of emission of the neutrons in the fragment frames were chosen by sampling Ψ from a Sin Ψ distribution weighted by $1 + b\ \mathrm{Sin}^2\Psi$, and δ from a uniform distribution on $[-\Pi,\Pi]$. Here Ψ is the angle between the direction of neutron emission and the fragment angular momentum axis (see Figure 2.5), and is in the range [O,Π]. The azimuthal angle δ is measured relative to an arbitrary axis in a plane perpendicular to the fragment angular momentum axis.

The anisotropy parameter b(A) was calculated for each fragment of mass A, nuclear temperature T and angular momentum J according to equation 2.4.2. Experimental data (Zi74,Di76) were used to determine the angular momentum J(A) of each fragment. The percentage reduction of the fragment moment of inertia from the rigid body value was an adjustable parameter specified as input in the model.

(vii) TRANSFORMATION TO THE LABORATORY FRAME

Neutron trajectories were transformed from the fragment frames to the laboratory frame by vector addition of the neutron and fragment velocities. The angle θ of emission relative to the fission axis is transformed to an angle θ_{lab} in the laboratory frame, while the azimuth ϕ is unmodified by the transformation. The direction cosines corresponding to the trajectory (θ_{lab},ϕ) were determined for each neutron.

Models including anisotropic emission resulting from fragment angular momentum required an additional spherical coordinate transformation (before the transformation to the laboratory) to determine the emission angles (θ,ϕ) corresponding to the direction (Ψ,δ).

(viii) STORAGE OF THE FISSION DATA

The parameters characterising each fission (eg fragment masses, neutron yields, energies, directions etc) were written into separate bytes of 36-bit computer words. On average the storage requirements were 8.5 words per simulated fission of ^{252}Cf, and 5.9 words per ^{235}U fission. Arrays containing 5000 words, ie the details of between 600 and 850 fissions, were written to a disc file as they became filled during programme execution. The simulated fission data were subsequently rewritten onto magnetic tape for permanent storage. A 2400 ft tape provided sufficient storage for the details of approximately 10^6 fissions.

3.3 SIMULATION OF FISSION EXPERIMENTS

(i) THE FISSION SPECTRUM

After transforming to the laboratory frame the laboratory neutron energies were tallied to yield the fission neutron spectrum. The calculated spectrum for ^{252}Cf was compared with the measurements of Green *et al* (Gr73), and the ^{235}U fission spectrum with the data of Werle and Bluhm (We72). Results are presented in Chapters 5 and 6.

(ii) NEUTRON-NEUTRON ANGULAR CORRELATION

The experiments reported here to measure the n-n angular correlation were simulated during scanning of the Monte Carlo fission data. The angles between the trajectories of neutrons emitted in each fission were calculated and the probabilities of detecting the neutrons in detectors having the same properties as those used in the actual experiments were determined. The experiments, and consequently the Monte Carlo calculations, were aimed at determining the energy dependence of the angular correlation. In the analysis of experimental data this was achieved by imposing several detector thresholds and determining the angular correlation for neutrons with energies greater than these thresholds. Likewise, a set of "detector thresholds" covering the range 0-3 MeV in 0.3 MeV steps was used during scanning of the simulated data. In order to maximise the efficiency of the simulation programme, all neutrons with energies E greater than the relevant threshold E_B were assumed to be "detected." Neutrons were assigned weights equal to the efficiencies $\varepsilon(E)$ for their detection, calculated from Owen's equation (Ow60):

$$\varepsilon(E) = \frac{E-E_B}{E}[1 - \exp(-n_H\sigma_H(E)x)]$$

where $\sigma_H(E)$ is the n-p scattering cross-section at energy E, and n_H is the density of protons in the scintillator of mean thickness x cm. Neutrons with energies below the threshold E_B were assigned zero weights. The simulated n-n angular correlation function at each threshold E_B was formed by randomly assigning one of every pair of neutrons to each "detector" and tallying the quantity $(\varepsilon_1\varepsilon_2/\text{Sin }\theta)$* as a function of the neutron-neutron angle θ_{nn} of the pair in the laboratory frame.

(iii) NEUTRON ANGULAR DISTRIBUTION

"Experiments" to determine the neutron angular distribution were performed by scanning the simulated fission data generated in the first stage of the Monte Carlo calculation. The calculated distributions were compared with the data of Bowman *et al* (Bo62a) and Skarsvåg and Bergheim (Sk63), who measured prompt neutron densities as a function of energy over a range of angles with respect to the light fragment direction. These measurements span the ranges 0°-180° and 0.4-11.3 MeV (for ^{235}U), and 11.25°-168.75° and 0.55-10.3 MeV (for ^{252}Cf). Both sets of measurements were corrected for the energy dependence of the neutron detector efficiencies. Bowman *et al* divided the measured neutron densities for each energy interval by the calculated detector efficiency, while Skarsvåg and Bergheim defined the measured densities such that they were independent of the detector efficiency. Thus the simulation of these experimental measurements simply involved scanning the fission data to determine the neutron angular distributions for a specified set of energy intervals. A set of 14 neutron energy

---

* Division by Sin θ is an approximation. The exact expression is $\varepsilon_1\varepsilon_2/\{\text{Cos}(\theta-\frac{\Delta\theta}{2}) - \text{Cos}(\theta+\frac{\Delta\theta}{2})\}$. It is found that for angular bins $\Delta\theta = 1^\circ$, as used in the present calculations, $\text{Sin }\theta\cdot\Delta\theta = \{\text{Cos}(\theta-\frac{\Delta\theta}{2}) - \text{Cos}(\theta+\frac{\Delta\theta}{2})\}$ to within $\sim$0.001% for all θ.

intervals was used, spanning the range 0-7 MeV in 0.5 MeV steps. Above 7 MeV the Monte Carlo data are too sparse for meaningful comparison with experiment.

3.4 CHECKS ON THE SIMULATION

A number of cross checks were built into the Monte Carlo simulation to confirm the validity of the calculation at intermediate stages. The fragment mass distribution and the variation of $\bar{\nu}$ with fragment mass obtained from the simulation were checked against the input parameters.

The calculated ratios ($\bar{\nu}_L/\bar{\nu}_H$) of neutron yields from light and heavy fragments were 1.15±0.01 for ^{252}Cf and 1.16±0.01 for ^{235}U, both values in good agreement with experiment. Experimental estimates of these ratios show some variation, ranging from 1.15±0.07 (Ap64) to 1.46 (Sk63) for ^{235}U and from 1.05 (Ga74) to 1.33 (Sk73) for ^{252}Cf.

The average total neutron yields ($\bar{\nu}$) and the neutron multiplicity distributions (P_ν) for fission of ^{252}Cf and ^{235}U obtained from the Monte Carlo simulation are compared with experimental measurements in Tables 3.1 and 3.2. The calculated values are generally in good agreement with experiment. In the case of the multiplicity distribution for ^{252}Cf, it should be noted that some statistically significant differences exist between P_ν values obtained in different sets of experimental measurements.

In order to check the transformation equations and the calculation of angular distributions and correlations in the

TABLE 3.1 Neutron yield parameters for spontaneous fission of ^{252}Cf. The values P_ν are the probabilities of emitting ν neutrons per fission, and σ_ν is the standard deviation of the P_ν distribution. Only statistical errors are shown.

	Monte Carlo Simulation (This work)	Boldeman (1974) (Bo74b)	Stoughton *et al* (1973) (St73)	Ribrag *et al* (1972) (Ri72)
$\bar{\nu}$	3.731 ± 0.010	3.738 ± 0.015	3.72 ± 0.06	3.756
σ_ν	1.25	1.25 ± 0.05	1.21 ± 0.06	1.25 ± 0.04
P_0	0.0026 ± 0.0003	0.0022 ± 0.0001	0.003 ± 0.008	0.0022 ± 0.0001
P_1	0.0270 ± 0.0008	0.0255 ± 0.0003	0.026 ± 0.003	0.0260 ± 0.0004
P_2	0.1207 ± 0.0018	0.1281 ± 0.0005	0.118 ± 0.082	0.1234 ± 0.0005
P_3	0.2709 ± 0.0026	0.2767 ± 0.0008	0.275 ± 0.095	0.2760 ± 0.0007
P_4	0.3222 ± 0.0029	0.3064 ± 0.0010	0.322 ± 0.060	0.3048 ± 0.0010
P_5	0.1902 ± 0.0022	0.1819 ± 0.0007	0.190 ± 0.030	0.1875 ± 0.0008
P_6	0.0563 ± 0.0012	0.0648 ± 0.0006	0.056 ± 0.020	0.0650 ± 0.0005
P_7	0.0093 ± 0.0005	0.0127 ± 0.0003		0.0132 ± 0.0004
P_8	0.0009 ± 0.0002	0.0016 ± 0.0002		0.0020 ± 0.0003

T A B L E 3.2 Neutron yield parameters for thermal neutron induced fission of ^{235}U. The notation follows that of Table 3.1

	Monte Carlo Simulation (This work)	Boldeman and Dalton (1967) (Bo67)
$\overline{\nu}$	2.444 ± 0.008	2.416 ± 0.008
σ_ν	1.15	1.11 ± 0.06
P_0	0.0226 ± 0.0008	0.0313 ± 0.0060
P_1	0.1787 ± 0.0022	0.1729 ± 0.0016
P_2	0.3348 ± 0.0029	0.3336 ± 0.0029
P_3	0.2972 ± 0.0028	0.3078 ± 0.0029
P_4	0.1331 ± 0.0019	0.1232 ± 0.0016
P_5	0.0293 ± 0.0009	0.0275 ± 0.0020
P_6	0.0038 ± 0.0003	0.0038 ± 0.0015
P_7	0.0004 ± 0.0001	

simulation, one run was made in which neutrons were assumed to be emitted isotropically from fragments at rest in the laboratory frame. The results indicated, as expected, an isotropic angular distribution and an isotropic angular correlation.

CHAPTER FOUR

EXPERIMENTAL METHODS

4.1 OUTLINE OF EXPERIMENTS

The ^{252}Cf measurements were made during five independent sets of experimental runs at the Southern Universities Nuclear Institute (SUNI), Faure, Cape. Run sets were of 3-14 day duration. Measurements on ^{235}U were made at the National Nuclear Research Centre, Pelindaba, during three experimental runs. Of these, the first two were largely feasibility studies, and the measurements reported here are from the third run series, which extended over nearly two months.

In each run set, measurements were made of neutron-neutron coincidences over a wide range of correlation angles. Data were acquired in multiparameter mode, with simultaneous monitoring of the random coincidence background. In all runs except the final set of measurements on ^{252}Cf, the parameters acquired were the energies of the recoil protons in the neutron detectors for each n-n coincidence event, and the coincidence time delay. In the final measurements on ^{252}Cf the time-of-flight technique was used for direct determination of the energies of coincident neutrons. The buffered data collected in each run were analysed on a UNIVAC 1106 computer at the University of Cape Town to yield the fission neutron angular correlation, and the dependence of this distribution on neutron energy.

4.2 FISSION SOURCES

^{252}Cf

Californium-252 decays both by spontaneous fission (3.1%) and α-emission (96.9%)

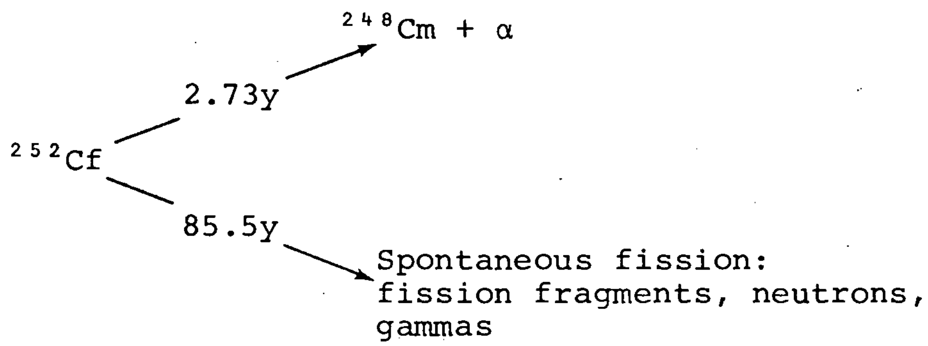

The resultant half-life is 2.638 years (Sp74a). Each fission results in the prompt emission of an average of 3.738 ± 0.015 neutrons with an average energy 2.15 MeV (Bo74b) and 7.95 gamma photons with average energy 0.88 MeV (Ho74). The delayed neutron yield is ∿0.85% of the neutrons emitted per fission (Am65). The neutron and gamma emission rates per μg of ^{252}Cf are 2.34×10^6 n/s and $1.3\times10^7 \gamma$/s respectively (An73).

The ^{252}Cf source used in the experiments comprised four afterloading cells, each with an active length of 15 mm. Each cell consisted of Cf_2O_3 deposited on a 15 mm-long platinum wire, and sealed in an 18 mm-long, 1 mm-diameter platinum-iridium capsule. The nominal total ^{252}Cf mass at the start of the experiments in July 1974 was 2.3 μg, decaying to 1.1 μg by the final series of measurements in March 1977. The corresponding fission neutron emission rates from the source are 5.3×10^6 n/s and 2.6×10^6 n/s.

During experimental runs the high gamma flux was attenuated by placing the source inside a 2 mm-thick lead sheath.

4.3

^{235}U

Uranium-235 decays predominantly by α-emission (∿100%) and very rarely by spontaneous fission (∿4×10^{-7}%).

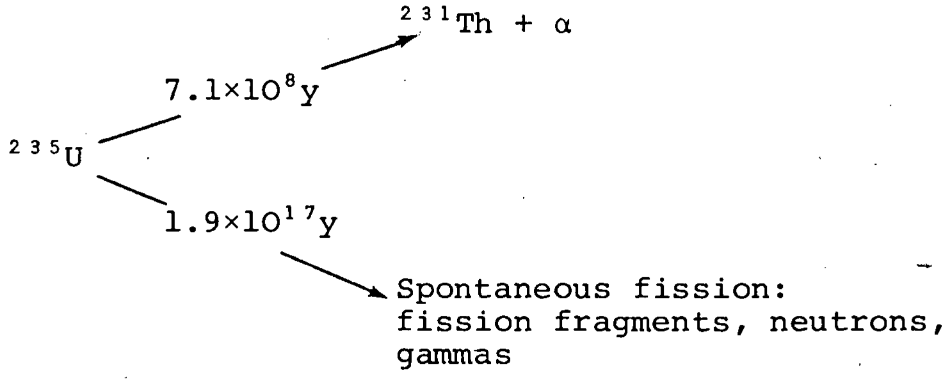

The resultant half-line is 7.1×10^{8}years (Ar71). It has a large cross-section (∿2.3×10^{3}b) for fission by sub-thermal neutrons, emitting on average 2.416 ± 0.008 prompt neutrons (Bo67) with average energy 1.98 MeV (Sm72) and 6.89 prompt gammas with average energy 0.97 MeV (Ho74). The delayed neutron yield from $^{235}U(n_{th},f)$ is ∿0,66% of the neutrons emitted per fission (Am65).

Secondary fissions in ^{235}U from fast fission neutrons are relatively unlikely, the fission cross-section being about 1.3b for incident neutrons with energies between 1-5 MeV (St65).

The source used in the experiments consisted of a thin disk (∿2 mm-thick×30 mm-diameter) of natural uranium (^{238}U) enriched to 30% in ^{235}U. Fissions were induced in ^{235}U by a collimated beam of sub-thermal (2.5 meV) neutrons from the 20MW ORR-type research reactor SAFARI 1 at Pelindaba. The neutron flux incident on the source was ∿3×10^{6}n cm^{-2}s^{-1}. The beam diameter was 20 mm, giving an active source area of 3.1 cm^{2} and a fission rate of ∿10^{7}s^{-1}. Source gamma radiation was attenuated by shielding the scintillation crystals with thin lead sheets.

The beam flux was monitored in order to account for changes in the fission rate in ^{235}U. (The angular correlation ratio $R(\theta)$ is inversely proportional to the source fission rate - see Section 4.6.) Between runs, variations in beam flux were generally less than 1%. Over a four week period a total flux change of ∿7% was recorded, resulting mainly from a replacement of reactor fuel elements, and reactor 'poisoning' by the build-up of fission products having large thermal-neutron capture cross-sections (eg $_{45}Rh$, $_{54}Xe$, $_{62}Sm$).

<u>^{238}U</u>

The effects of the large proportion of ^{238}U in the uranium sample are negligible. Like ^{235}U, ^{238}U decays predominantly by α-emission (∿100%) and rarely by spontaneous fission (4.55×10^{-5}%).

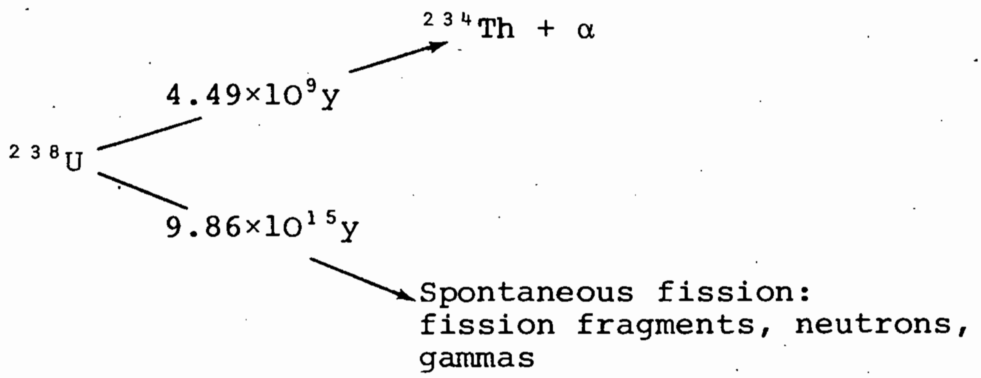

The resultant half-life is 4.49×10^{9}years (Eℓ70). The probabilities of fission of ^{238}U induced by the sub-thermal neutron beam or by fast neutrons from fission of ^{235}U are negligible. Sub-thermal neutron energies are far below the ^{238}U fission threshold (∿1.3 MeV), and the average cross-section for fission of ^{238}U by neutrons emitted from fission of ^{235}U is ∿310mb (Ca72).

Interpretation of the angular correlation measurements rests on a comparison of the experimental results and the predictions of the evaporation model, in which neutrons are assumed to be emitted from fully accelerated fragments. In the present experiments thick sources were used and the fission fragments were stopped in the platinum-iridium canister (for ^{252}Cf) or the uranium target (for ^{235}U). In both sources the fission fragment range is $\sim 5\times10^{-4}$cm (Ni61, and range tables in No70), and the fragments are stopped in about 10^{-12}s after scission.

Fraser (Fr52) showed that the upper limit on the emission time of prompt neutrons was 4×10^{-14}s. From tables of heavy ion ranges (eg No70), it is found that average fission fragments lose about 5 MeV of kinetic energy in the targets in about 10^{-14}s. This energy loss decreases the fragment velocity by about 3%. However it is likely that neutron emission occurs much earlier during the time interval 10^{-21}–4×10^{-14}s (Sk73). Hence the effects on prompt neutron emission of using thick sources are considered to be negligible.

4.3 APPARATUS AND EXPERIMENTAL GEOMETRIES

Several different organic scintillators were used during the experiments. Details of these scintillators and the photomultiplier tubes on which they were mounted are given in Table 4.1. The scintillators, which were chosen for their excellent pulse shape discrimination (PSD) properties, were optically coupled with silicone fluid to 5 cm-diameter magnetically shielded photomultiplier tubes. Total light collection was increased by surrounding the non-coupled scintillator surfaces with diffuse reflector (NE562) painted on thin aluminium foil. The cylindrical anthracene crystal was coupled to the photomultiplier via a polished lucite light guide in order to improve uniformity of light collection at the cathode.

TABLE 4.1 Details of the scintillators and photomultiplier tubes used in the experiments

SOURCE	RUN SERIES	DETECTOR 1				DETECTOR 2			
		PM TUBE	SCINTILLATOR	SHAPE	VOLUME (cm^3)	PM TUBE	SCINTILLATOR	SHAPE	VOLUME (cm^3)
	A	RCA 6810	Anthracene	Cylinder	12.3	56 AVP	NE 213	Cylinder	27.6
	B	RCA 6810	Anthracene	Cylinder	12.3	56 AVP	NE 213	Cylinder	27.6
^{252}Cf	C	RCA 6810	Anthracene	Cylinder	12.3	56 AVP	NE 213	Cylinder	27.6
	D	RCA 6810	Anthracene	Cylinder	12.3	RCA 6810	Anthracene	Wedge	6.7
	E	RCA 6810	NE 213	Cylinder	98.2	RCA 6810	NE 213	Cylinder	98.2
	E	Fission 'start' timing detector				58 AVP	NE 102	Disk	40.2
^{235}U	F	RCA 8575	Stilbene	Cylinder	9.6	RCA 8575	Stilbene	Cylinder	31.4

Experiments on ^{252}Cf were carried out with the dectectors and source mounted in a horizontal plane at least 3 m from the closest concrete walls and floor of the neutron pit at SUNI. The source was suspended above the midpoint of the experimental table on a thin nylon thread in order to minimise the scattered neutron background. One detector and the source were fixed in the horizontal plane and the other detector was rotated about a vertical axis through the source to vary the n-n correlation angle θ (see Figure 4.1). Distances between source and scintillators varied in different run series, and also at different angles θ. The main criteria governing the choice of distances were the angular resolution and the coincidence rate (for $\theta \geq 45^{\circ}$), and the amount of space required to insert shadow shields between the two detectors (for $\theta < 45^{\circ}$).

In run series A to D, detector-source distances were typically 20-30 cm for measurements made at $\theta \geq 45^{\circ}$. At these distances the scintillators subtended angles of 4° to 7° with respect to the source. For smaller angles one detector was moved back to 40-80 cm from the source, giving correspondingly finer angular resolution. In run series E, where time-of-flight was used to determine neutron energies, all measurements were made at 80 cm from the source to improve energy resolution. For these measurements the scintillators subtended angles of $3{\cdot}5^{\circ}$ at the source.

Measurements on ^{235}U were made with the detectors and source in a vertical plane, perpendicular to the incident neutron beam from the SAFARI 1 reactor at Pelindaba. One detector was fixed in the vertical plane and the other detector was rotated about a horizontal axis through the source to vary the correlation angle θ. The main detector-source geometries used in run series F were : fixed detector distances of 18 or 30 cm and corresponding moveable detector distances of 40 or 69 cm. In the two configurations the detectors subtended angles of $\sim6^{o}$ and $\sim3^{o}$ at the source.

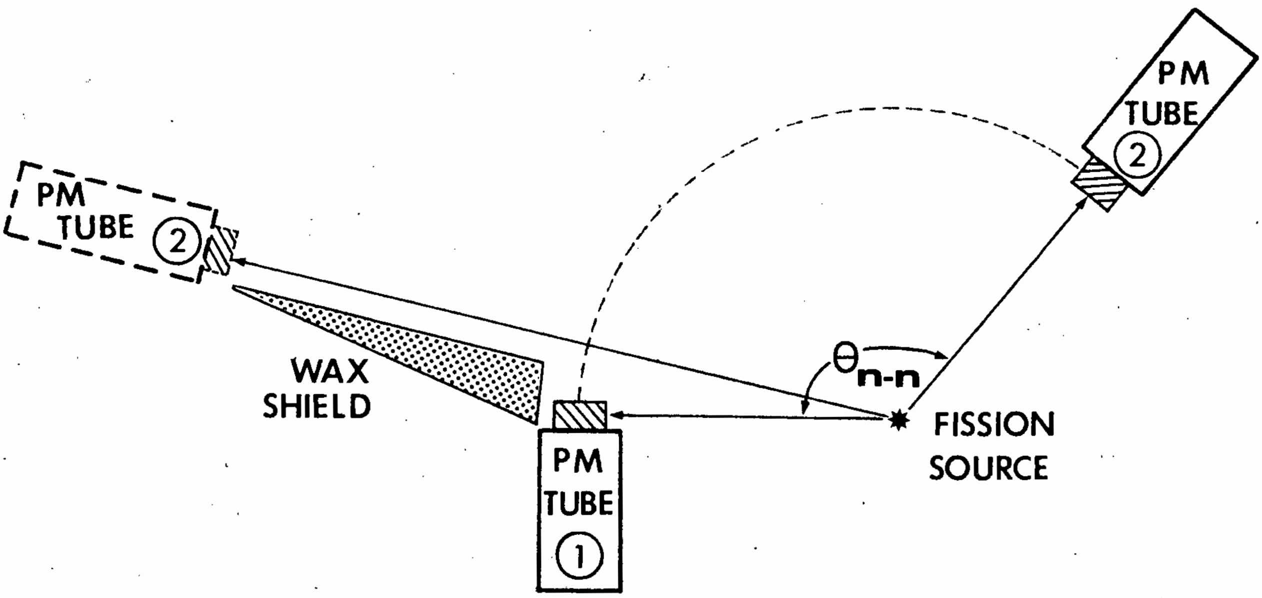

Figure 4.1 Illustration of the two detector-source geometries for angular correlation measurements at small and large angles θ. At small angles detector 2 is moved back to allow the insertion of a wax shadow shield between the scintillators.

SCATTERING EFFECTS

As indicated above, all small angle measurements require the insertion of shadow shields between the two detectors to attenuate spurious coincidences arising from neutron scattering from one detector to the other. This scattering background was carefully investigated.

The angular correlation ratio R(θ) was defined so as to be independent of the detector-source distance. This meant that comparative measurements could be made at different distances (for fixed small θ) to test the effects of shadow shields of different thicknesses. Measurements of the transmission of (unscattered) ^{252}Cf fission neutrons through various thicknesses of wax showed that shields of thickness 20 cm would provide adequate attenuation of this scattered component. Shadow shields used for both ^{252}Cf and ^{235}U work consisted of wax (or borated wax) blocks specially cut to the optimum shape and thickness for each angle. Shields were generally 20-30 cm in length and of the minimum thickness required to effectively shadow detector 2, while at the same time keeping the amount of scattering material placed near the neutron detectors at a minimum. The positioning of the shadow shield is illustrated in Figure 4.1.

4.4 ELECTRONIC CONFIGURATIONS AND DATA COLLECTION

A schematic diagram of the basic experimental configuration used in all except run series E is shown in Figure 4.2. Each detector provides three output signals : L, the linear pulse which depends on the energy of the recoil particle in the scintillator; S, the "shape" or PSD output pulse, with amplitude characteristic of the nature of the recoil particle; and the fast timing output. Figure 4.2 shows how the outputs from each detector are processed by the four main components of the circuit. These are:

(i and ii) The "slow" electronics associated with each detector, used to identify neutron events on the basis of the characteristic scintillation decay curves for recoil protons (<u>ie</u> neutron events) and electrons (<u>ie</u> gamma events).

(iii) The "fast" (nanosecond) timing circuitry used to measure the time of each coincidence event in order to separate real coincidences from the random coincidence background.

(iv) A coincidence logic system used to provide a gating pulse for acceptable n-n coincidence events.

Detailed block diagrams of typical circuits used for ^{252}Cf and ^{235}U measurements are shown in Figures 4.3 and 4.4.

There are two main differences between the circuits. Firstly, for ^{252}Cf, pulse shape discrimination (PSD) was usually achieved by using the S output from PSD circuitry (Br59) coupled to the photomultiplier base. The zero cross-over technique (Aℓ61) of particle identification was used for ^{235}U measurements. The other major difference was dictated by the data acquisition systems available in the two laboratories. At SUNI, three parameters (L_1, L_2 and T_{12}) were acquired on-line by a PDP15 computer and written to a magnetic buffer tape for subsequent off-line analysis. Data acquisition for ^{235}U measurements was limited to a two-parameter analyser and consequently on-line time analysis was performed. This was achieved by using the outputs of single channel analysers with windows set on the peak and background of the coincidence time delay spectrum in order to route $L_1 \cdot L_2$ coincidence events

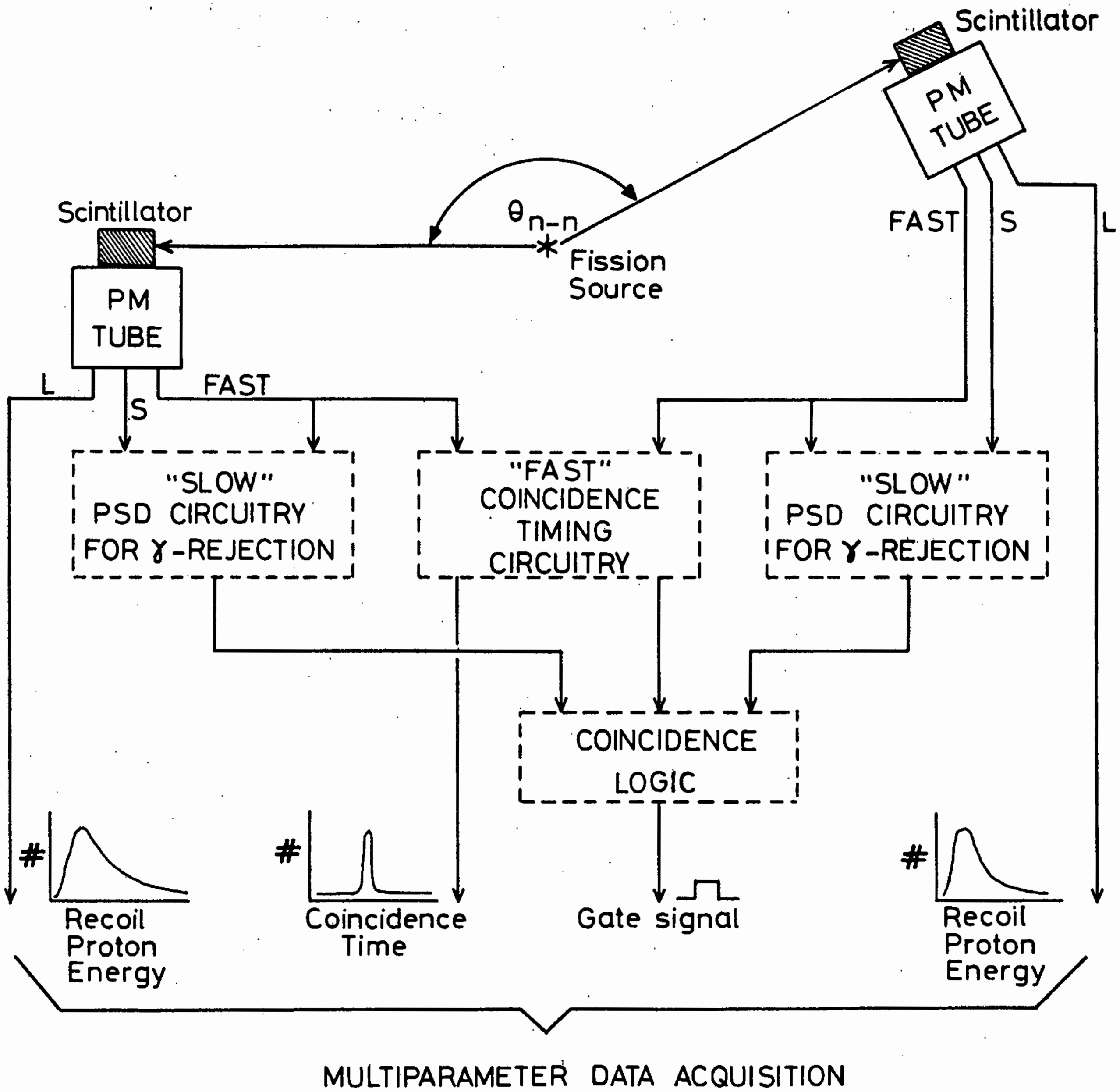

Figure 4.2 Schematic diagram of the experimental configuration for ^{252}Cf measurements. For the ^{235}U measurements, L signals were routed into "foreground" or "background" subgroups of a two parameter analyser memory using logic signals from single channel analyser windows set on the peak and background of the coincidence time delay spectrum.

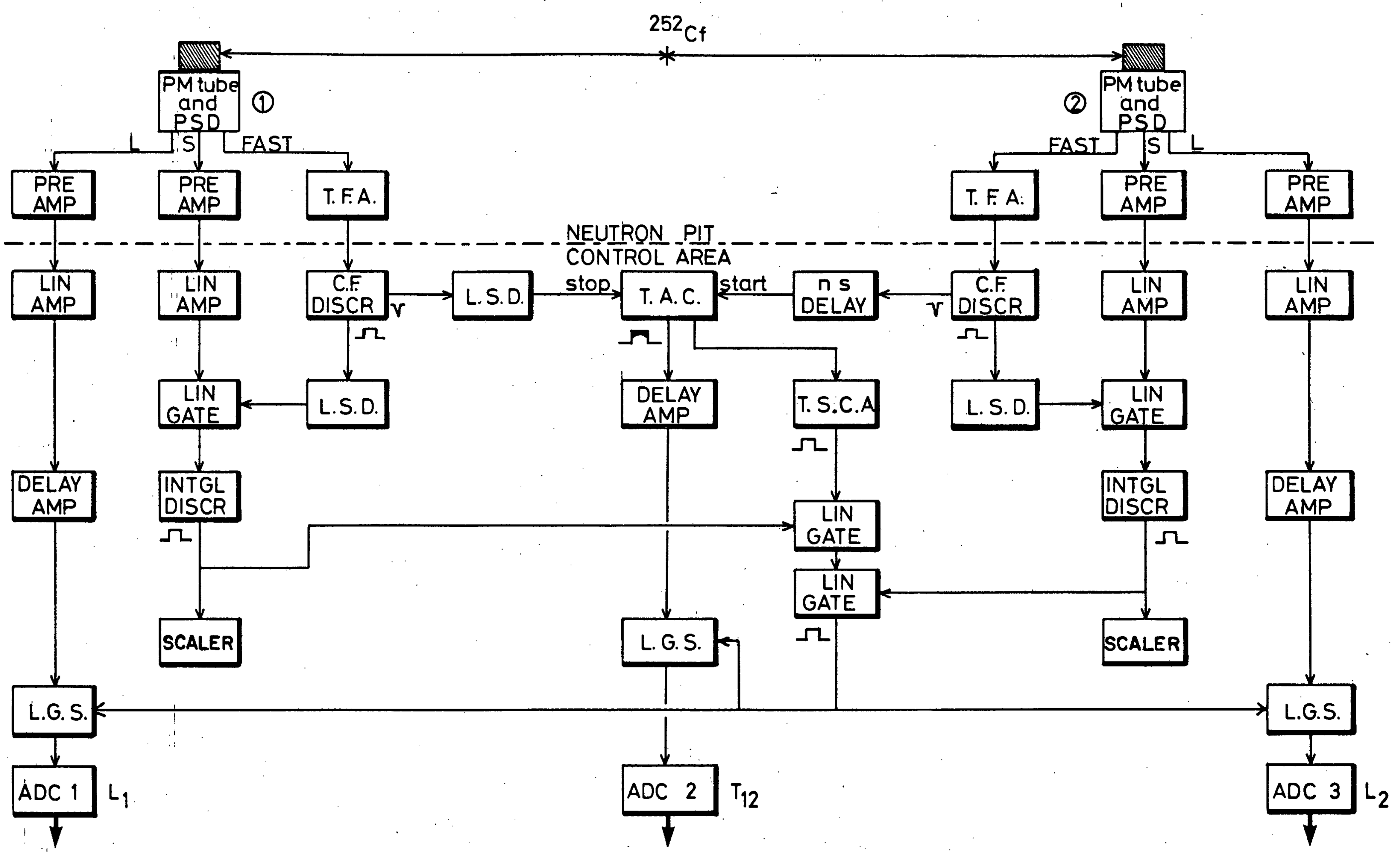

Figure 4.3 Block diagram of the electronic configuration used for most ^{252}Cf fission neutron angular correlation measurements. The ADC outputs give the energies of recoil protons in the neutron detectors (L_1 and L_2), and the coincidence time delay (T_{12}). These signals were routed to a PDP 15 computer and stored on magnetic tape.

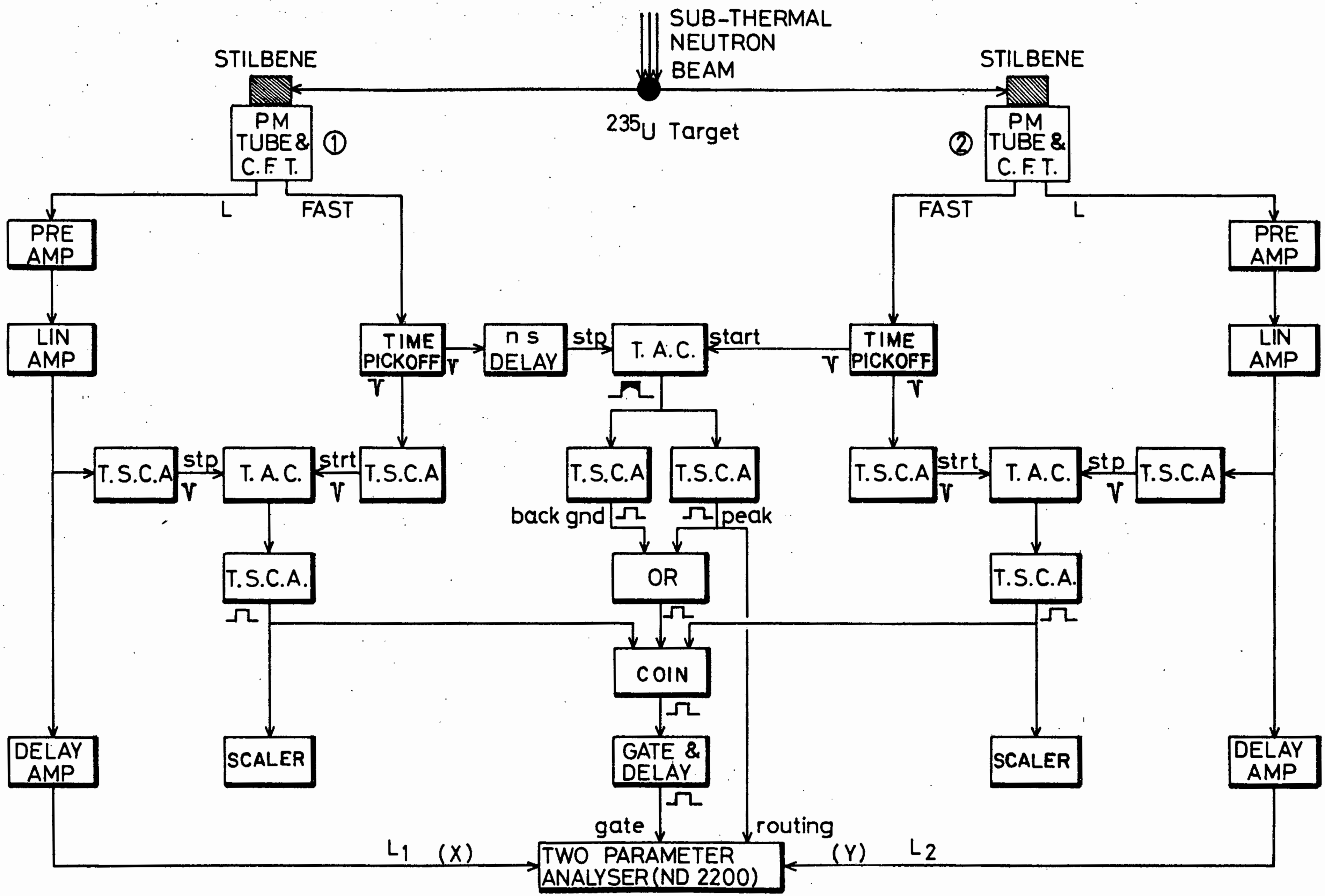

Figure 4.4 Block diagram of the electronic configuration used for ^{235}U fission neutron angular correlation measurements.

into "foreground" and "background" subgroups of the analyser memory. Time delay spectra for foreground n-n and background n-n coincidences were monitored in every run, and these provided a check on the single channel analyser window settings.

Two-parameter spectra were outputted onto paper tapes and subsequently repunched onto cards in condensed format. Scanning and analysis of magnetic tapes and card outputs was performed on a UNIVAC 1106 computer at the University of Cape Town.

TIME-OF-FLIGHT MEASUREMENTS

The fact that about 90% of fission γ-rays with energies greater than 100 keV are emitted at times shorter than 1 ns after scission (Sk70,Sk75) means that detection of a prompt γ-ray may be used to signal the start of a fission event. This provides a means of determining fission neutron energies using the time-of-flight method. (Time-of-flight measurements are normally made using thin sources and requiring the detection of a fission fragment as a "start" signal.)

Figure 4.5 is a schematic diagram of the electronic configuration used in time-of-flight angular correlation measurements (run series E). This configuration differs from that shown in Figure 4.2 by the addition of two fast timing circuits for neutron flight time measurement. Prompt γ-rays (or rarely, prompt neutrons) detected in a plastic scintillator (12.7 cm diameter × 0·3 cm thick) placed against the ^{252}Cf source provided timing pulses signalling the occurrence of fission events. These pulses were used as "stop" signals for the measurement of

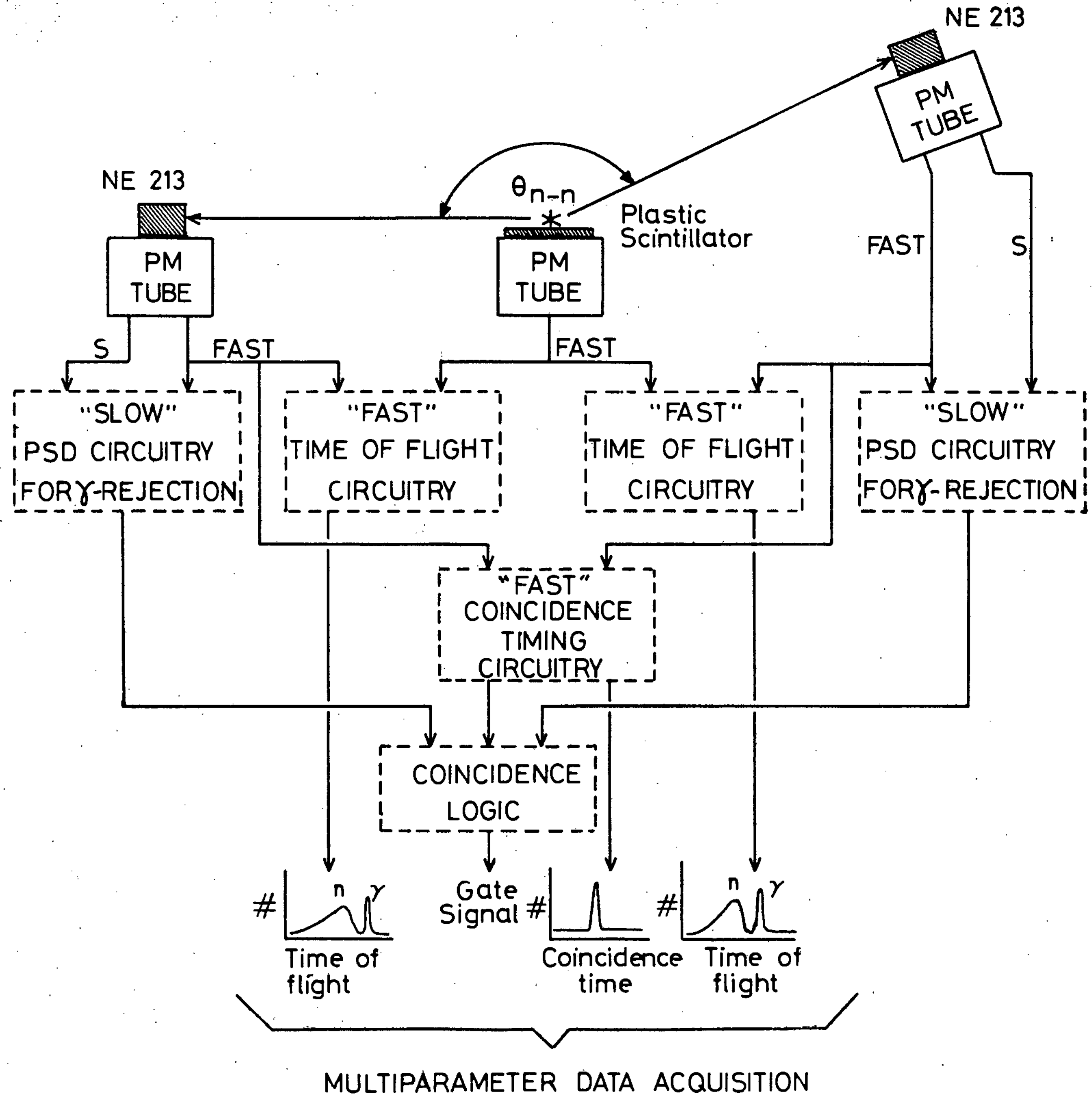

Figure 4.5 Schematic diagram of the experimental configuration for time-of-flight angular correlation measurements.

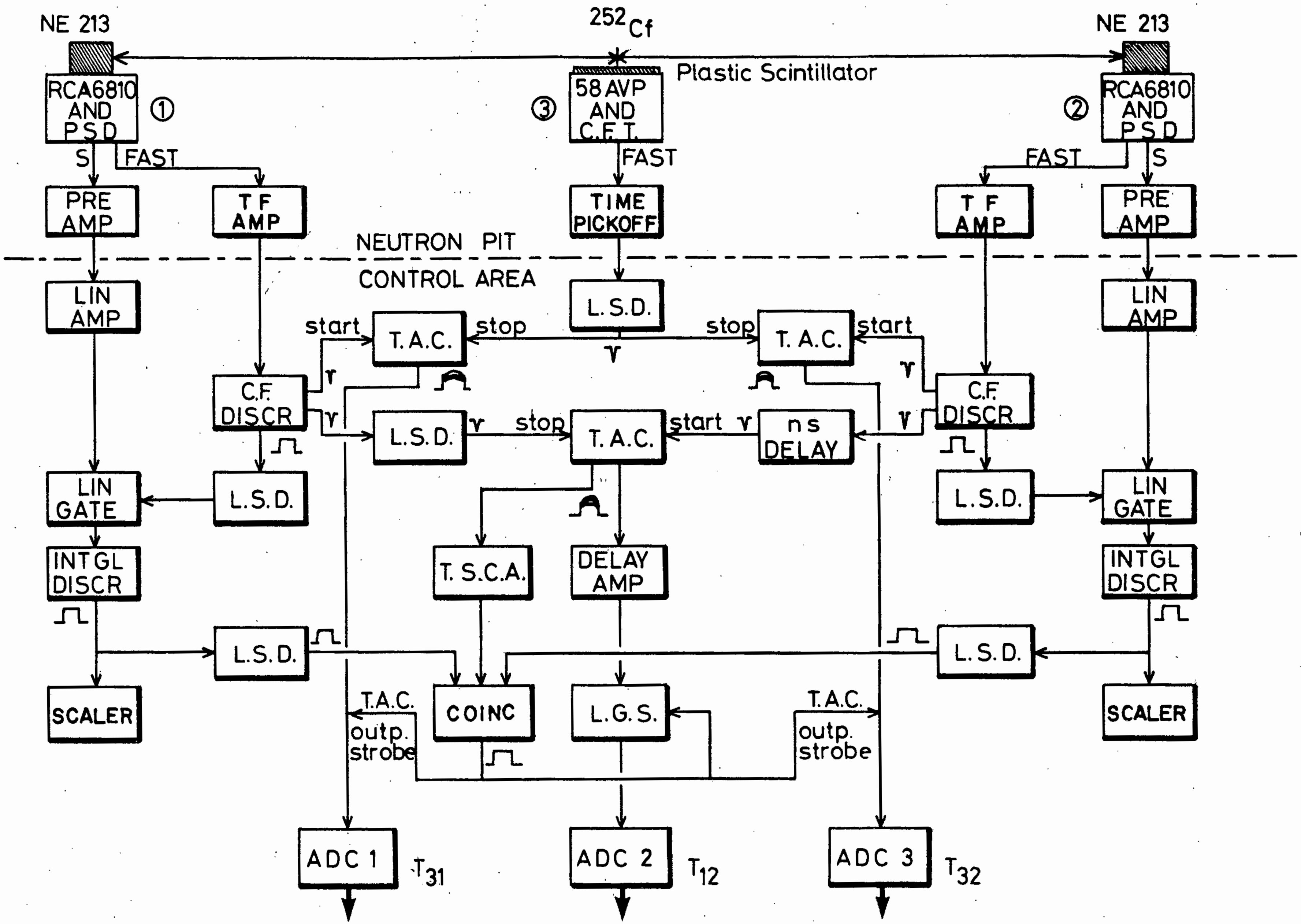

Figure 4.6 Block diagram of the electronic configuration used for time-of-flight angular correlation measurements. Outputs of the ADC's give the flight times (T_{31} and T_{32}) and the coincidence time delay (T_{12}). These outputs were routed to a PDP 15 computer and stored on magnetic tape.

neutron flight times in view of the high count rate in this detector. The large diameter of this scintillator and its proximity to the source reduced the possibility of any additional directional correlation (between the γ-ray and the n-n pair) being introduced into the measurements.

A complete block diagram of the electronic circuit used for time-of-flight work is shown in Figure 4.6. During the experiment, three TAC output signals (T_{31}, T_{32} and T_{12}) for each n-n coincidence event were routed to a PDP15 computer and written onto magnetic tape.

4.5 CALIBRATIONS

Every run set included several calibration runs and checks on detector performance. The main calibrations are detailed below.

(i) Determination of the "true zeroes" of the recoil proton pulse height (L) scales. This was achieved by measuring the position of the Compton edge corresponding to a specific gamma photon for two or three different gain settings of the L linear amplifier.

(ii) Pulse height scales were calibrated in terms of Compton electron energies for a variety of gamma sources. (eg ^{60}Co, ^{22}Na, ^{137}Cs, ^{54}Mn and ^{88}Y.) From these calibrations, and scintillator response curves for Compton electrons and recoil protons (Br56), pulse height scales were calibrated in terms of equivalent proton energy (and hence minimum incident neutron energy).

(iii) Gamma rejection efficiencies of the PSD systems were checked periodically using ^{60}Co or ^{22}Na sources. Rejection efficiencies were generally better than 99.5%. A lower PSD rejection efficiency ($\gtrsim$98%) was permitted in runs where the time-of-flight technique was used, and provided additional n-γ discrimination.

(iv) Proton pulse height spectra for single fission neutrons incident on the detectors were recorded for use in subsequent energy analysis of the $L_1 \cdot L_2$ coincidence spectra (see Section 4.6). Likewise, single neutron time-of-flight spectra were recorded for use in the energy analysis of time-of-flight coincidence matrices.

(v) Time scale calibrations were performed by introducing calibrated nanosecond delays into the "STOP" pulse inputs of the TAC's. In run series E the position of the prompt fission γ peak, which corresponded to a 2.7 ns flight time, was used to determine time zero.

(vi) Recoil proton detection thresholds were determined either by direct measurement using monoenergetic neutron beams from the $^{7}Li(p,n)^{7}Be$ reaction, or relative to the positions of Compton edges for several gamma sources. In the time-of-flight run set an additional method was used for direct calibration of the <u>neutron</u> detection threshold. The method used a contour plot of neutron flight time versus corresponding recoil proton pulse height in the detector being calibrated. The neutron threshold energy was calculated using the measured flight time corresponding to the proton pulse height cut-off determined from the contour plot. This method is illustrated in Figure 4.7.

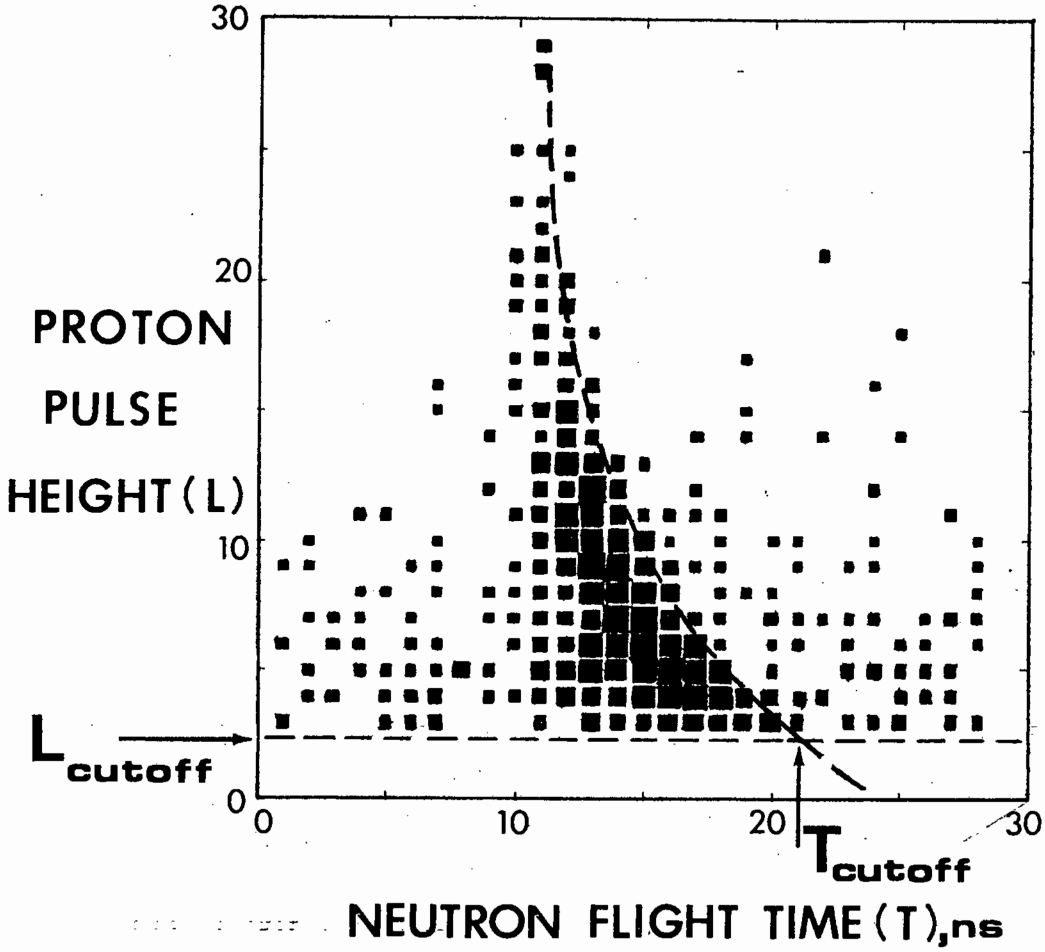

Figure 4.7 The method used during time-of-flight runs for determination of the neutron detection threshold. The threshold energy was calculated from

$$E_{threshold} = (72.3D/T_{cutoff})^2$$

where D = flight path in metres.

DETECTOR EFFICIENCY

Computer simulation of the n-n angular correlation experiments requires a knowledge of the energy dependence of the efficiency (relative or absolute) of the neutron detectors. The Monte Carlo simulation programme was designed to calculate the absolute detector efficiency $\varepsilon(E)$ using the equation (Ow60):

$$\varepsilon(E) = \frac{E-E_B}{E}\left[1 - \exp(-n_H \sigma_H(E) x)\right]$$

where E = energy of the incident neutron

E_B = bias of the neutron detector

n_H = density of protons in scintillator

$\sigma_H(E)$ = n-p scattering cross-section at energy E

x = mean scintillator thickness.

This equation takes no account of the presence of carbon nuclei, or the possibility of multiple n-p scatters in the organic scintillators. Experimental justification for the use of this equation was therefore desirable.

A novel experimental method (Sm77) was used in run series E to determine the relative efficiencies of the neutron detectors. The method is based on the time-of-flight measurement of the spectrum of prompt neutrons from ^{252}Cf spontaneous fission. Many accurate measurements (see Section 2.1) of the ^{252}Cf fission spectrum have shown that it may be represented by a Maxwellian spectrum of the form

$$N(E) \propto \sqrt{E}\, \exp(-E/T)$$

where N(E) is the fraction of neutrons per unit energy range, E is the neutron energy in MeV, and $T \simeq 1.41$ MeV (Gr73). Experimentally determined relative efficiency functions for the neutron detectors, defined as the ratio of the measured neutron spectrum (using time-of-flight) to the Maxwellian spectrum, are shown in Figure 4.8. Agreement between the calculated and measured relative efficiency curves is good, and the use of Owen's equation (Ow60) in the simulation programme appears to be justified.

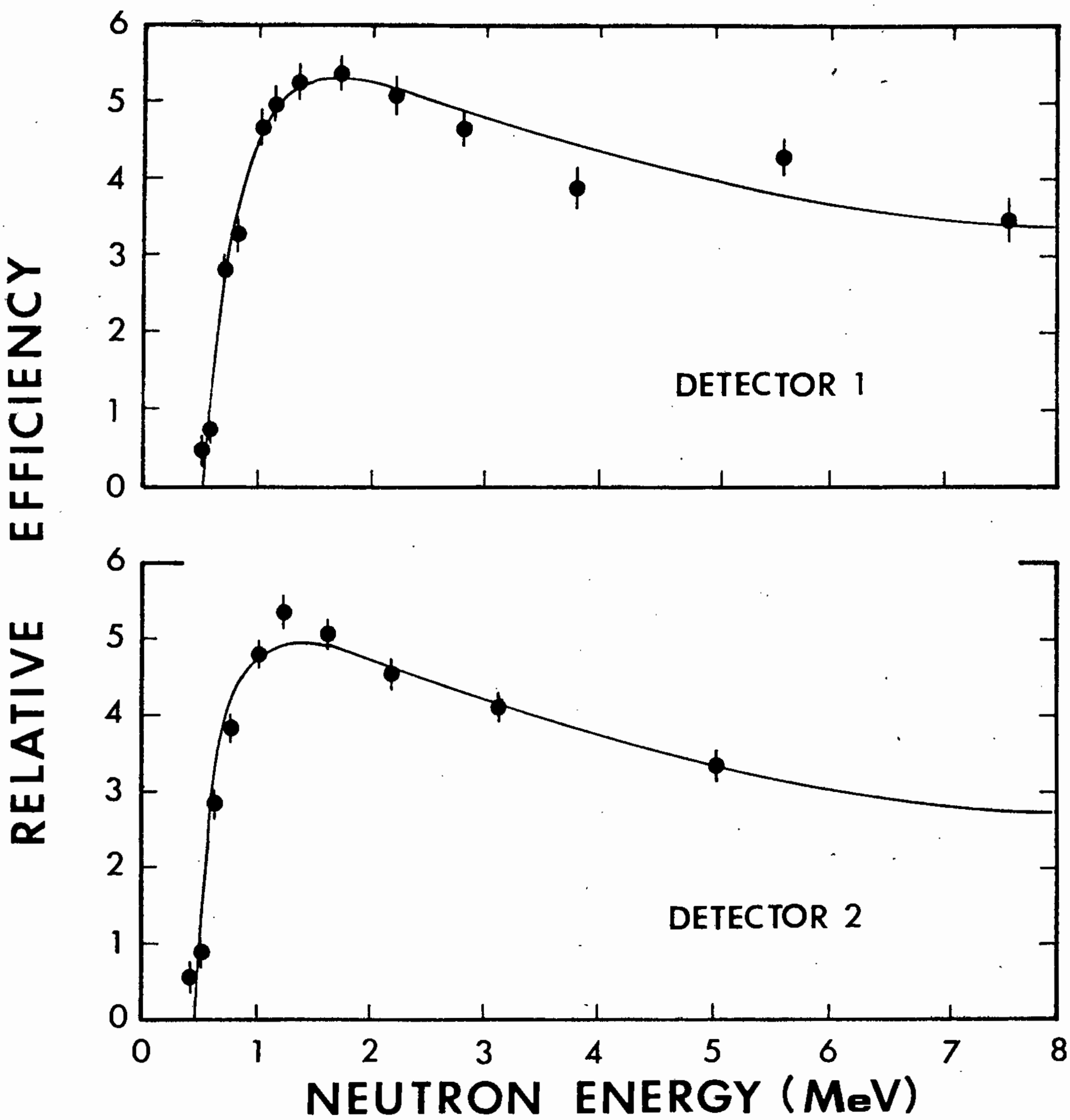

Figure 4.8 Relative efficiencies of the neutron detectors used in run series E. The points represent the ratios of the measured spectrum (from time-of-flight) to the Maxwellian spectrum $N(E) \propto \sqrt{E}\ \exp(-E/1.41)$. The curves represent the detector efficiencies according to Owen's equation. Normalisation of points and curves is arbitrary.

4.6 ANALYSIS

CORRECTION FOR ACCIDENTAL COINCIDENCES

As outlined in Section 4.4, multiparameter magnetic tape data acquisition for ^{252}Cf measurements enabled the coincidence time delay T_{12} (see Figure 4.9) to be recorded for each n-n coincidence event and so provide a means of subtracting accidental coincidences from the true rate. On playback the time spectrum of the coincidence events in each run was formed (Figure 4.9). Real n-n coincidences appear as a peak, typically 50 ns wide, superimposed on a background of accidental coincidences. Since the accidental coincidence background is uniformly distributed in time, the true coincidence rate may be determined by subtracting the average background level from the events in the time peak. The accidental rate was generally less than 10% of the true rate.

"Foreground" and "foreground + background" $L_1 \cdot L_2$ pulse height matrices were formed for each run by scanning the magnetic tapes with windows set on: (i) the time peak, to accept real + background events and (ii) spanning most of the time range, to include the time peak and 2 to 4 times the background - this window was made as large as possible for optimum statistical accuracy. True coincidence rates were then determined by subtraction of "foreground" and "foreground + background" data, suitably adjusted for differences in window widths.

In ^{235}U runs, separate peak and background pulse height matrices were acquired simultaneously by using windows set on the time peak and background to route $L_1 \cdot L_2$ events into

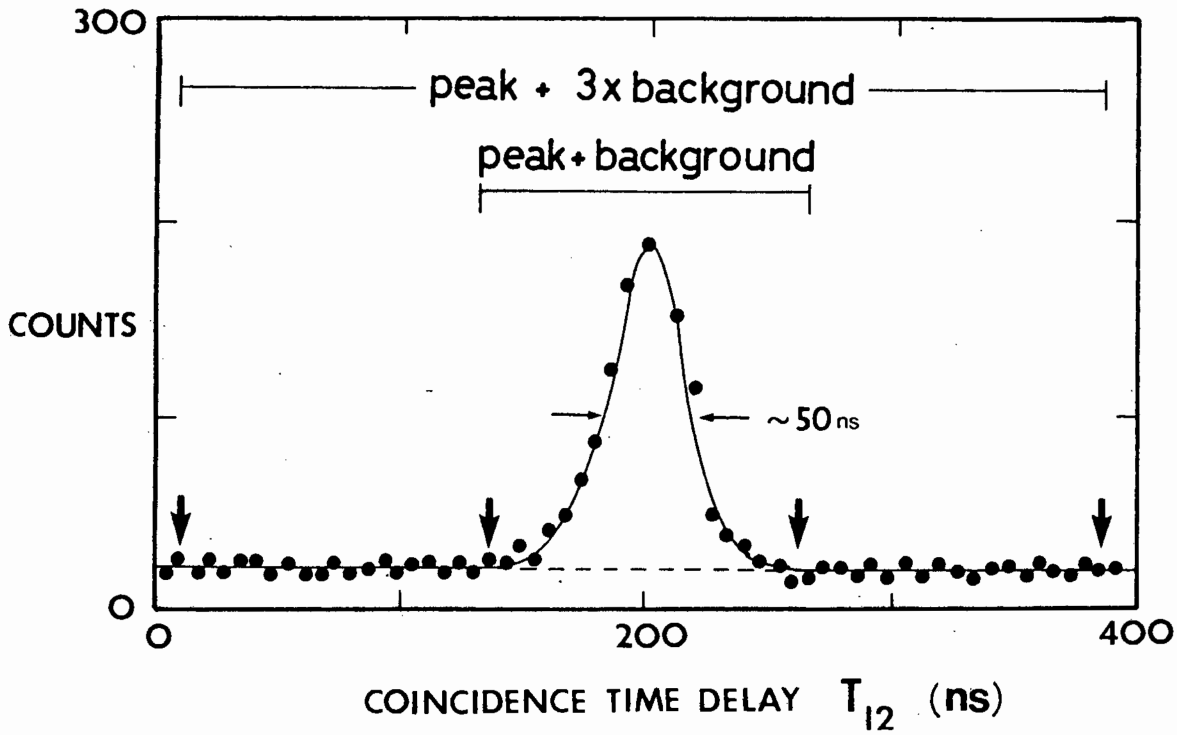

Figure 4.9 A typical time delay spectrum for n-n coincidences. Time windows used in scanning were positioned as shown.

separate memory groups. After calibration of the time window widths, the true coincidence rates were determined as for ^{252}Cf by foreground/background subtraction.

DETERMINATION OF THE ANGULAR CORRELATION

Preliminary analysis (Pr75) was based on the total count rates above the detection thresholds (∿0.6 MeV) of the neutron detectors. ie the analysis used the total number of true coincidences in the $L_1 \cdot L_2$ matrix. A ratio, proportional to the angular correlation, was determined from the measured singles count rates N_1 and N_2 of the two detectors and the coincidence rate $N_c(\theta)$ at angle θ. Count rates determined in the ^{252}Cf experiments were processed in the following manner.

Let N_f be the fission rate (per unit time) of the source, $\overline{\nu}$ the average neutron yield per fission, and Ω_1 and Ω_2 the solid angles subtended by the two detectors. Then, since Ω_1 and Ω_2 are small ($<< 4\Pi$), the singles count rates are:

$$N_1 = \Omega_1 \ \varepsilon_1 \ \bar{\nu} \ N_f/4\Pi \qquad 4.6.1$$

and $$N_2 = \Omega_2 \ \varepsilon_2 \ \bar{\nu} \ N_f/4\Pi \qquad 4.6.2$$

where ε_1 and ε_2 are the average efficiencies of the detectors for detecting a fission neutron. The rate of true coincidence counts is given by:

$$N_c(\theta) = \Omega_1\Omega_2 \ \varepsilon_1\varepsilon_2 \ \bar{\nu} \ N_f \ P(\theta)/4\Pi \qquad 4.6.3$$

where $P(\theta)$ represents the number of fission neutrons emitted per unit solid angle at angle θ to, and in coincidence with, the νth fission neutron. We define a ratio

$$R(\theta) = N_c(\theta)/N_1N_2 = 4\Pi P(\theta)/\bar{\nu} \ N_f \qquad 4.6.4$$

Thus $R(\theta)$ is proportional to the angular correlation $P(\theta)$, independent of the experimental geometry (Ω_1 and Ω_2), and insensitive to small variations in instrumental stability insofar as these affect ε_1 and ε_2.

Experimental runs were of short duration compared with the ^{252}Cf half-life, and the fission rate per unit time of this source was effectively constant in each run. However, for ^{235}U, measurements extended over nearly two months, during which time the source fission rate was subject to fluctuations in the thermal neutron beam flux. Experiments on $^{235}U(n_{th},f)$ incorporated a monitor of the incident beam flux in order to correct for variations in the source fission rate N_f. Fission rate variations were compensated by using coincidence and singles count rates per unit beam monitor count to calculate the ratio $R(\theta)$. (For ^{252}Cf, count rates per unit time were used in equation 4.6.4.) As a result, for ^{235}U, $R(\theta)$ has the dimension of beam monitor counts, and it has units of time for ^{252}Cf measurements.

ENERGY ANALYSIS BASED ON RECOIL PROTONS

The method above was initially used to determine the n-n angular correlation for all neutrons with energies greater than the detection thresholds. Later analysis was aimed at investigation of the energy dependence of R(θ) (reflecting the energy dependence of P(θ)), by determining the coincident and singles count rates in different regions of the $L_1 \cdot L_2$ pulse height matrices. This was achieved by imposing "detection thresholds" at different energies during analysis.

Axes of the $L_1 \cdot L_2$ pulse height matrices and the singles pulse height spectra for each detector were calibrated in terms of proton energy (see Section 4.5). Energy analysis was performed at a set of 9 or 10 proton energies L_{min} spanning the energy range 0.6-3.0 MeV. The total number of real coincidences N_{co}, in which both pulse heights L_1 and L_2 were greater than L_{min}, was determined for each energy level L_{min} (see Figure 4.10). The corresponding singles rates above each threshold were estimated by multiplying the measured singles rate by the fraction (f) of neutrons with energies (proton pulse heights) greater than L_{min}. Thus the coincidence and singles rates were determined for each energy threshold and used in equation 4.6.4 to determine R(θ).

ENERGY ANALYSIS BASED ON NEUTRON FLIGHT TIMES

The analysis of time-of-flight coincidence matrices ($T_{31} \cdot T_{32}$) at each n-n correlation angle θ was similar to that performed on the pulse height matrices. The number of n-n coincidences was determined within a time region (region A in Figure 4.11a) bounded by neutron flight times T_{min} and T_{max}.

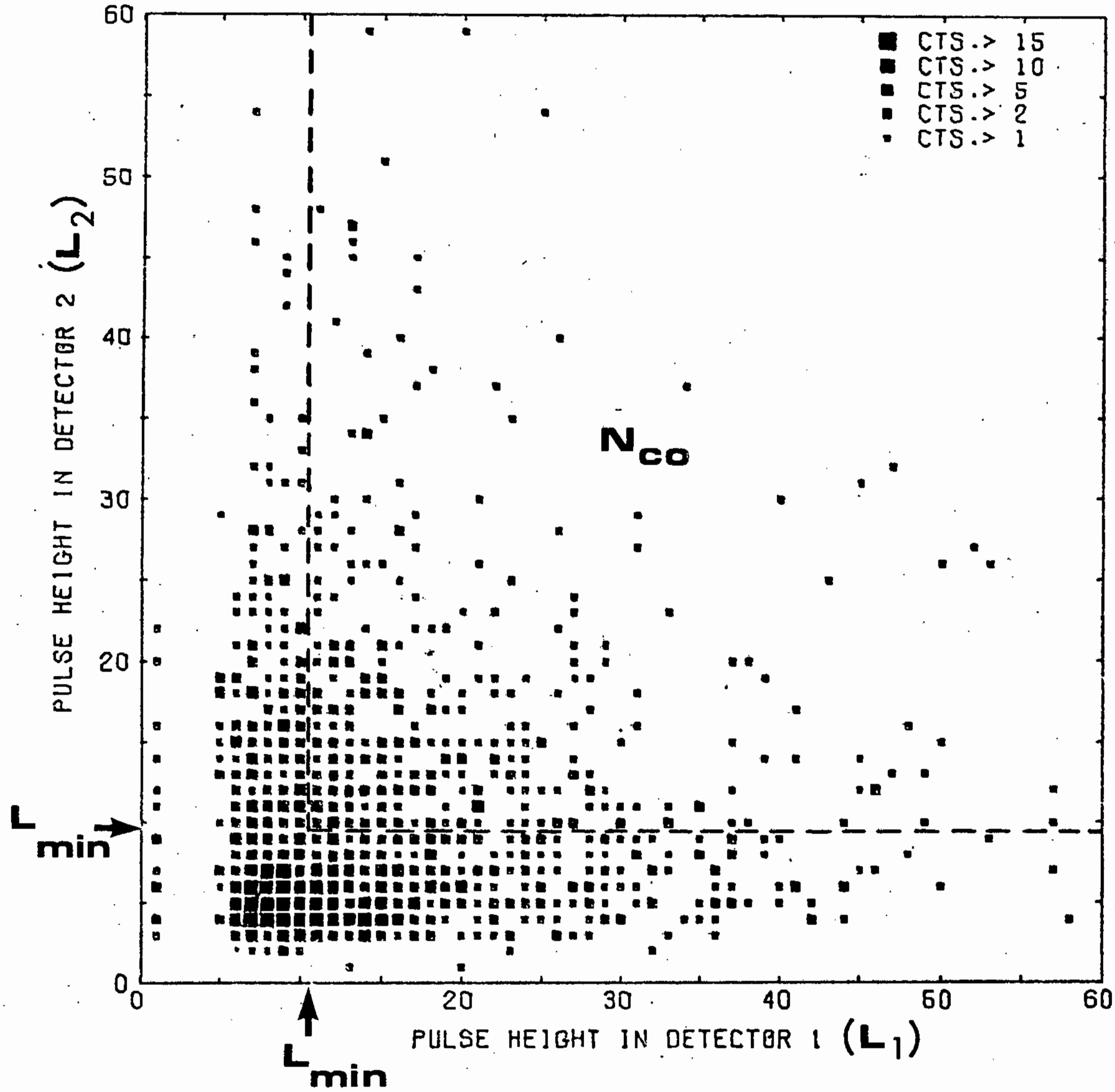

Figure 4.10a A count density plot of a recoil proton-pulse height matrix, showing typical thresholds L_{min} used in the energy analysis. N_{co} is the total number of coincidences between neutrons with energies greater than the proton energy corresponding to the pulse height value L_{min}.

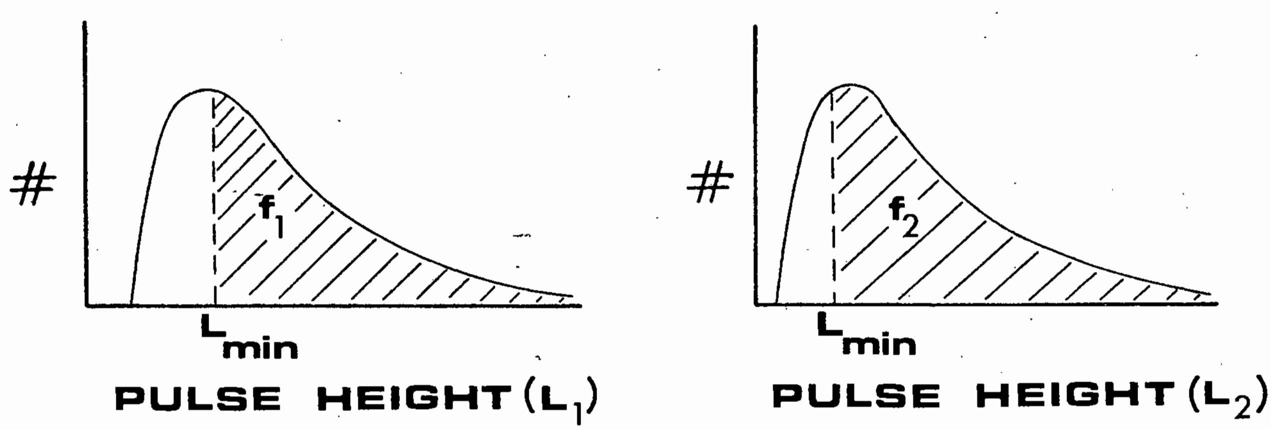

Figure 4.10b Schematic illustration of singles pulse height spectra, showing the fractions f_1 and f_2 of neutrons with energies (proton pulse heights) greater than L_{min}.

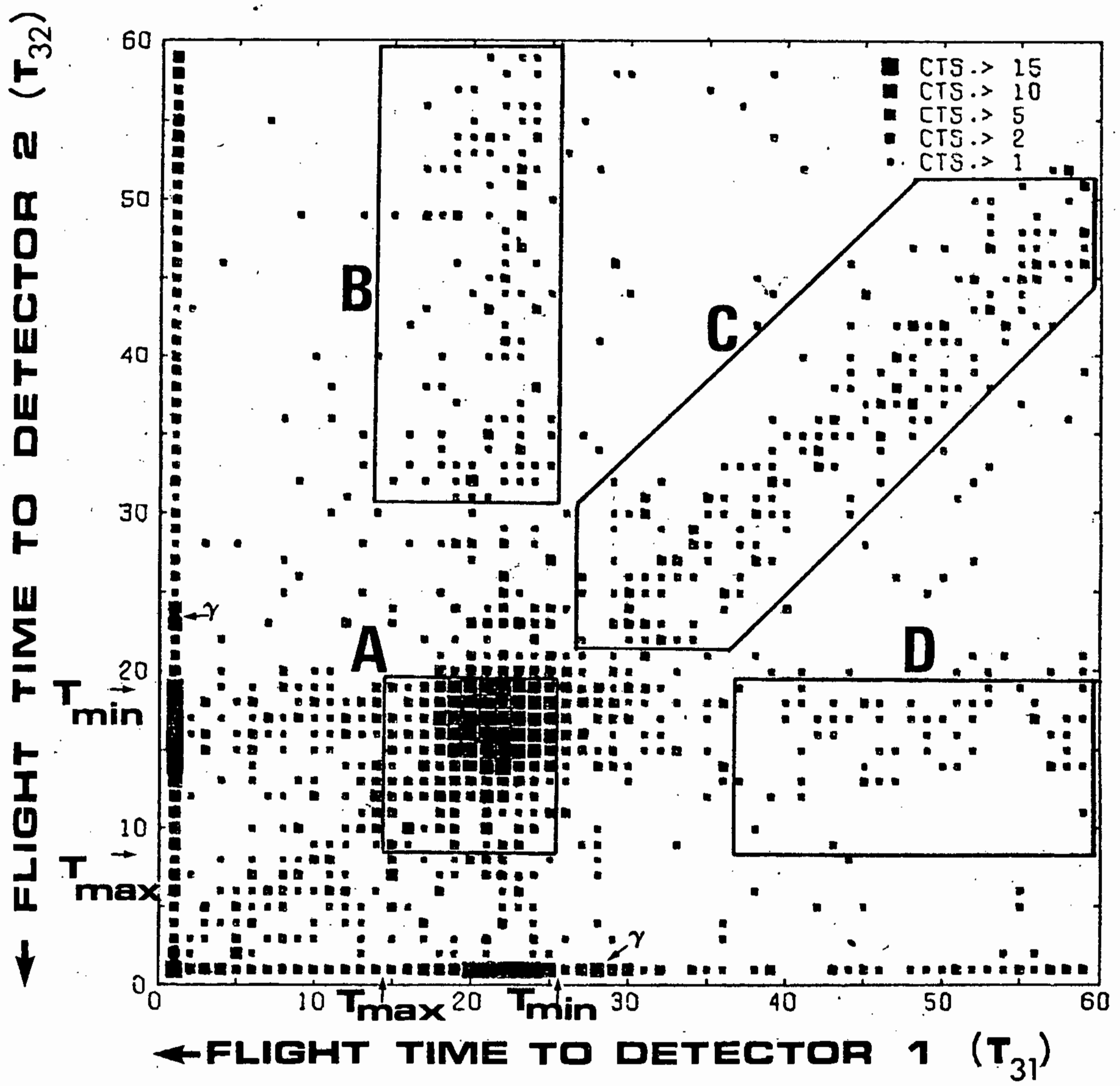

Figure 4.11a A count density plot of a typical n-n coincidence time-of-flight matrix. Background contributions to the real n-n coincidence region A defined by flight times T_{min} and T_{max} are estimated from the counts present in the regions marked B,C and D. Events in regions B,C and D correspond to accidental coincidences in detectors 2,3 and 1 respectively. (eg counts in region C are real n-n coincidences "stopped" by a background fission γ-ray in detector 3.) Points lying on the axes represent singles events which bypassed the coincidence gating requirement. The prompt γ peaks resulting from the small γ-breakthrough may be recognised in these spectra.

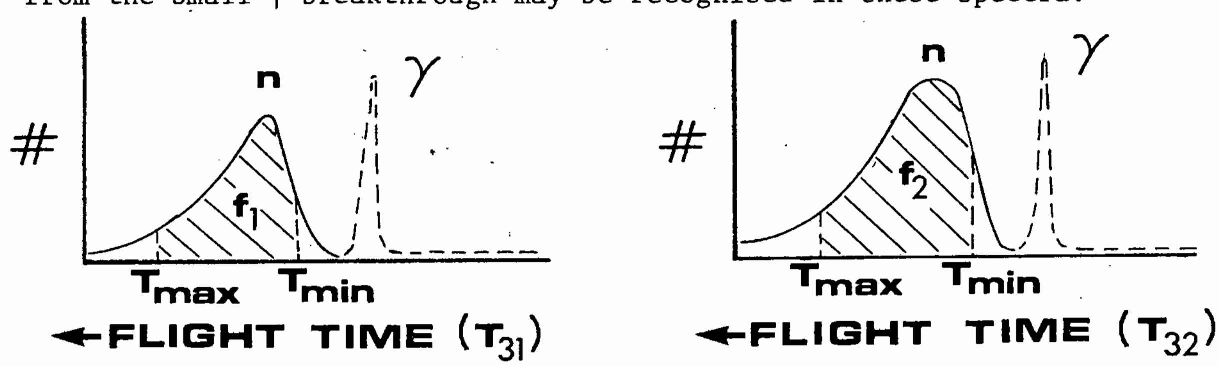

Figure 4.11b Schematic illustrations of singles time-of-flight spectra, showing the fractions f_1 and f_2 of neutrons within the energy region defined by flight time limits T_{min} and T_{max}.

T_{max} corresponds to the detection threshold of the neutron detector. In analogy with the proton recoil-based energy analysis, several thresholds T_{max} were set during analysis and the total number of n-n coincidences in the energy regions defined by T_{min} and T_{max} were determined.

Correction of the total coincidence rate for accidental coincidences is illustrated in Figure 4.11a. The coincidences lying in the regions B, C and D result from accidental events occurring in detectors 2, 3 and 1 respectively. These regions extend beneath the peak of true n-n coincidences (region A). Corrections to the number of coincidences in region A were made by estimating the contributions arising from events in regions B, C and D.

Singles count rates for different energy regions were estimated by multiplying the measured count rates by the fraction (f) of neutrons within the energy region defined by flight time limits T_{min} and T_{max} (see Figure 4.11b). The angular correlation $R(\theta)$ was calculated for each energy region using equation 4.6.4 and the coincidence and singles rates determined by the above methods.

CHAPTER FIVE

RESULTS

5.1 ANGULAR CORRELATION OF NEUTRONS FROM ^{252}Cf (sf)

Data sets for each run series were analysed as described in Section 4.6 to determine the n-n angular correlation $R(\theta)$. During each run series more than one run was usually made at each angle. After checking for internal consistency, multiple measurements at each θ were combined to give a weighted mean value of $R(\theta)$, individual measurements being assigned weights proportional to the inverse squares of their standard deviations.

Absolute values of $R(\theta)$ varied in different run series, reflecting changes in the source strength and the effects of small differences in the γ-rejection efficiencies used in each series. The absolute value of $R(\theta)$ increases as the source fission rate decreases (see equation 4.6.4). The calculated decrease in source strength was sufficient to account for the difference (a factor of 1.2) between absolute values of $R(\theta)$ obtained in run series A and B. A larger variation ($\sim$2.6) between $R(\theta)$ values in run series A and C is thought to be due mainly to small differences in the γ-rejection efficiencies of the detectors used in the two run series. Small changes in the γ-rejection efficiency (although still $\geq$99%) change the singles count rates much more rapidly than the coincidence rate, with a resulting change in $R(\theta)$.

The measurements of the n-n angular correlation for neutrons with energies $\geq$0.6 MeV, based on recoil protons (run series A) and time-of-flight (run series E), are shown in Figure 5.1. Data from run series E, in which measurements were taken at only three angles (20^0, 90^0, 180^0), are normalized to the run series A measurement at 90^0. The prediction of a Monte Carlo model, in which all neutrons were assumed to be emitted isotropically in the frames of the fully accelerated fragments, is also shown in Figure 5.1. The predicted distribution is normalized to the experimental measurements in the angular region 80^0-180^0, where the distributions are in best agreement. Whereas the evaporation model predicts a backward peaking of the correlation, ie an enhanced angular correlation for neutrons emitted at large angles to one another, the measurements show a nearly symmetric correlation which is slightly enhanced at small angles.

ENERGY DEPENDENCE OF R(θ)

Energy thresholds used in the recoil proton-based energy analysis corresponded to particular channel numbers on the axes of the $L_1 \cdot L_2$ coincidence pulse height matrices. Consequently these energies varied in different run series. In order to combine the results of different run series, each set of R(θ) values calculated for each series was used to interpolate R(θ) at a set of equally spaced energy thresholds (0.8, 1.3, 1.8, 2.3 and 2.8 MeV). Results obtained in run series A to D were then combined at each angle after normalization of R(90^0) values at the energy threshold 0.8 MeV, and after checking for consistency within experimental uncertainties. The results obtained from an energy analysis of run series E (time-of-flight) showed some

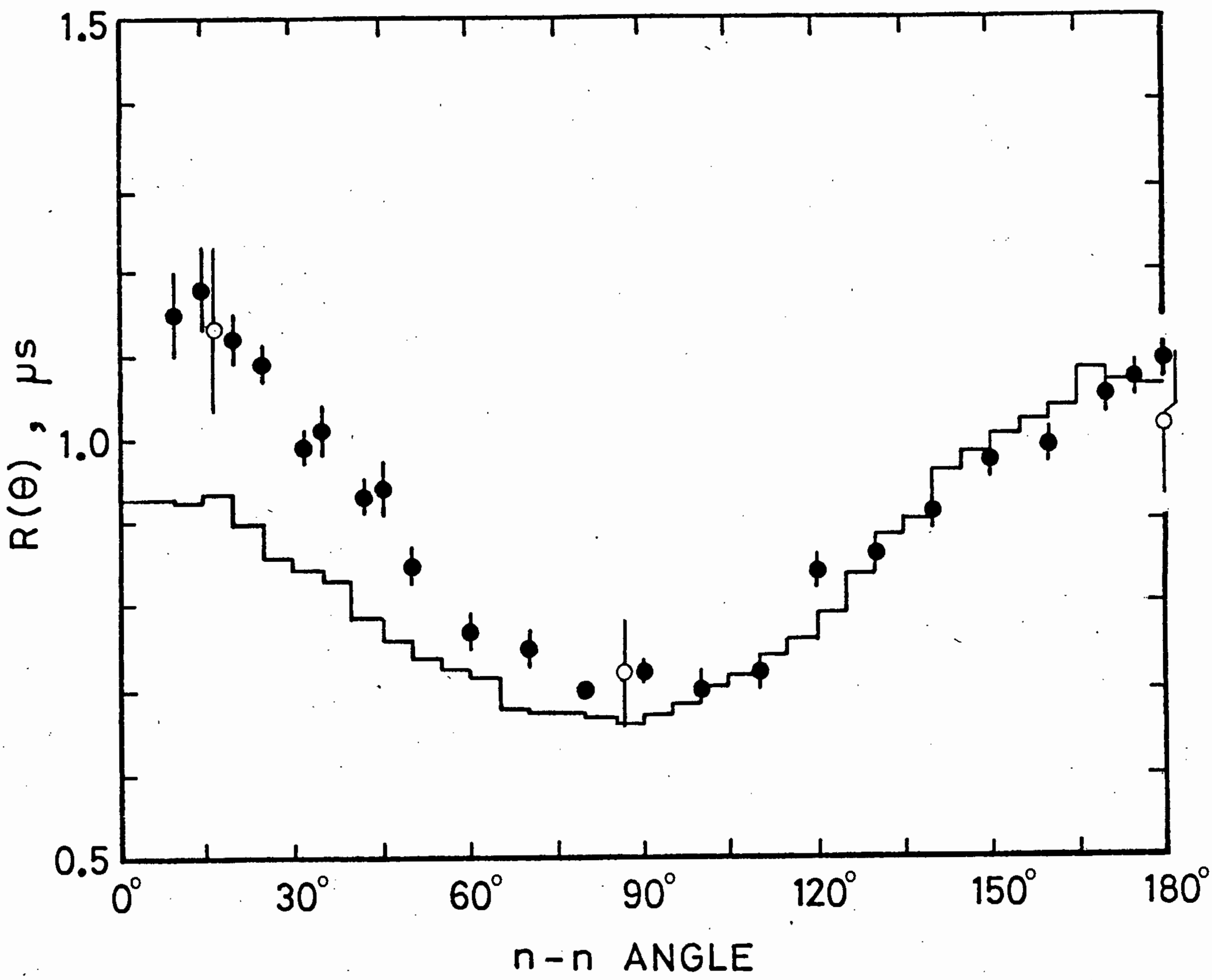

Figure 5.1 The n-n angular correlation R(θ) for neutrons with energies ≥0.6 MeV from ^{252}Cf (sf), showing experimental measurements from run series A (solid circles), time-of-flight measurements from run series E (open circles), and Monte Carlo prediction (histogram). Run series E measurements are normalized to those of run series A at 90^0, and the histogram is normalized to the measurements in the angular region 80^0-180^0. Error bars indicate the statistical uncertainties in the measurements (one standard deviation).

systematic differences (see Figure 5.5) and were not combined with other measurements.

The threshold energy dependence of the n-n angular correlation (determined from recoil proton measurements) is shown in Figure 5.2. The most marked effect on R(θ) with increasing neutron energy is the increased peaking of the correlation at small and large angles relative to $R(90^{\circ})$. This effect is qualitatively understood as follows. Neutrons with the highest energies are those that are emitted along the fission axis in the direction of fragment motion, since they receive the largest translational velocity component. Thus, measurements at high energy thresholds preferentially select these neutrons, thereby enhancing the small-angle correlation (axial neutrons emitted by the same fragment) and the large-angle correlation (axial neutrons emitted by opposite fragments) relative to the 90° correlation.

At high energies counting statistics are poor as a result of the Maxwellian form of the fission spectrum, and the indirect (recoil proton) method of measuring neutron energies.

To facilitate comparison of the measured energy dependence of R(θ) and model predictions, the ratios of small (10° to 20°) and large (170° to 180°) angle measurements of R(θ) to those at intermediate angles (80° to 100°) were calculated for each energy threshold.* The energy dependence of these ratios reflects the change in the angular correlation distribution with

---

*These ratios were defined as the mean of R(θ) values within angular ranges, rather than at specific angles, so as to reduce the effects of scatter and possible wayward trends of individual measurements.

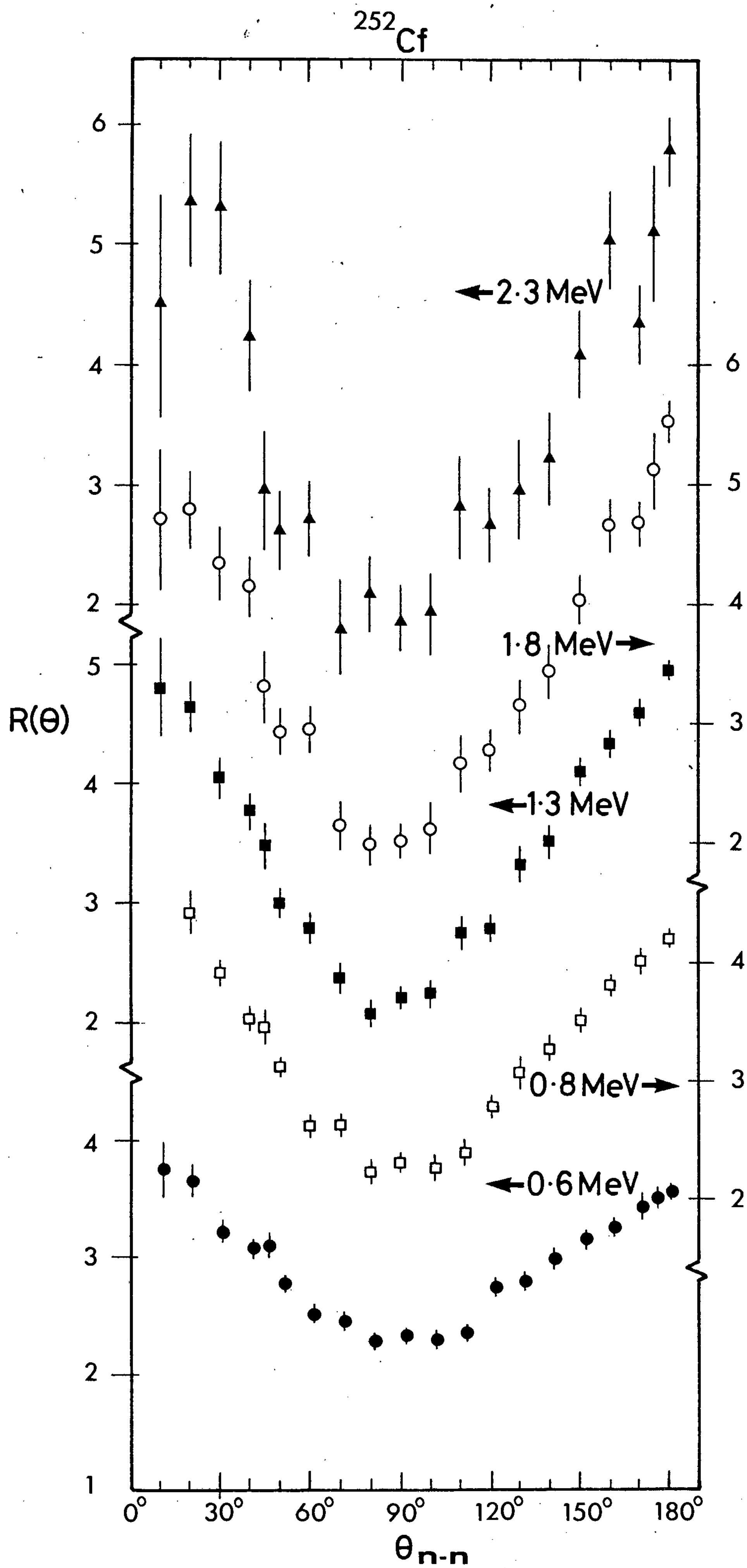

Figure 5.2 The n-n angular correlation R(θ) at different neutron energy thresholds for neutrons from ^{252}Cf (sf). Arrows indicate the appropriate scales for data at each threshold.

increasing neutron energy. The measured (via recoil protons) and predicted ratios are shown in Figure 5.3. It is seen that for energies $\lesssim$2.5 MeV the evaporation model predicts an angular correlation which is backward peaked (ie at 180^0), while the measurements suggest a small forward peaking below $\sim$1 MeV and an approximately symmetric distribution above 1 MeV. The measurements and the model predictions show a marked discrepancy at energies $\gtrsim$2 MeV, indicating that the angular correlation of neutrons in this energy region is more isotropic than is expected on the assumption of evaporation from moving fragments.

The computer model was modified to include the emission of a small (10%) component of scission neutrons emitted isotropically in the laboratory frame with an evaporation spectrum having mean energy 2.6 MeV (ie a scission component identical to that included in the analysis of Bowman *et al*). The angular correlation predicted by this model is shown in Figure 5.4(a). As before, the model predicts an angular correlation peaked at large angles and the discrepancy at small angles remains. For neutrons with energies $\gtrsim$2 MeV the "fit" between the experimental data and the model predictions appears to be improved. Figure 5.4(b) shows the angular correlation predicted by a model including a 20% isotropic scission component. Comparison with experimental measurements clearly disfavours the existence of a large scission neutron component of this nature.

The threshold energy dependence of R(θ) obtained from time-of-flight measurements is compared with recoil proton-based data in Figure 5.5. It is seen that for threshold energies $\gtrsim$0.8 MeV large-angle measurements are systematically lower for the time-

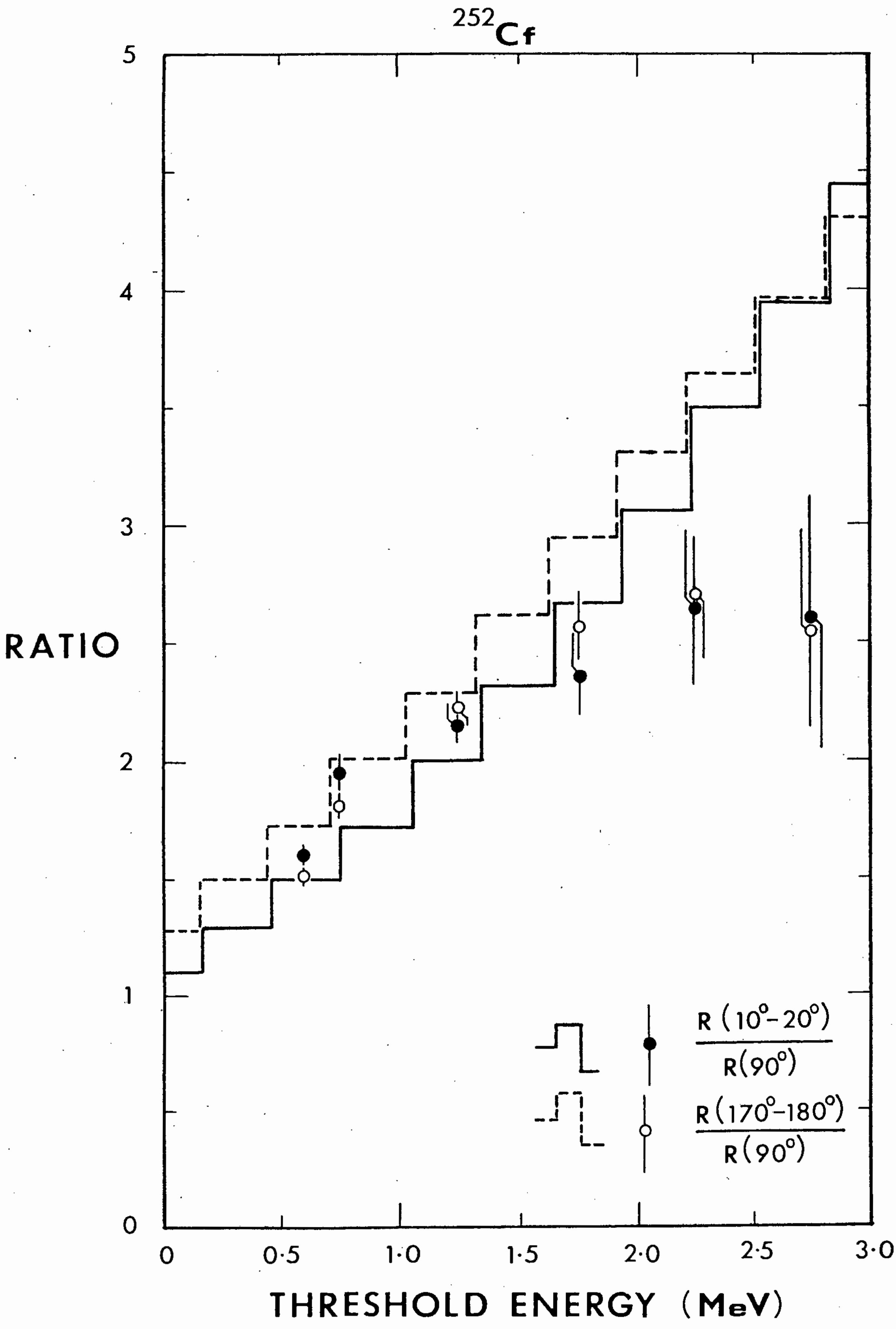

Figure 5.3 The threshold energy dependence of the n-n angular correlation for ^{252}Cf (sf), showing measurements (points) and Monte Carlo predictions (histograms) for a model which assumed isotropic neutron evaporation in the frames of the fully accelerated fragments.

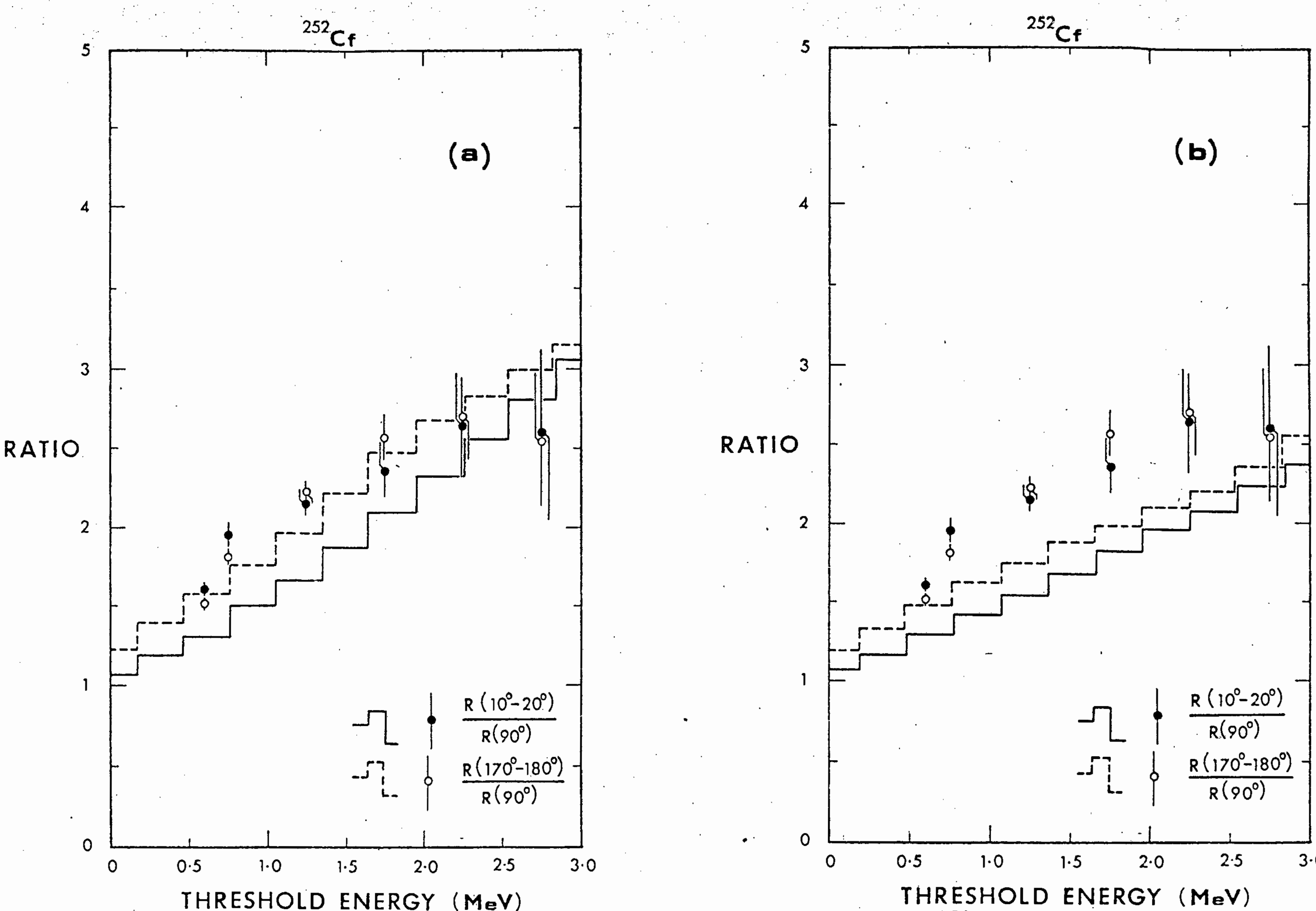

Figure 5.4(a) The threshold energy dependence of the n-n angular correlation for ^{252}Cf (sf), showing measurements (points) and Monte Carlo predictions (histograms) for a model which assumed a 10% scission component emitted isotropically in the laboratory frame, and isotropic evaporation of the remaining 90% of the neutrons from the moving fragments. (b) Comparison of measurements and the Monte Carlo predictions for a model which included a 20% scission component.

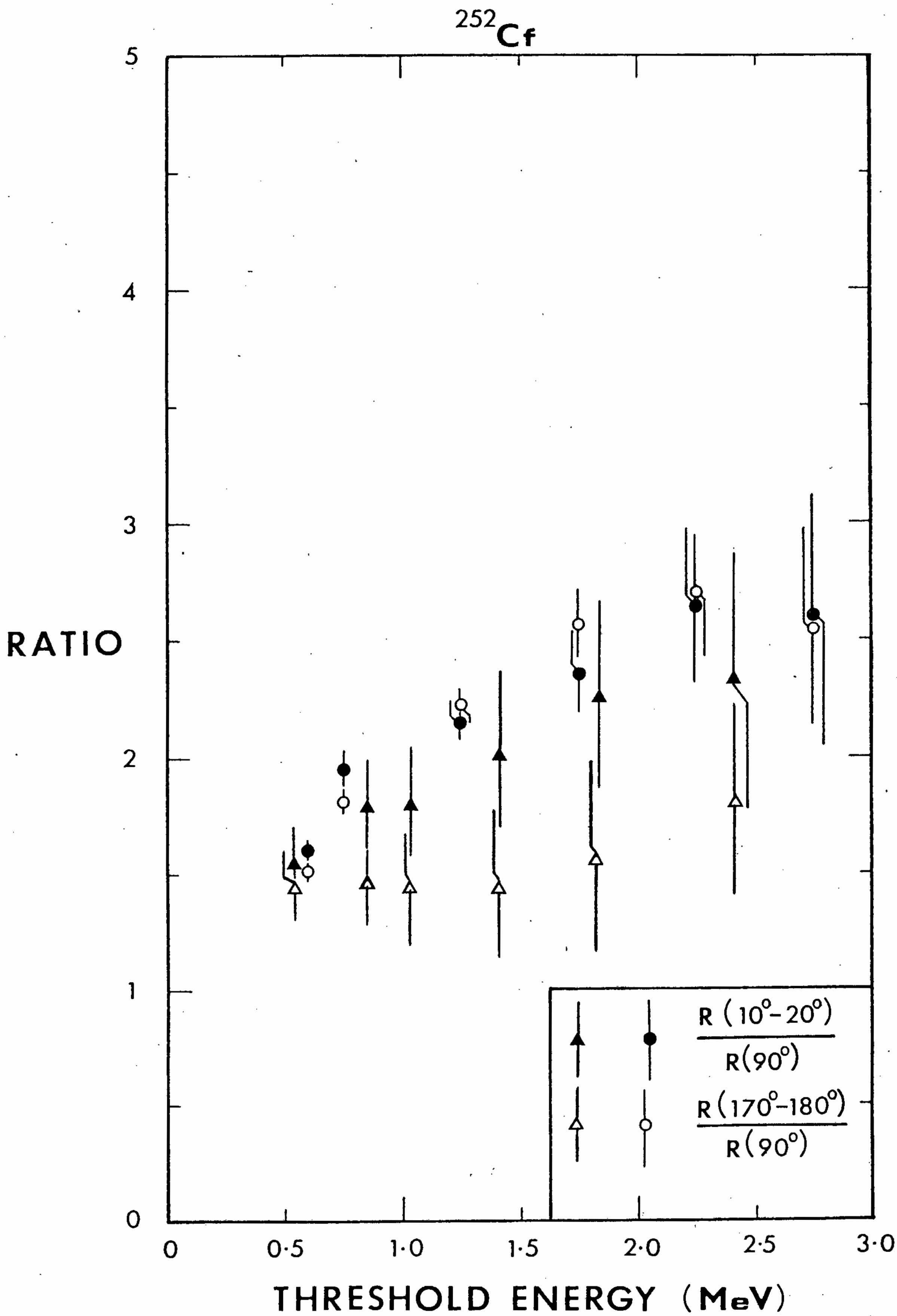

Figure 5.5 Comparison of measurements of the threshold energy dependence of the n-n angular correlation for ^{252}Cf (sf) from run series A to D (circles) and run series E (triangles).

of-flight run, while small-angle measurements obtained via the two methods are mostly in agreement within the statistical uncertainties. The large systematic differences between large-angle measurements are attributed to the fact that, in the time-of-flight run series, only one measurement (which appears to be suspect) was made at 180^{0}, while several were made at 20^{0} and 90^{0}. The recoil proton-based measurements are considered to be more reliable, since they are based on a large number of (consistent) measurements from four independent run series. Moreover, the energy resolution of the time-of-flight measurements was considerably poorer than that obtained via recoil protons. The time resolution of the system used for time-of-flight measurements, as indicated by the width of the prompt γ-peak, was $\sim$9 ns. Thus, the resulting energy resolution was of the order of $\pm$0.4 MeV for a neutron energy of 1.0 MeV. Recoil proton energies determined relative to Compton edges of γ-sources were estimated to be accurate to within $\pm$0.1 MeV at 1.0 MeV.

The n-n correlation measurements based on recoil protons, obtained in run series A to D are used exclusively in further comparisons with model predictions.

5.2 ANGULAR CORRELATION OF NEUTRONS FROM $^{235}U(n_{th},f)$

The angular correlation of neutrons with energies $\geq$1.0 MeV from $^{235}U(n_{th},f)$ is shown in Figure 5.6, together with evaporation model predictions of this measurement. The model predictions are for the cases where (i) all neutrons were assumed to be evaporated isotropically from moving fragments and (ii) 15% of the neutrons were emitted isotropically at scission and the remainder from the moving fragments. (The effects of fragment angular momentum were not taken into account). The results indicate that the angular correlation for $^{235}U(n_{th},f)$ is similar to that observed for ^{252}Cf (sf). In both reactions the observed n-n correlation is more strongly peaked at small angles than is expected for an evaporation model - which predicts large-angle peaking.

The present measurements cannot be compared directly with those of De Benedetti *et al* (De48), since the operating thresholds of the detectors used in that experiment are not known. Those early measurements (see Figure 2.8 on p 2.25) suggested a flat correlation distribution at angles <90^{0}. However this result is based on only two small-angle measurements, at 30^{0} and 60^{0}. The measurement at 30^{0} was corrected for spurious coincidences caused by single neutrons scattering from one detector to the other. The correction method employed used measurements obtained for a Po-Be source which emits single neutrons via the reaction $^{9}Be(\alpha,n)^{12}C$. This method is liable to considerable error as a result of the different energy spectra for neutrons from fission and from the Po-Be source. Further errors

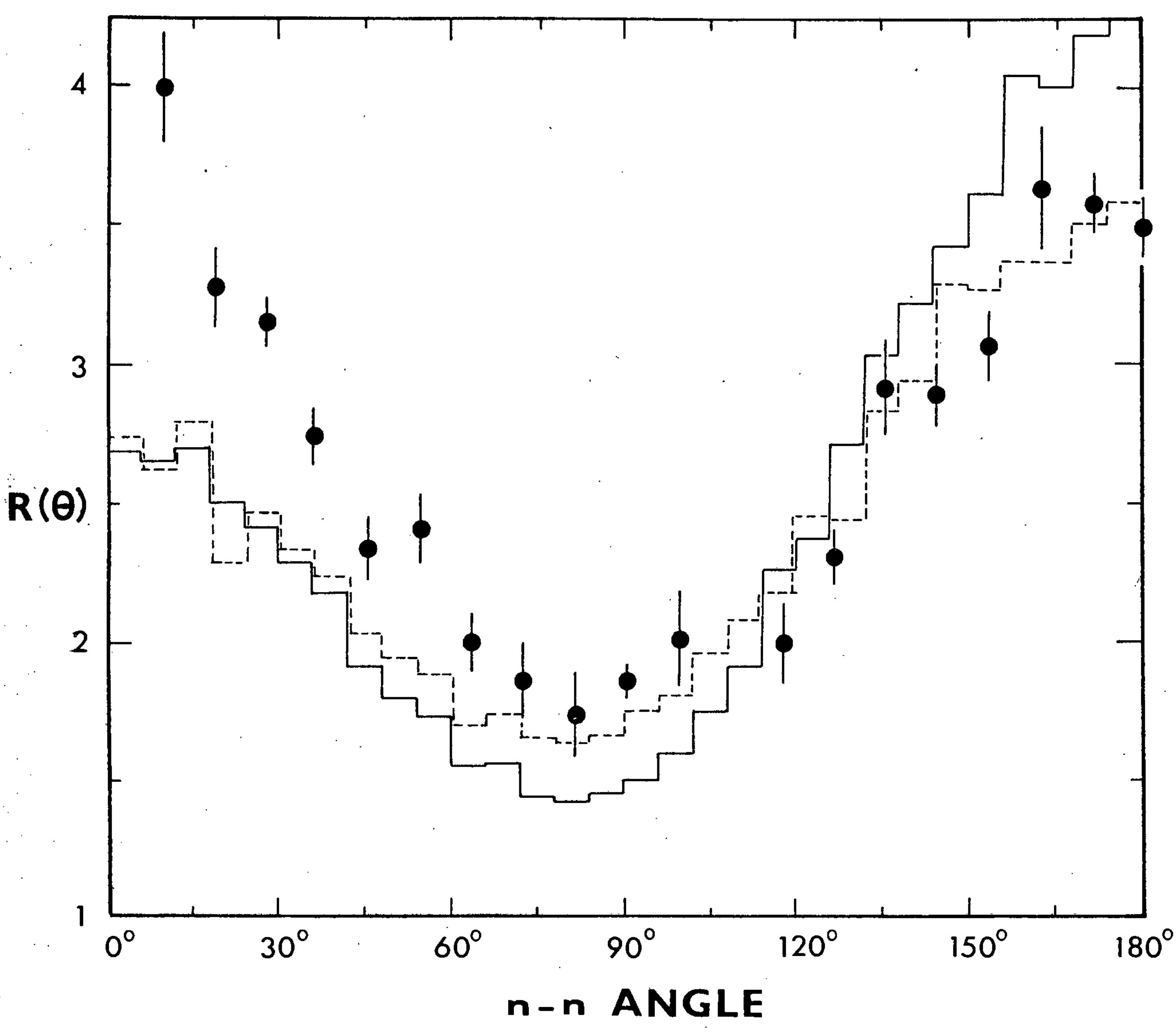

Figure 5.6 The n-n angular correlation for neutrons ($E_n \geq 1.0$ MeV) from fission of ^{235}U, compared with the Monte Carlo predictions for models which assumed (i) isotropic evaporation of all neutrons from the fragments (solid histogram) and (ii) inclusion of a 15% isotropic scission component (broken histogram). Histograms are normalized to the measurements in the angular range 90^0-180^0. Error bars indicate the statistical uncertainties in the measurements (one standard deviation).

would be introduced by differences in the source strengths, which are unlikely to have been identical. For these reasons, and in view of the excessive background coincidence rate (3 to 5 times the true rate), it is considered that the present measurements, showing small-angle peaking, are superior and correctly reflect the n-n angular correlation.

The results of an analysis of the two parameter ($L_1 \cdot L_2$) spectra to investigate the energy dependence of the angular correlation are given in Figure 5.7. Measurements are shown for neutron energy thresholds of 1.0, 1.8 and 2.5 MeV. The general trend is for the angular correlation to become more strongly peaked at small and large angles relative to the value at 90^o. The energy dependent trends of the angular correlation were described in terms of the ratios $R(10^o \text{ to } 20^o)/R(80^o \text{ to } 100^o)$ and $R(170^o \text{ to } 180^o)/R(80^o \text{ to } 100^o)$, which are plotted in Figure 5.8 together with the predictions of the evaporation model. As observed for ^{252}Cf, the measured angular correlation for neutrons with energies $\gtrsim 2$ MeV appears to be more isotropic than is predicted.

Inclusion of an isotropic scission component (see Figure 5.9) identical to that used by Skarsvåg and Bergheim (Sk63) (15%; mean energy 1.8 MeV) has an effect on the angular correlation similar to that found for ^{252}Cf (sf). A backward peaking of the angular correlation is again predicted by the model, and it appears that the inclusion of an isotropic scission component cannot explain the observed discrepancies.

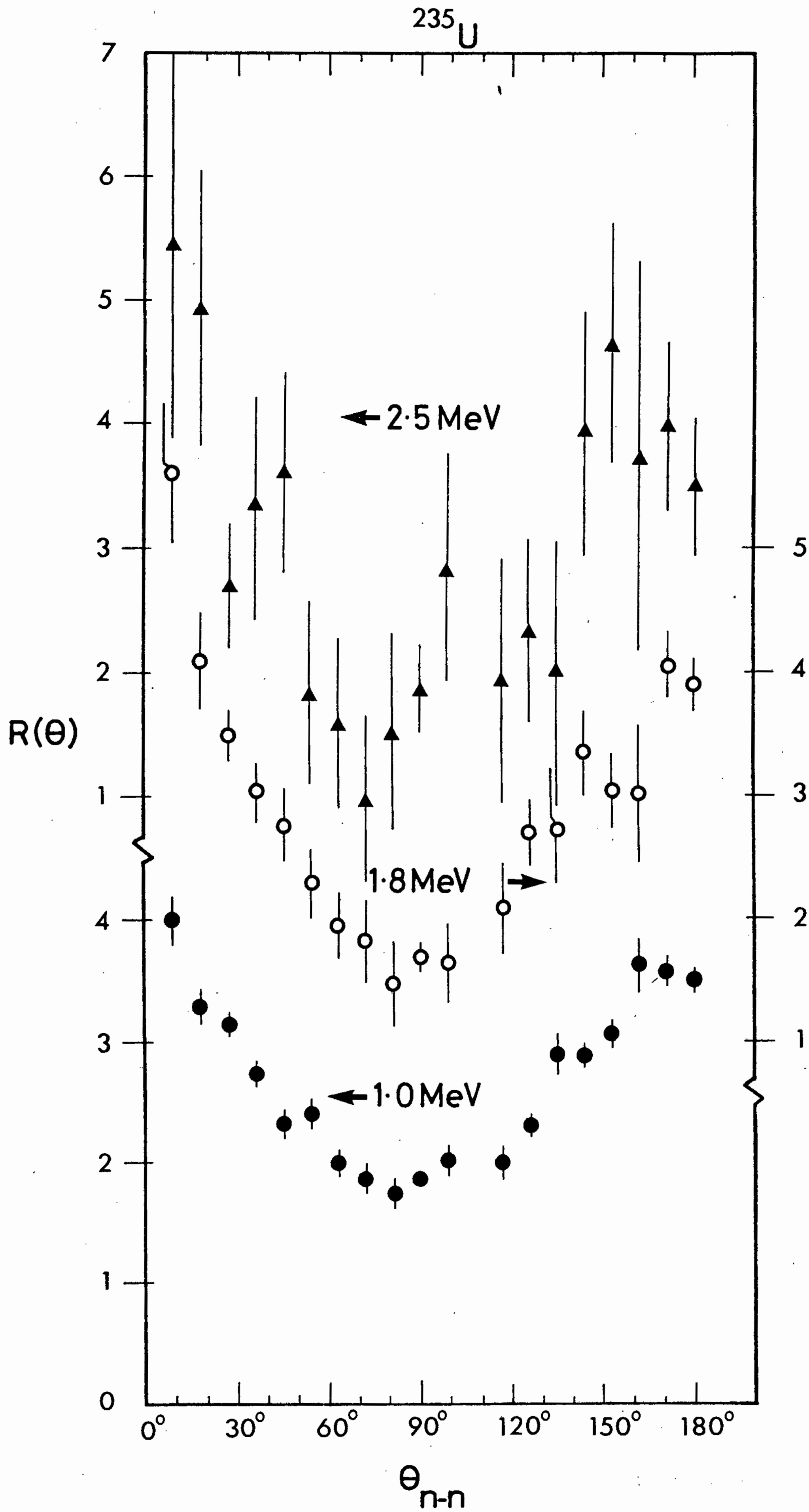

Figure 5.7 The n-n angular correlation R(θ) at different neutron energy thresholds for neutrons from $^{235}U(n_{th},f)$. Arrows indicate the appropriate scales for data at each threshold.

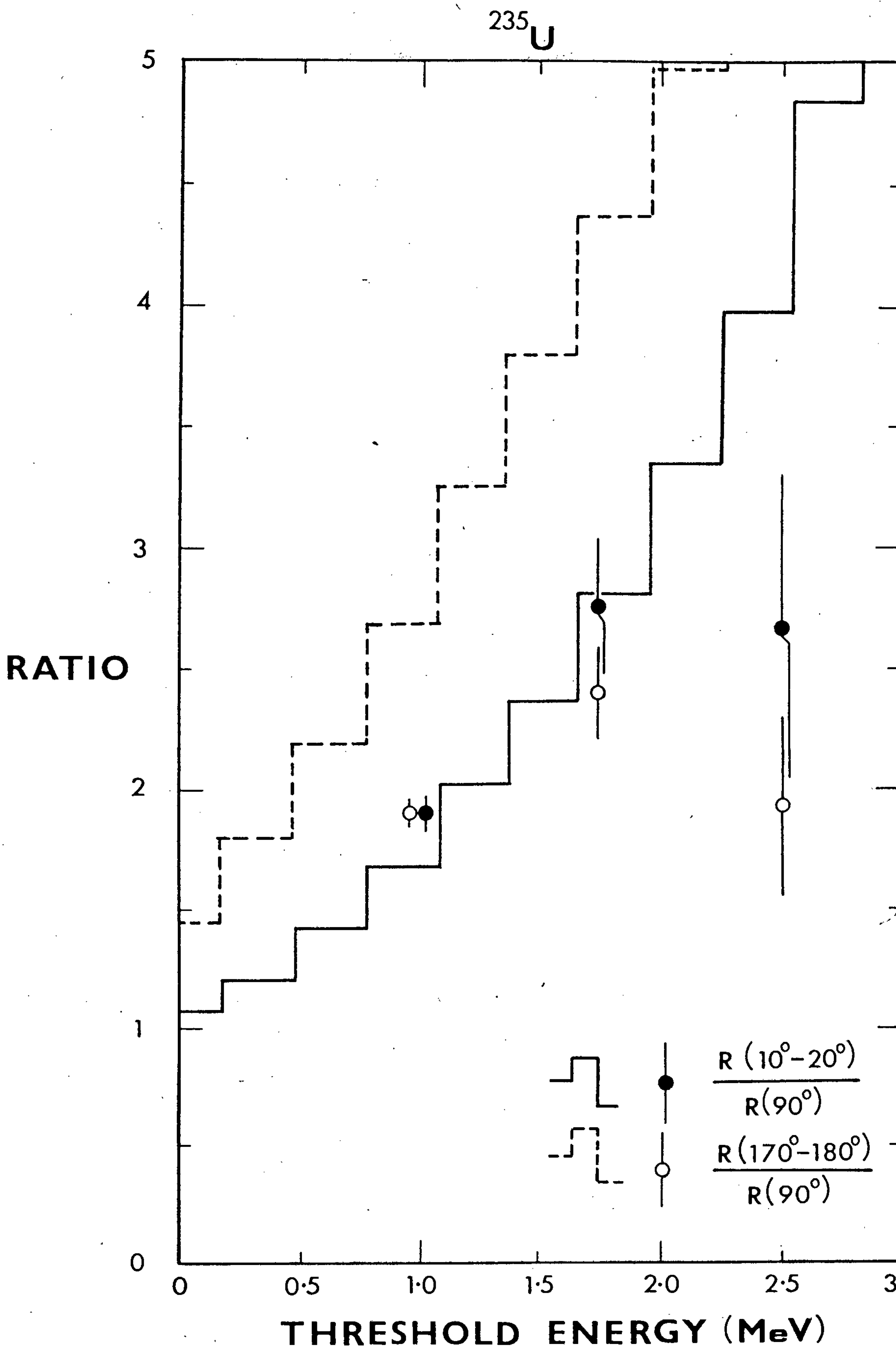

Figure 5.8 The threshold energy dependence of the n-n angular correlation for $^{235}U(n_{th},f)$, showing measurements (points) and Monte Carlo predictions (histograms) for a model which assumed isotropic evaporation of all neutrons from the fully accelerated fragments.

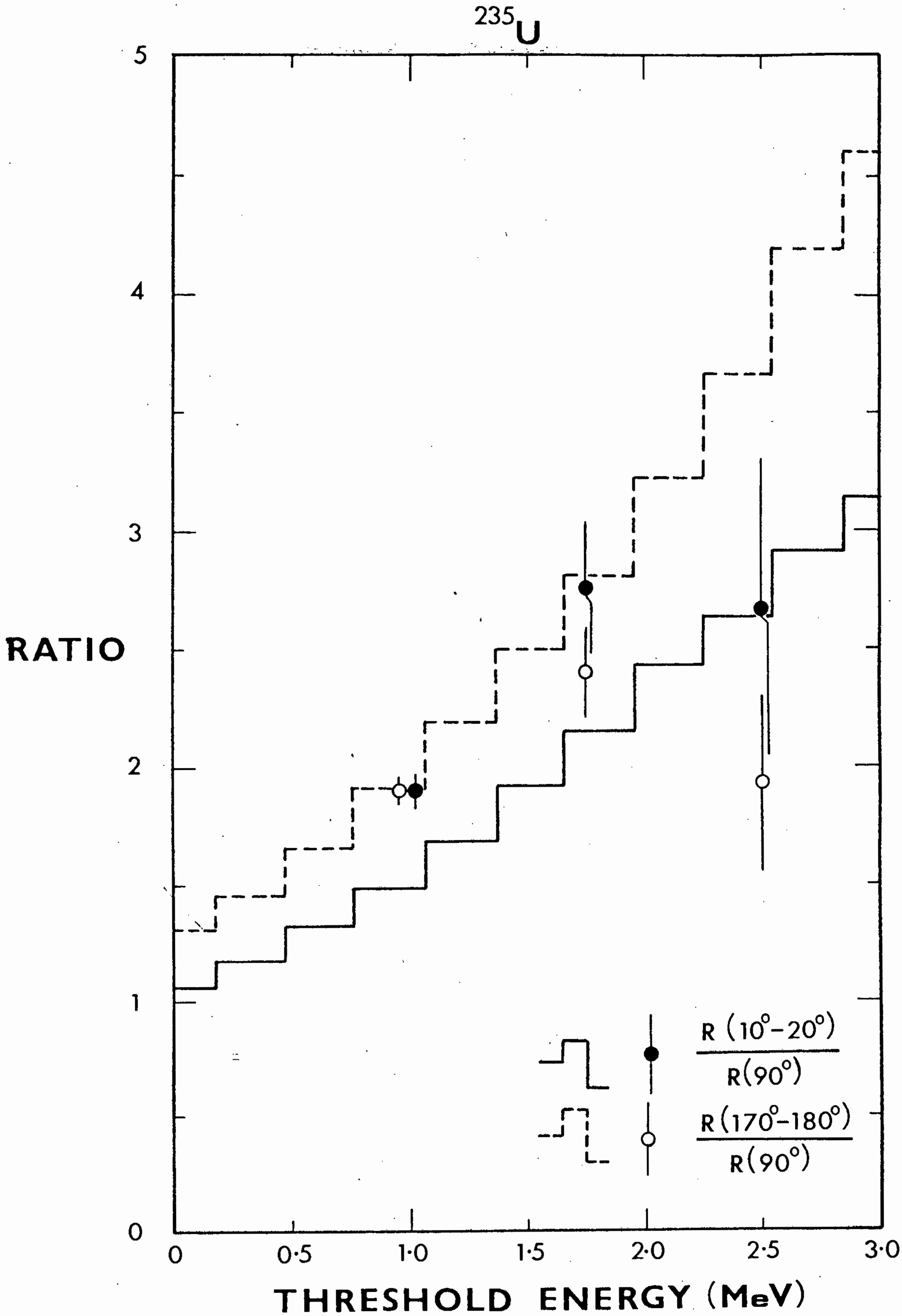

Figure 5.9 The threshold energy dependence of the n-n angular correlation for $^{235}U(n_{th},f)$, showing measurements (points) and Monte Carlo predictions (histograms) for a model which assumed a 15% isotropic scission component, and isotropic evaporation of the remaining 85% of the neutrons from the moving fragments.

5.3 COMPARISON OF EVAPORATION MODEL PREDICTIONS AND OTHER DATA. NEUTRON ANGULAR DISTRIBUTION.

The Monte Carlo predictions of the neutron angular distribution relative to the light fragment direction were compared with the measurements of Bowman *et al* (Bo62a) and Skarsvåg and Bergheim (Sk63). Comparisons were made for evaporation models which included scission neutron components identical to those used in the analyses (Bo62a,Sk63) of the original data. The angular distribution measurements were simulated using neutron detection thresholds of 0.55 MeV for ^{252}Cf and 0.40 MeV for ^{235}U, as used in the original experiments. The simulated distributions were normalized to the data in the angle range $\theta = 40^{\circ}$-140° and are shown in Figure 5.10 together with the data and curves showing the fits of analytical models (Bo62a,Sk63). Whereas the curves fit the data well, the predictions of the present Monte Carlo evaporation model are too low at small ($\theta \lesssim 30^{\circ}$) and large angles ($\theta \gtrsim 150^{\circ}$). For ^{252}Cf (sf), the discrepancy between the two calculated distributions was investigated by modifying the Monte Carlo programme so as to use the fixed (i.e. mass-independent) values used in the analytical calculation (Bo62a) for the fragment velocities, temperatures, and neutron yields. The modified Monte Carlo prediction (Figure 5.10(a), broken histogram) is in close agreement with the analytical calculation, indicating that the discrepancy between the two predictions may be attributed to the different assumptions made in the models. The strongest effect on the predicted angular distribution was found to result when the Monte Carlo sampling method used to choose neutron emission energies, which takes account of the mass dependence of the nuclear temperature,

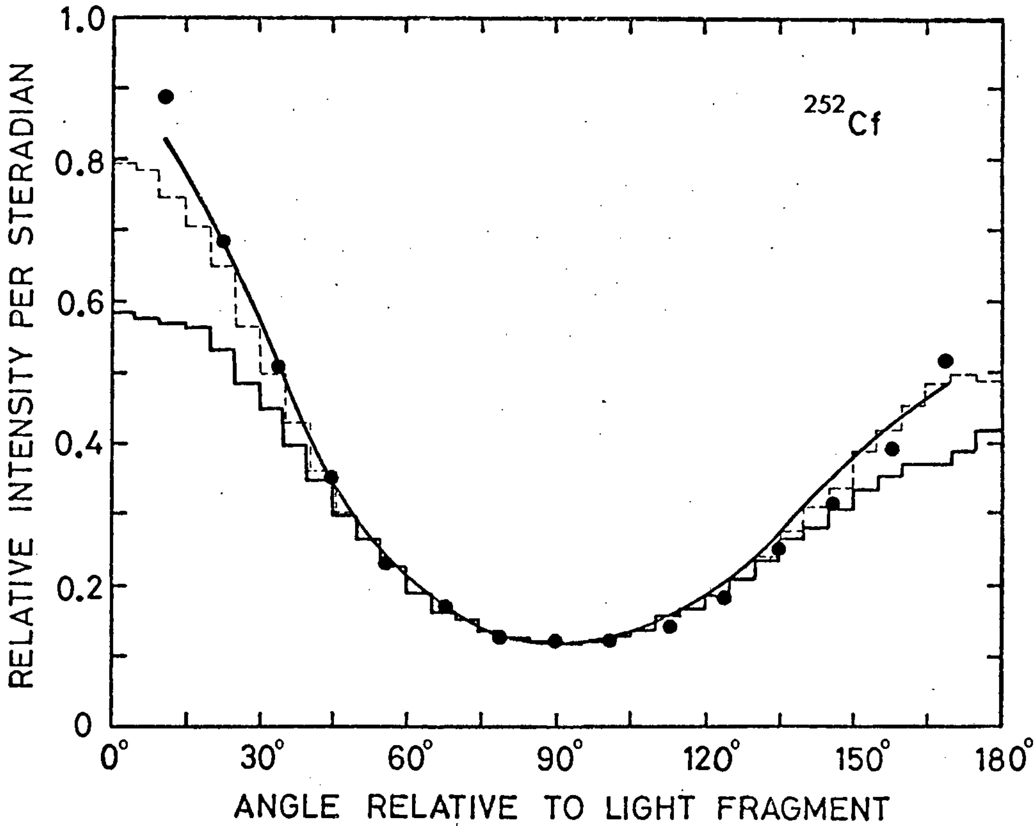

Figure 5.10(a) Simulated angular distribution of neutrons from ^{252}Cf (sf) (solid histogram). The points show experimental data (Bo62a) and the curve is the prediction of an analytical calculation (Bo62a). The broken histogram is the prediction of a modified Monte Carlo calculation (see text).

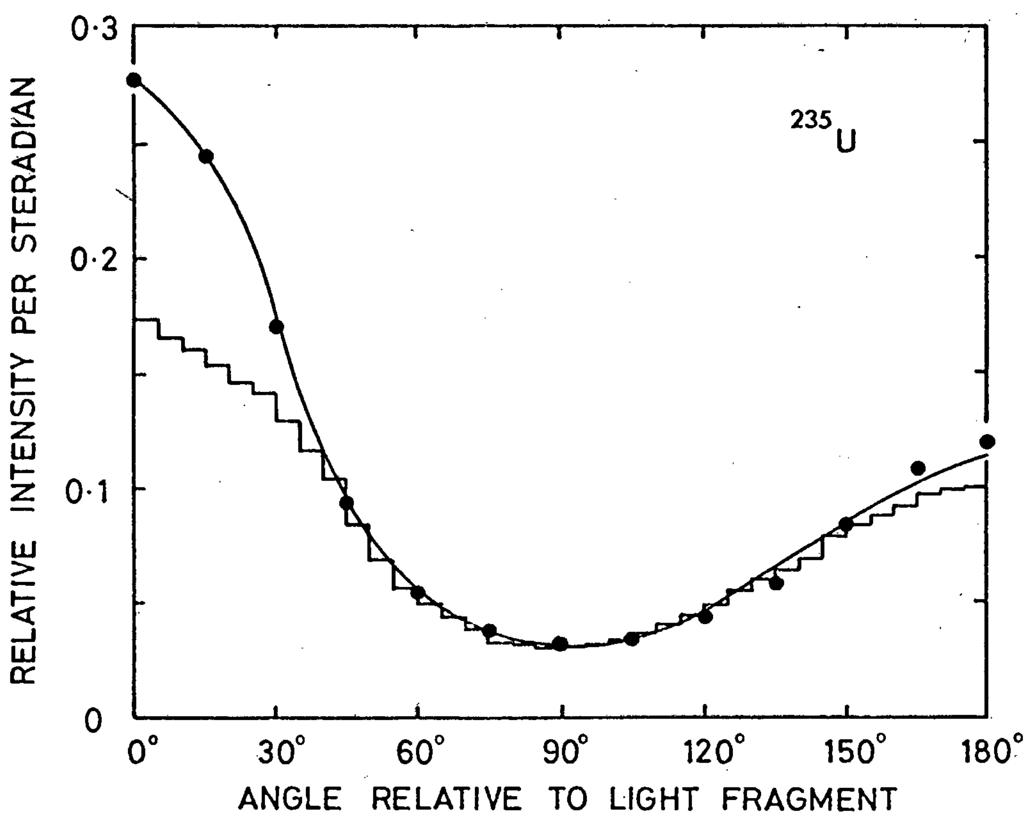

Figure 5.10(b) Simulated angular distribution of neutrons from fission of ^{235}U (histogram). The points show experimental data (Sk63) and the curve is the prediction of an analytical calculation (Sk63). Standard deviations of the data in this and the above Figure are smaller than the point size.

was replaced by sampling from a mass-independent, three-component evaporation spectrum as used in (Bo62a). The present Monte Carlo calculation is more realistic than the analytical method insofar as it includes the effects of the observed strong mass dependence of the neutron emission characteristics. Thus it is considered that the solid histogram shown in Figure 5.10(a) is a better representation of the angular distribution of the evaporation model (+ 10% scission), despite the poorer agreement with experiment.

The angular distributions shown in Figure 5.10 are averages for all neutrons with energies greater than the detector thresholds. A more stringent test of the evaporation model is provided by comparing the predicted and measured angular distributions at different neutron energies. As in the case of the n-n angular correlation, the energy dependent trends in the angular distribution may be represented by the changes in the ratios of neutron yields at small and large angles (measured relative to the light fragment direction) to the yield at right angles to the fission axis. The predictions of evaporation models for ^{252}Cf (sf) and $^{235}U(n_{th},f)$, in which all neutrons were assumed to be evaporated isotropically in the moving fragment frames, are compared with experimental data in Figures 5.11 and 5.12. For both fission reactions there are marked discrepancies. The measurements suggest an enhanced axial emission of neutrons with energies $\lesssim 2$ MeV, while at higher energies ($\gtrsim 3$ MeV) neutron emission appears to be more isotropic than is predicted by the evaporation model. The effects of including isotropic scission neutron components are shown in Figure 5.13.

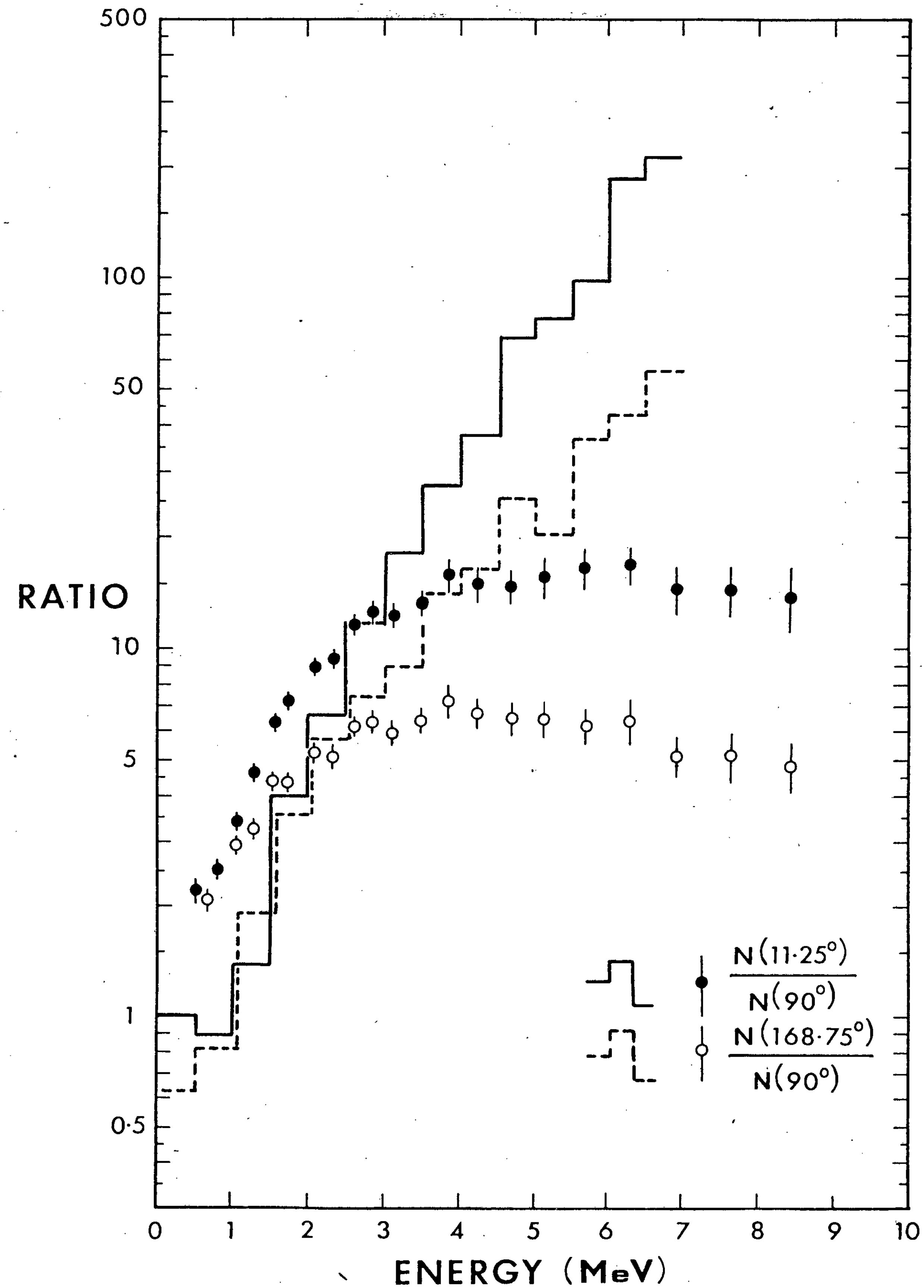

Figure 5.11 The energy dependence of the neutron angular distribution for ^{252}Cf (sf), showing measurements (points) and Monte Carlo predictions (histograms) for a model which assumed isotropic neutron evaporation in the fully accelerated fragment frames. The points were calculated from data in Bo62a (Tables IV and V). For clarity, not all low energy points have been plotted.

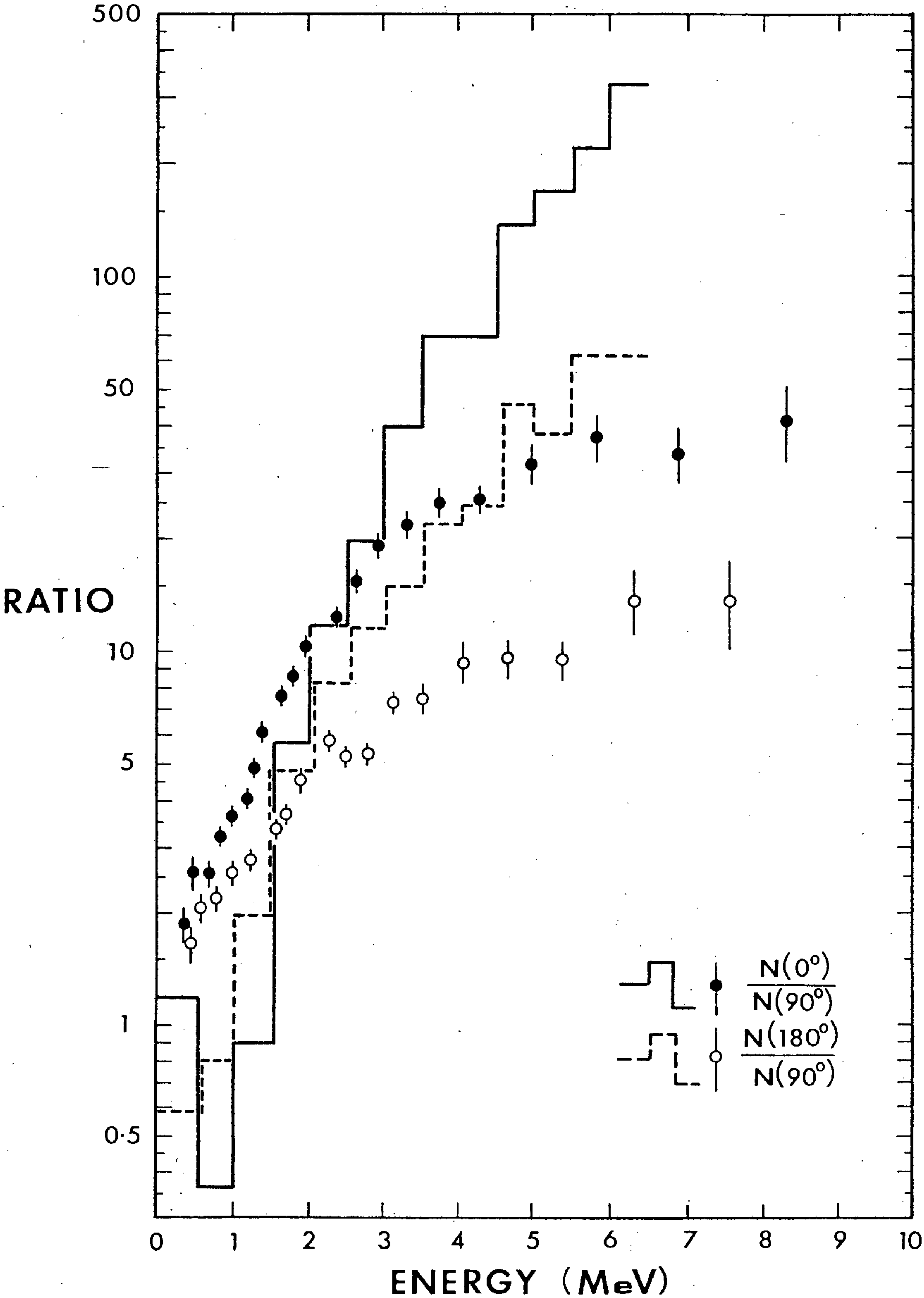

Figure 5.12 The energy dependence of the neutron angular distribution for fission of ^{235}U, showing measurements (points) and Monte Carlo predictions (histograms) for a model which assumed isotropic neutron evaporation in the fully accelerated fragment frames. The points were calculated from data in Sk63 (Tables 3 and 4).For clarity, not all low energy points have been plotted.

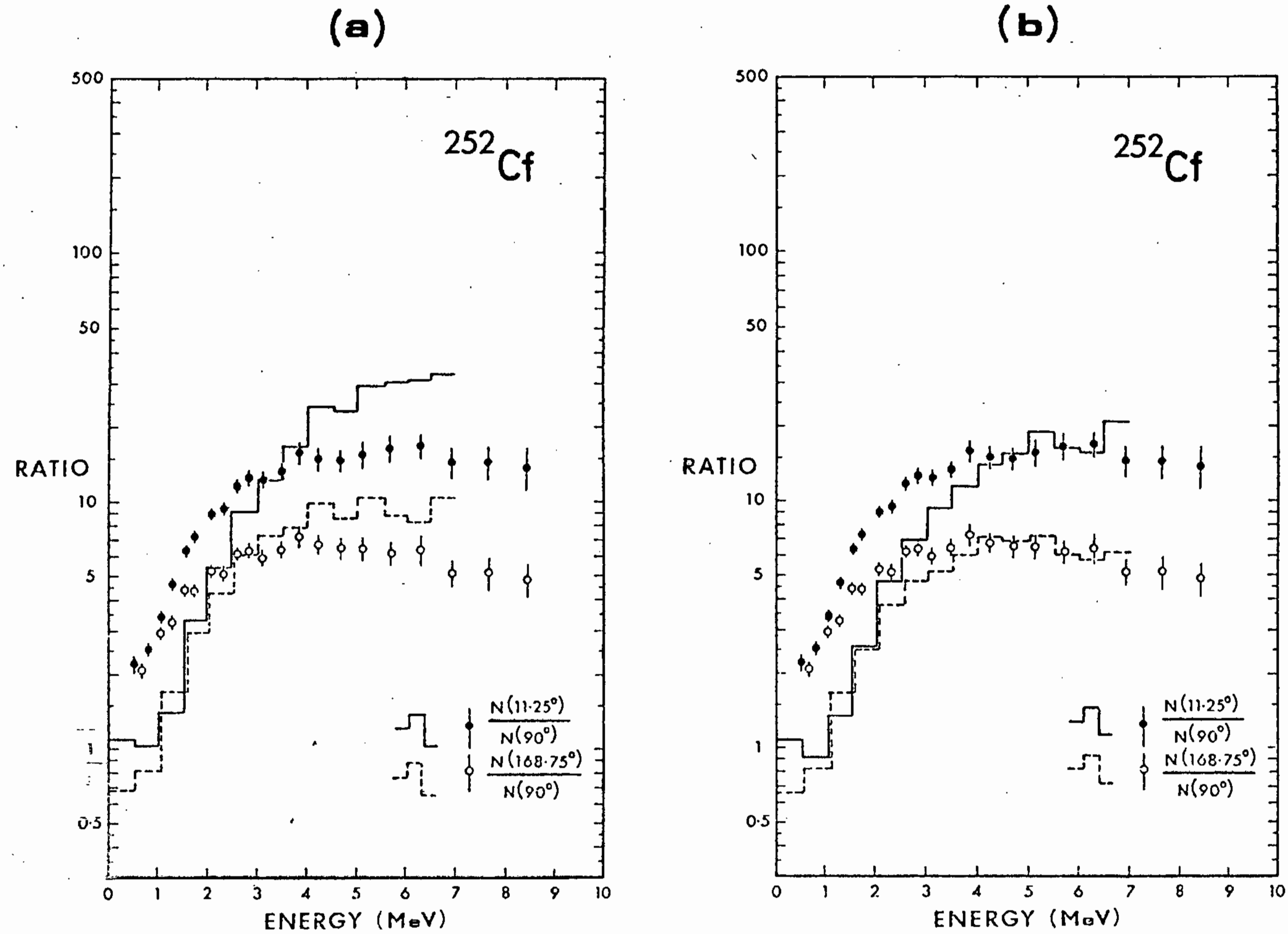

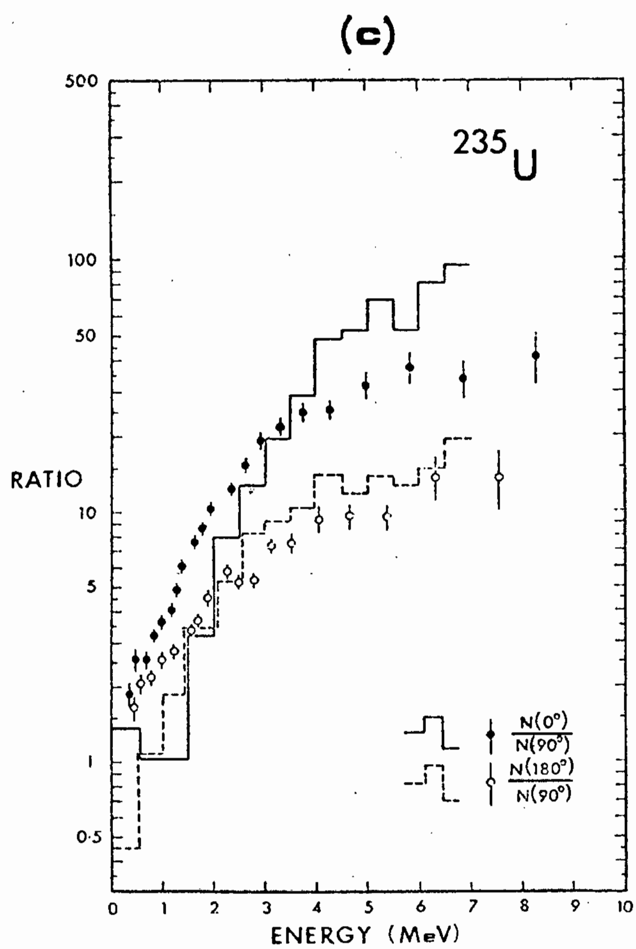

Figure 5.13 The energy dependence of the neutron angular distributions for fission of ^{252}Cf and ^{235}U, showing measurements (points) and Monte Carlo predictions (histograms) for evaporation models which include isotropic scission components as in Bo62a and Sk63: (a+b) 10% and 20% scission respectively, with an evaporation spectrum, $\overline{E}$ = 2.6 MeV; (c) 15% scission with an evaporation spectrum, $\overline{E}$ = 1.8 MeV.

Results indicate an improved fit between model predictions and experiment for neutron energies $\gtrsim$3 MeV - at the expense of an increased discrepancy at lower energies. Since most neutrons are in the low energy region of the fission spectrum ($E_{mean} \simeq 2.1$ MeV), the overall result is a worsening of the fit between experiment and prediction by the inclusion of scission components of this nature.

FISSION SPECTRUM

The calculated neutron spectra were compared with the measurements of Green *et al* (Gr73) and Werle and Bluhm (We72), whose measurements are shown in Figures 5.14 and 5.15. (These measurements were selected since they enable a detailed comparison to be made with model predictions over a large energy range.) In Figures 5.14 and 5.15 the ratios of the measured fission spectra for ^{235}U and ^{252}Cf to "best fit" Maxwellians are plotted to demonstrate the deviations from a pure Maxwellian spectrum. The fission spectra predicted by the evaporation model (also plotted as a ratio to the relevant Maxwellian) are compared with these measurements in Figure 5.16. Discrepancies indicate that some mechanism needs to be included in the evaporation model in order to increase the neutron yield for energies $\lesssim$1.5 MeV and $\gtrsim$5.5 MeV and to decrease the yield for $1.5 \lesssim E \lesssim 5.5$ MeV.

Inclusion of isotropic scission neutron components leads to predicted fission spectra shown in Figure 5.17. The effects on the calculated spectra are seen to be small. The major discrepancies observed for the pure evaporation model are still present, and clearly some mechanism other than a scission component of this nature must be included in the model.

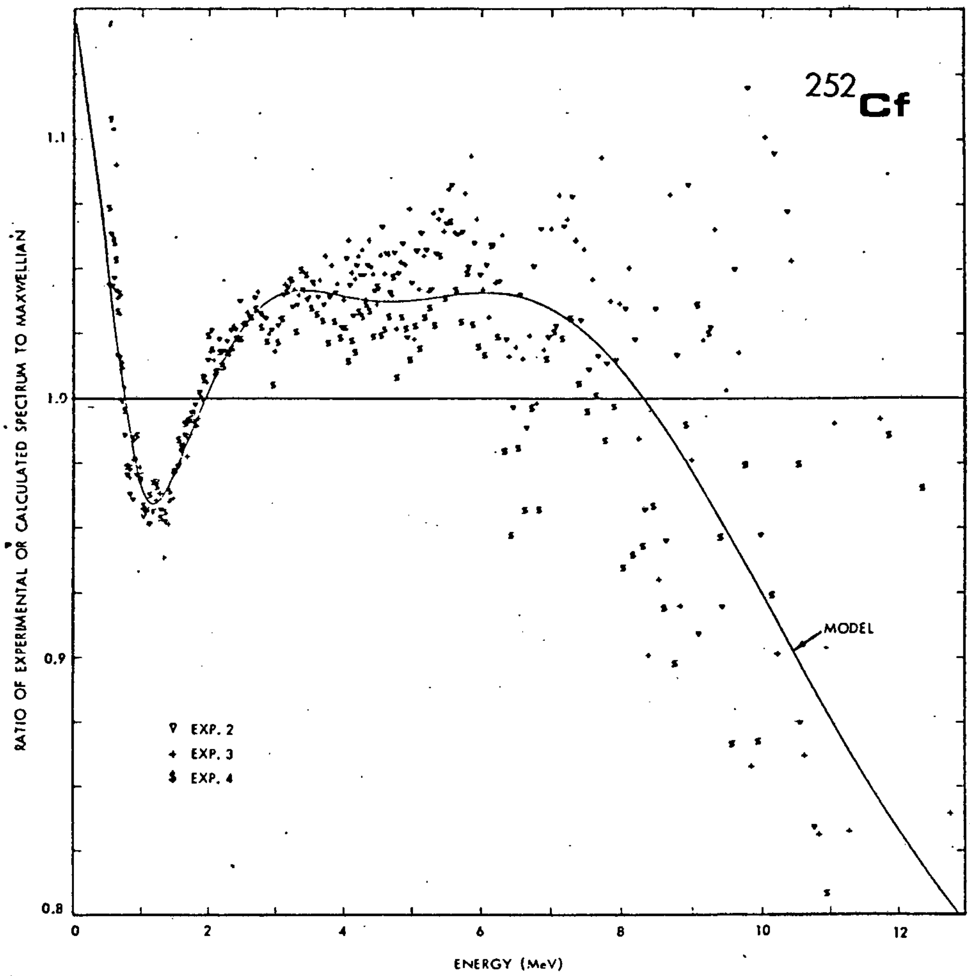

Figure 5.14 Measurements (Gr73) of the neutron energy spectrum for ^{252}Cf (sf). The points and curve are ratios of the measured and calculated spectra to a Maxwellian ($\overline{T}$ = 1.406 MeV). The curve, which represents a model fit (by Gr73), is used to represent the measured spectrum in all subsequent comparisons with the Monte Carlo predictions. (Figure from Gr73).

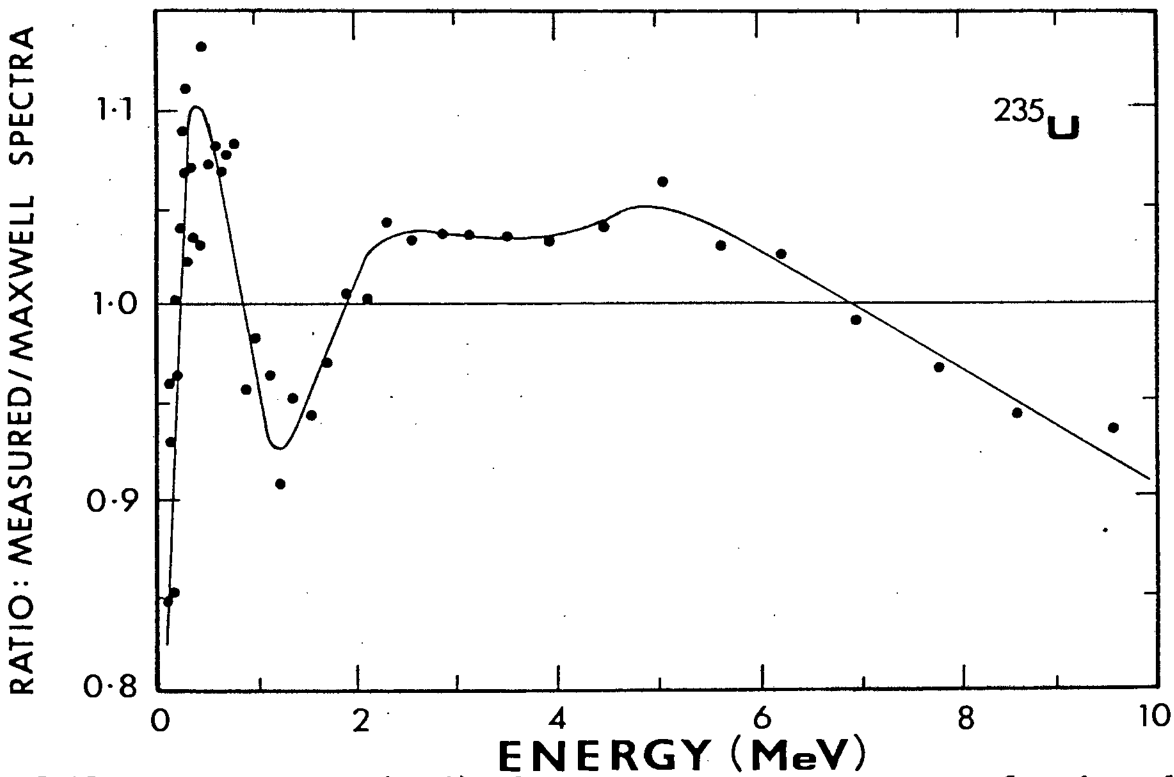

Figure 5.15 A measurement (We72) of the neutron energy spectrum for thermal fission of ^{235}U. The points, which were calculated from data in We72 (Figure 7), are the ratios of measurements to a fitted Maxwellian ($\overline{T}$ = 1.32 MeV). The curve, which is simply a guide to the eye, is used in subsequent comparisons with the Monte Carlo predictions.

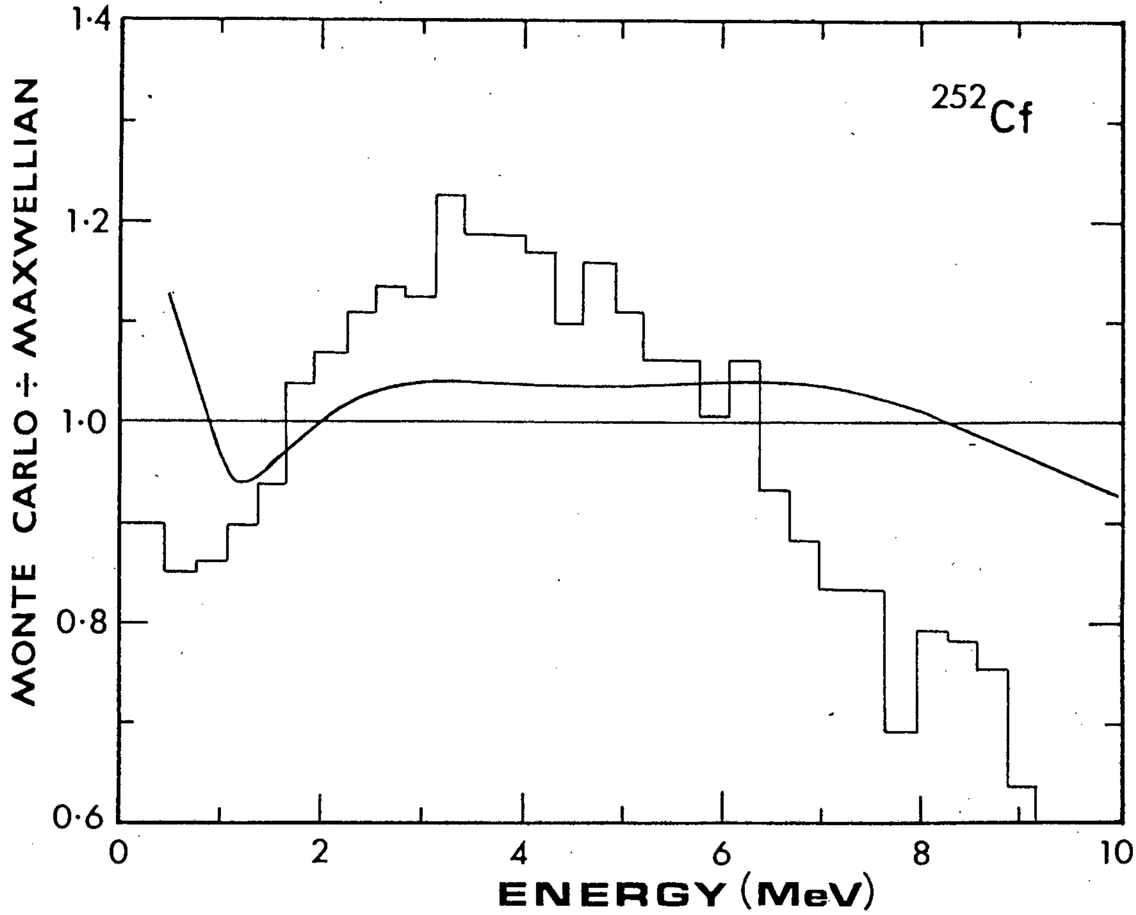

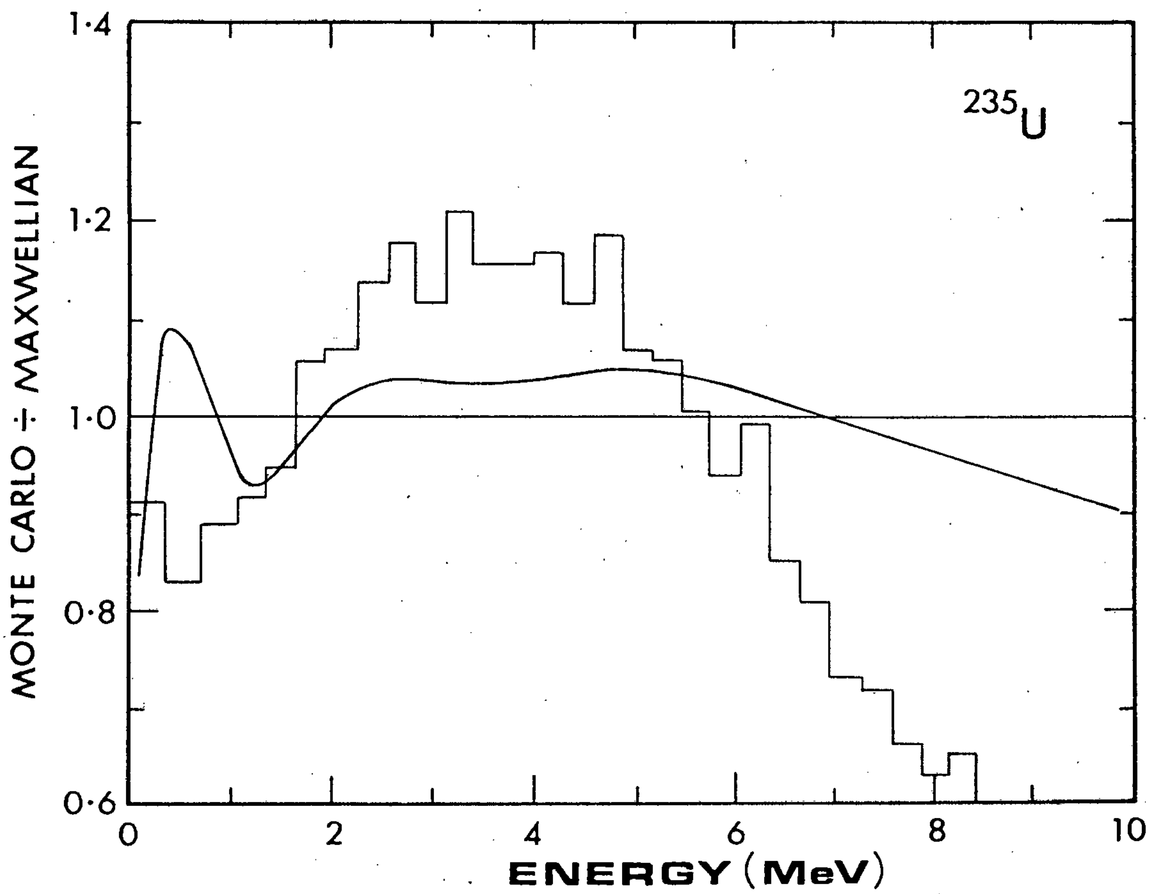

Figure 5.16 Calculated fission spectra (histograms) for a model which assumed isotropic neutron evaporation in the fully accelerated fragment frames. The curves represent measurements (We72,Gr73) of the fission spectra.

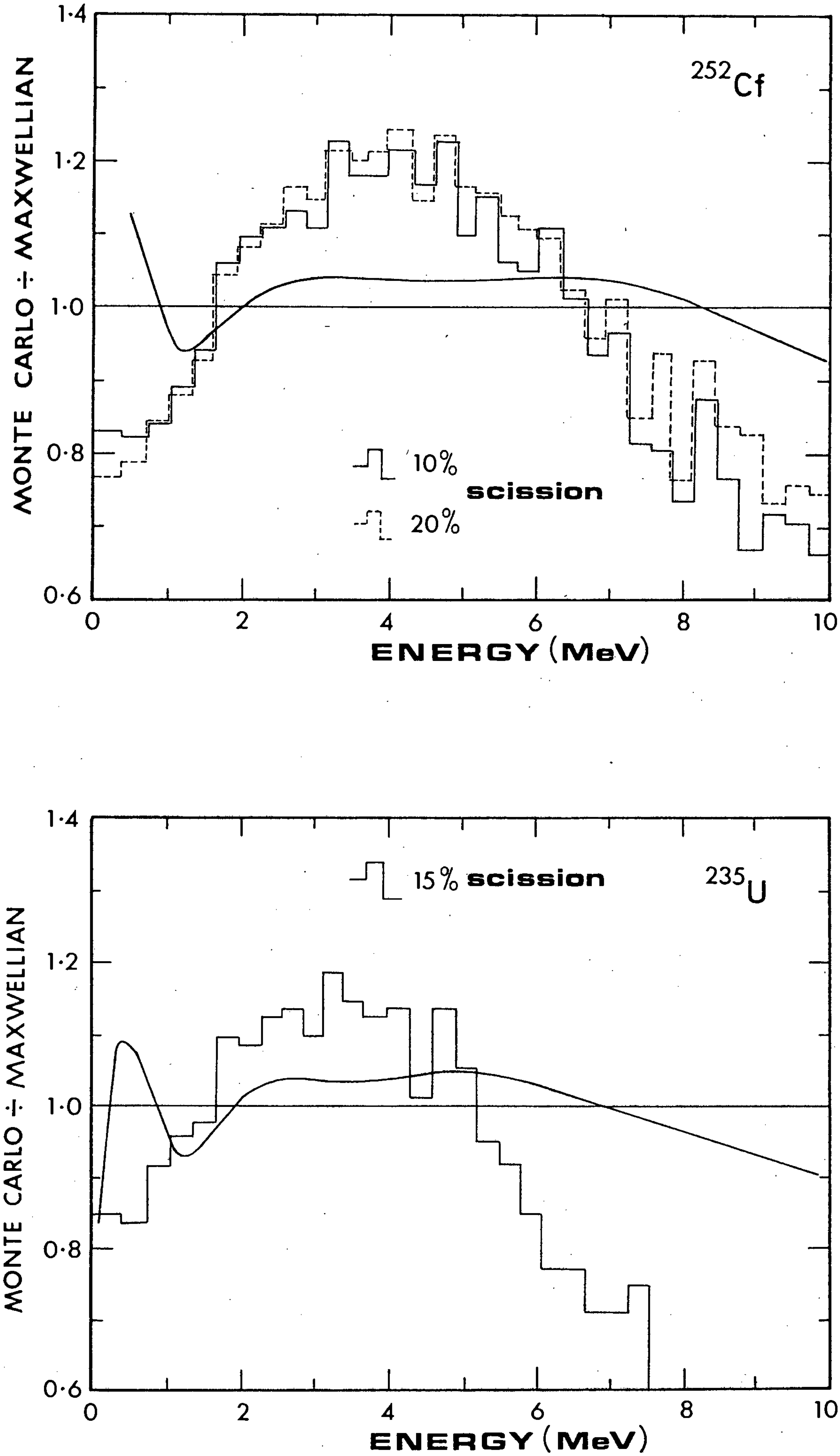

Figure 5.17 Calculated fission spectra (histograms) for a model which assumed isotropic evaporation from the moving fragments, plus an isotropic scission component. The curves represent measurements (We72,Gr73) of the fission spectra.

CHAPTER SIX

DISCUSSION

6.1 MODIFICATIONS TO THE EVAPORATION MODEL

Results presented in Chapter Five demonstrated the inadequacy of an isotropic evaporation model for fission neutron emission. Briefly, the discrepancies were:

(i) The measured n-n angular correlation is more strongly peaked at small angles than is predicted by the evaporation model. The energy dependence of this distribution shows a marked deviation over $\sim$2 MeV, where the measurements suggest a more isotropic correlation than is predicted.

(ii) Measurements of the neutron angular distribution suggest enhanced axial emission at energies $\lesssim$2 MeV. For energies $\gtrsim$3 MeV the observed angular distribution is more isotropic than is expected to result from the evaporation model.

(iii) The measured fission spectrum shows enhanced emission of neutrons with energies $\lesssim$1.5 MeV and $\gtrsim$5.5 MeV, and a deficient yield for $1.5 \lesssim E \lesssim 5.5$ MeV.

It is concluded that some modification of the neutron emission processes is required in order to explain the experimental data. Possible modifications to the evaporation model to account for these discrepancies are discussed below.

FRAGMENT ANGULAR MOMENTUM

It was noted in Section 2.4 that the high angular momenta of the fission fragments is expected to result in anisotropic neutron emission in the centre of mass frames. The effects of fragment angular momentum were incorporated in the simulation model by assuming that neutron emission in the fragment frame was of the form $1+b\ \mathrm{Sin}^2\Psi$ (see Figure 2.5), where b is the anisotropy parameter. The value of b was calculated for each fragment on the assumption that the moment of inertia of the fragment was reduced to 50% of the rigid body value. The predictions of this model (without a scission component) are shown in Figures 6.1 and 6.2. Comparison with the results of the evaporation model (Figure 6.3) shows that the effects of fragment angular momentum are small (assuming that a $1+b\ \mathrm{Sin}^2\Psi$ anisotropy accurately represents these effects), but lead to an increased discrepancy in the predicted n-n angular correlation. An increase in the anisotropy parameter b, which would result, for example, from a reduction of the fragment moment of inertia to less than 50% of the rigid body value, has the effect of increasing this discrepancy. It appears, therefore, that fragment angular momentum does not have a strong effect on the neutron emission distributions.

POLAR EMISSION

The possibility of enhanced polar emission of neutrons is suggested by recent measurements of the angular distribution of light charged particles (LCP) emitted in ternary fission. Feather (Fe69) has pointed out the analogy between the emission of LCP in ternary fission and scission neutron emission, which

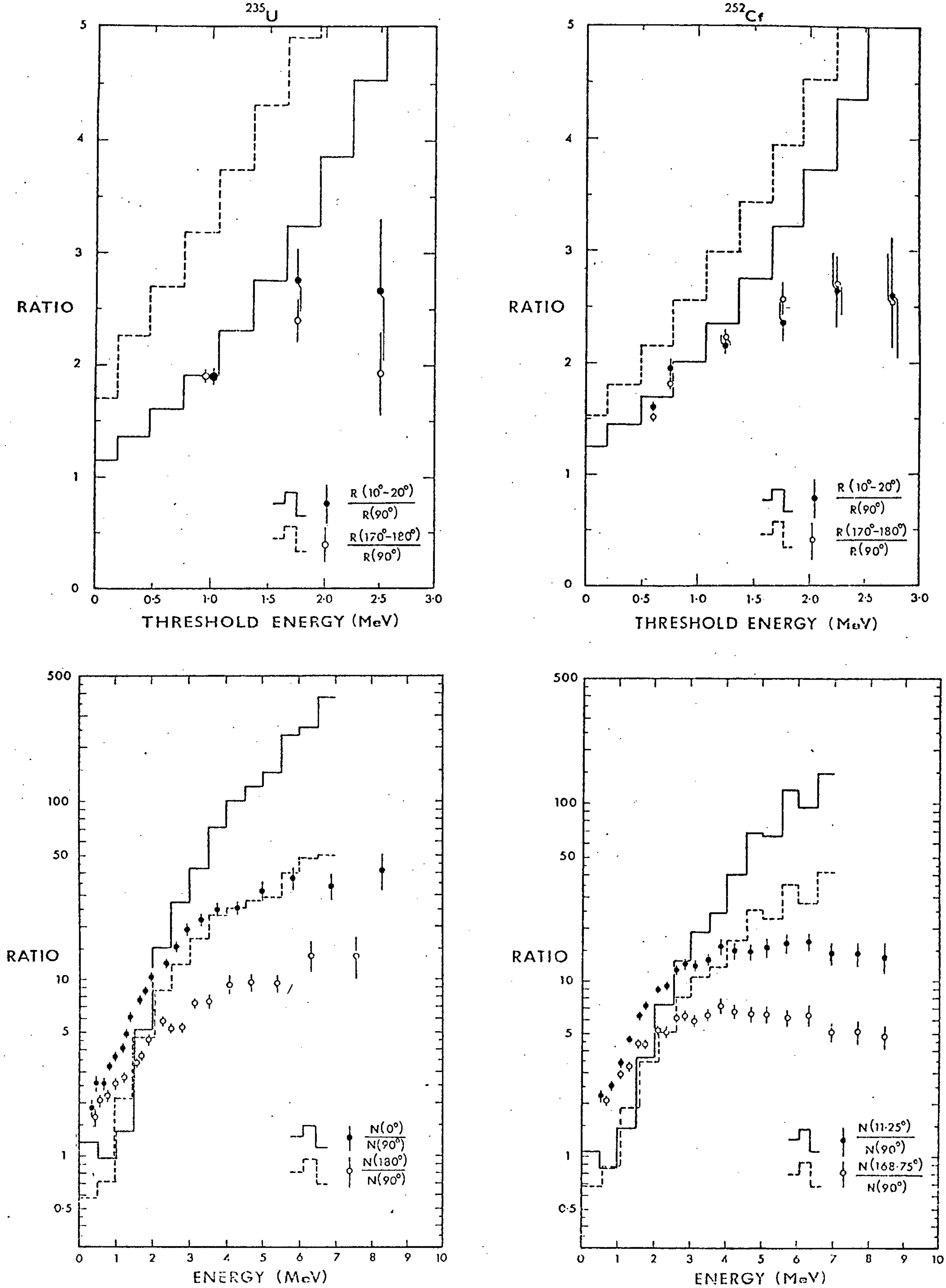

Figure 6.1 The threshold energy dependence of the n-n angular correlation (upper figures), showing measurements (points) and Monte Carlo predictions (histograms) for a model in which it was assumed that neutron angular emission was of the form $1+b\ \mathrm{Sin}^2\Psi$ in the fragment frame. No scission component was included in the model. In the lower figures, measurements (Bo62a,Sk63) of the neutron angular distribution for fission of ^{235}U (left) and ^{252}Cf (right) are compared with the predictions of this model.

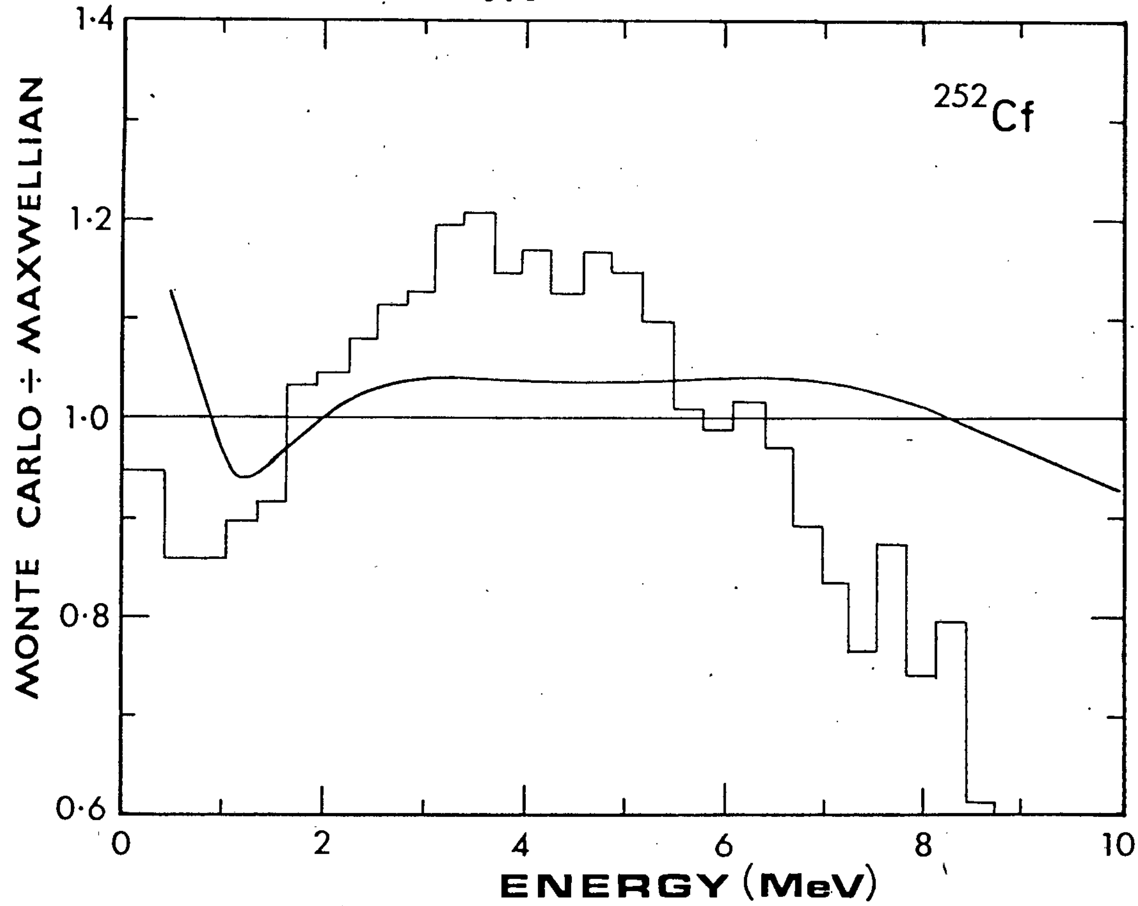

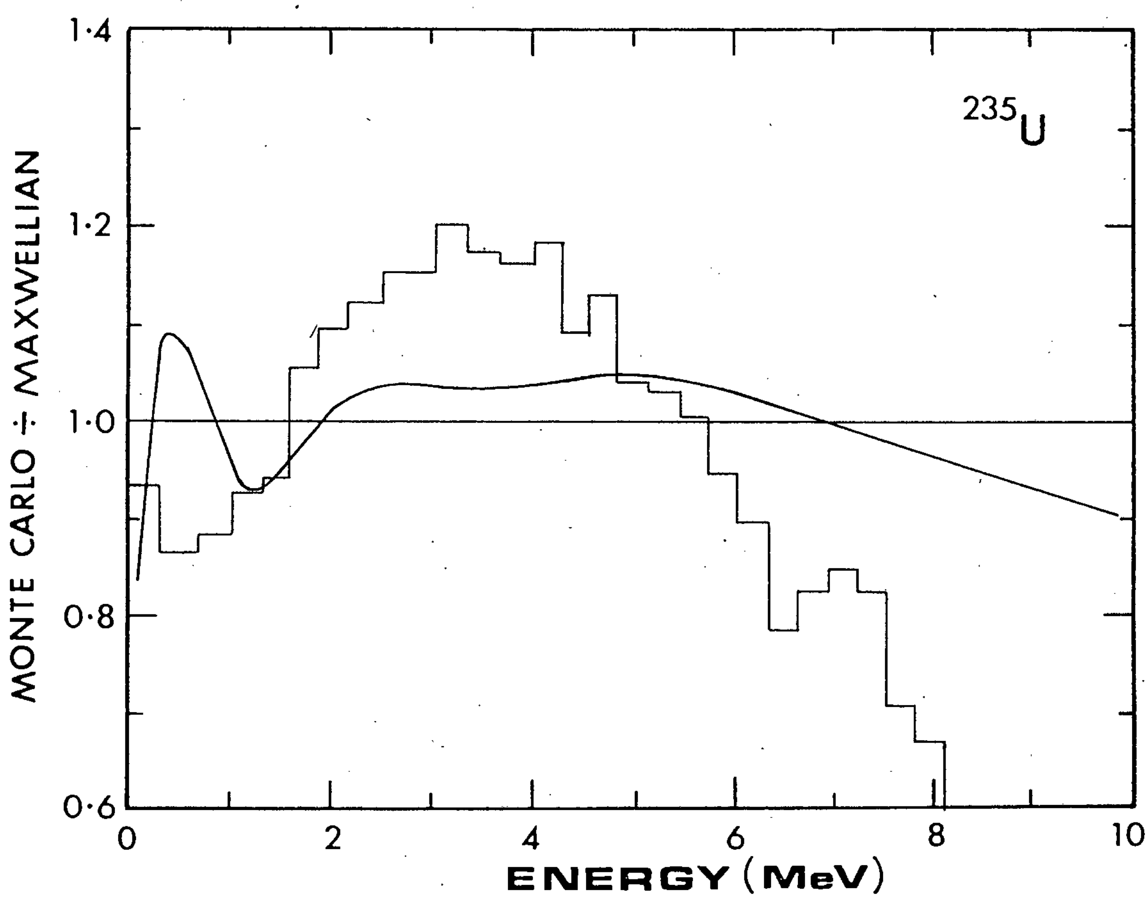

Figure 6.2 Calculated energy spectra (histograms) for a model which assumed a $1+b\ \mathrm{Sin}^2\Psi$ neutron angular distribution in the fragment frame, and no scission component. The curves represent measurements of the spectra for fission of ^{235}U (We72) and ^{252}Cf (Gr73).

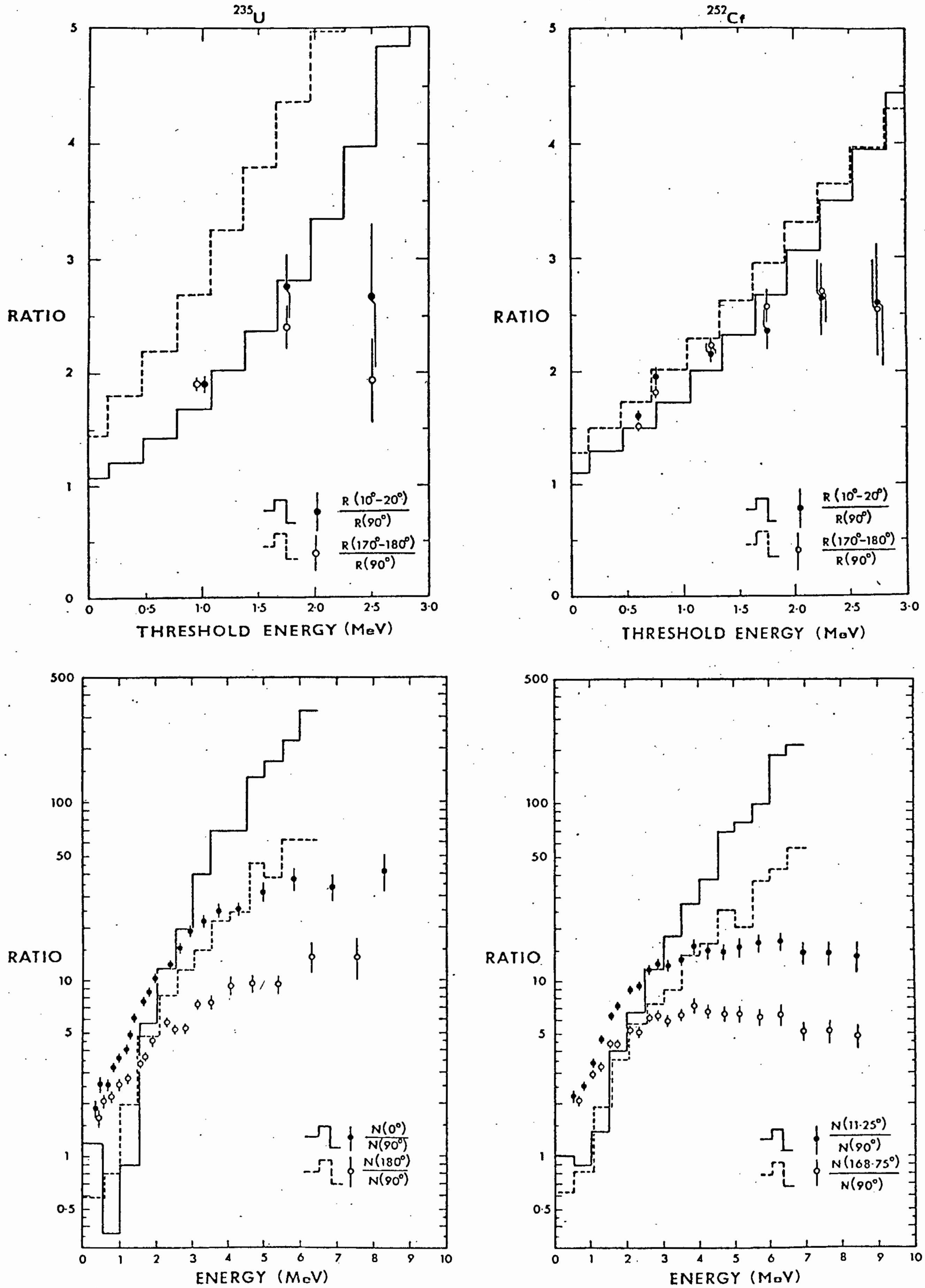

Figure 6.3 The threshold energy dependence of the n-n angular correlation (upper figures), showing measurements (points) and Monte Carlo predictions (histograms) for a model which assumed isotropic neutron evaporation in the fully accelerated fragment frames. No scission component was included in the model. In the lower figures, measurements (Bo62a,Sk63) of the neutron angular distribution for fission of ^{235}U (left) and ^{252}Cf (right) are compared with the predictions of this model.

may be regarded as a mode of ternary fission which is accompanied by the emission of an uncharged light particle. The angular distribution of the bulk of LCP from ternary fission is peaked in the direction perpendicular to the fission axis, and may be understood in terms of Coulomb focussing of the LCP by the recoiling fragments. Recent measurements (eg Pi70c,Pi74a, Pi74b, Pi75,Ad74,Wi76a) have however determined that an unexpectedly large LCP component is emitted along the fission axis, a phenomenon known as polar emission. Polar LCP detected have included p, d, t and α, from thermal neutron induced fission of ^{235}U and spontaneous fission of ^{252}Cf. In the case of proton-accompanied fission a particularly strong polar proton component has been reported (Ad74,Pi74b). If scission neutrons and LCP originate from the same emission mechanism then a polar neutron yield is to be expected.

Various hypotheses have been advanced to explain polar emission. Halpern (Ha71) suggested that the process may be similar to that assumed to result in normal LCP emission in ternary fission i.e. *"the snapping back of the nuclear surface just after scission"* (in this case the outer, polar surface). Asghar *et al* (quoted in Pi74) have suggested that Fresnel-like diffraction of ternary LCP emitted in the region between the fission fragments may give rise to enhanced polar emission. Piasecki *et al* (Pi74a) proposed that polar LCP resulted from in-flight evaporation from the outer poles of fully accelerated fission fragments, supporting this hypothesis with detailed calculations. More recently however, Piasecki *et al* (Pi75) concluded that, while some polar enhancement through LCP evaporation was possible, it appeared that the particles were emitted according to some other mechanism. It is interesting to recall at this point the early suggestion by Hill and Wheeler (Hi53) that enhanced axial neutron emission may result from the rapid contraction of the fragment walls along the fission axis after the instant of scission. De Benedetti *et al* (De48) also speculated that *"energy could be concentrated through ripple propagation"* at the outer poles of the fragments shortly after scission. Interpretation of the present discrepancies as evidence for polar emission of neutrons is somewhat speculative but, whatever the emission mechanism, polar LCP yields are well established and an analogous polar neutron yield is plausible.

The effects of including enhanced polar neutron emission in the computer model were evaluated for (i) evaporation emission from the fragments, plus a 15% polar scission neutron component and (ii) preferential polar emission from the moving fragments, with no scission component.

(i) POLAR SCISSION NEUTRONS

In this model a 15% scission component was assumed to be emitted according to an evaporation spectrum with temperature T = 0.5 MeV. An angular distribution given by $1 + \text{Cos}^2\theta$ (in the laboratory frame) was assumed for this component, where θ is the angle between the fission axis and the emitted neutron. Emission of the remaining 85% of the neutrons was assumed to be from the fragments and of the form $1+b\ \text{Sin}^2\Psi$ ie including the effects of fragment angular momentum. The resulting angular correlation, angular distribution and energy spectrum of fission neutrons emitted according to this model are shown in Figures 6.4 and 6.5 As expected, the discrepancies between the

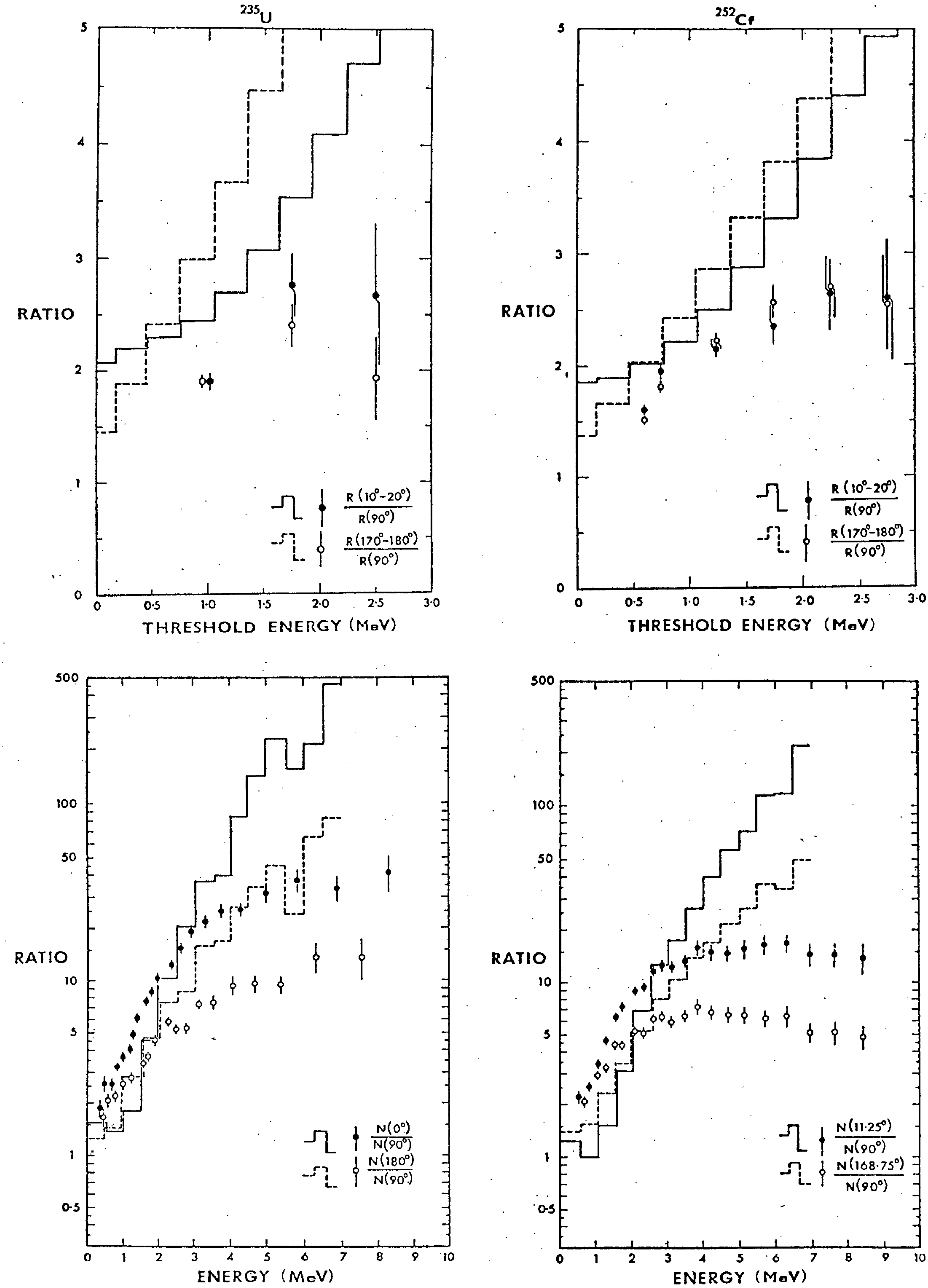

Figure 6.4 The threshold energy dependence of the n-n angular correlation (upper figures), showing measurements (points) and Monte Carlo predictions (histograms) for a model which assumed a 15% polar scission component with angular distribution $1 + \mathrm{Cos}^2\theta$, and emission of the remaining 85% of neutrons from the fragments according to $1{+}b\ \mathrm{Sin}^2\Psi$. In the lower figures, measurements (Bo62a,Sk63) of the neutron angular distribution for fission of ^{235}U (left) and ^{252}Cf (right) are compared with the predictions of this model.

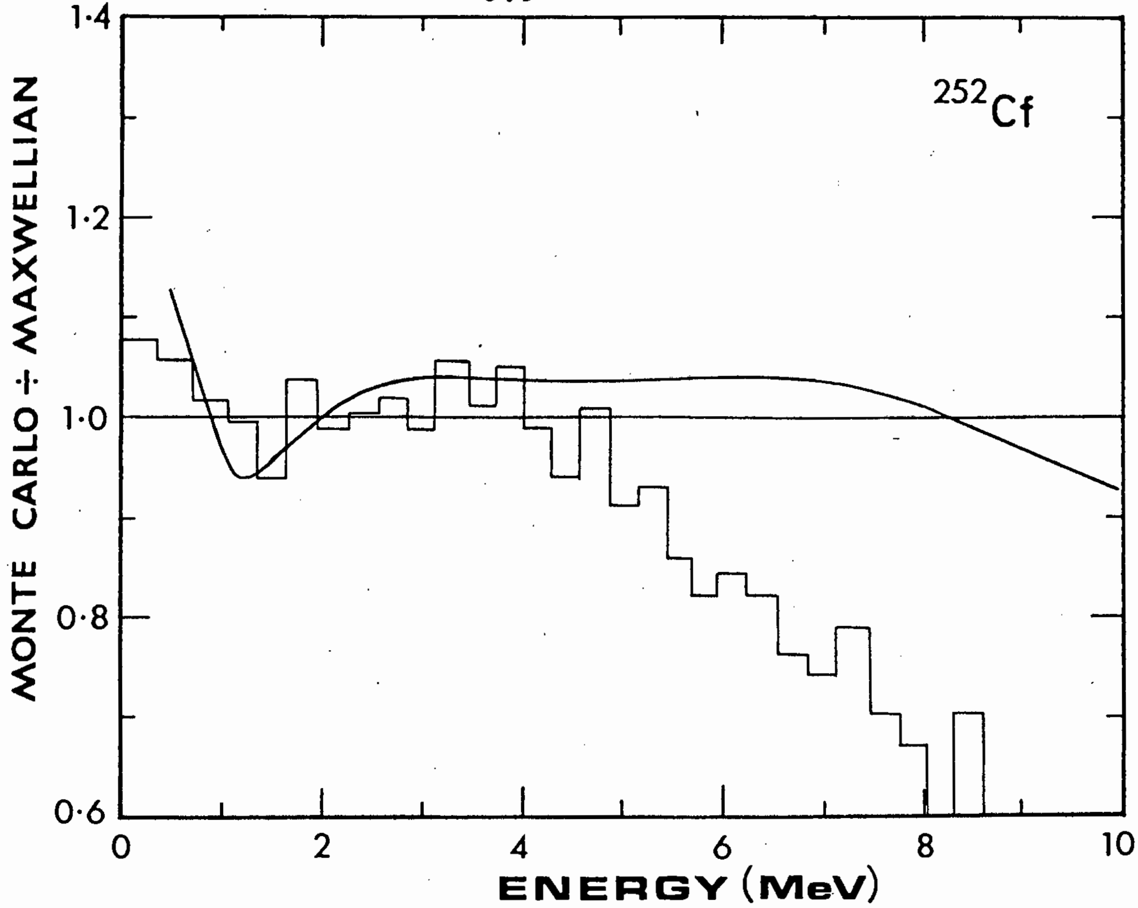

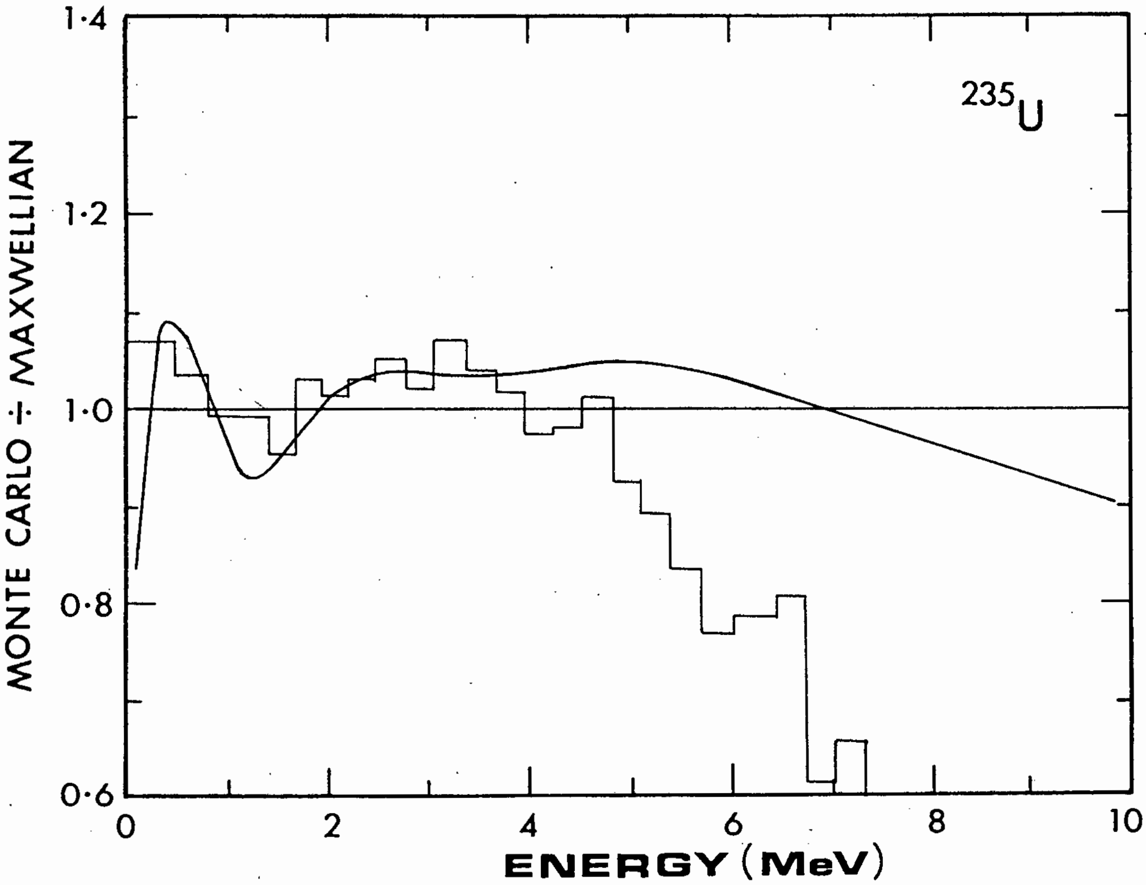

Figure 6.5 Calculated energy spectra (histograms) for a model which assumed a 15% polar scission component with angular distribution $1 + \cos^2\theta$ and emission of the remaining 85% of the neutrons from the fragments according to $1+b\ \sin^2\Psi$. The curves represent measurements of the spectra for fission of ^{235}U (We72) and ^{252}Cf (Gr73).

measured and predicted angular distribution and energy spectrum are reduced at low energies, although discrepancies at high energies remain. It is noted that the predicted n-n angular correlation is peaked at small angles for neutron threshold energies <0.5 MeV.

(ii) POLAR FRAGMENT NEUTRONS

In this model all neutrons were assumed to be emitted from the moving fragments with an angular distribution given by $1 + \cos^2\theta$ in the fragment frame. The predicted distributions are shown in Figures 6.6 and 6.7. In general the deviations from the experimentally measured distributions appear to be greater than for the pure evaporation model (Figure 6.3). The predicted fission spectrum reproduces the general form of the observed spectrum, but large discrepancies remain.

ANISOTROPIC SCISSION AND FRAGMENT NEUTRON EMISSION

Green *et al* (Gr73) concluded from their analysis of the neutron spectrum and angular distribution from fission of ^{252}Cf that a 25% scission neutron component was emitted preferentially at 90^0 to the fission axis, and that fragment neutron emission was strongly anisotropic, directed preferentially along the fission axis. The present Monte Carlo calculation was modified to use the neutron emission parameters deduced by Green *et al*. Thus, 25% of the neutrons were assumed to be emitted at scission with an evaporation spectrum at temperature T = 1.384 MeV and angular distribution $1-0.368 \cos^2\theta$. The remaining 75% of the neutrons were assumed to be evaporated from the fragments with an angular distribution given by $1+1.54 \cos^2\theta$ in the fragment frames. The distributions predicted by this model are shown

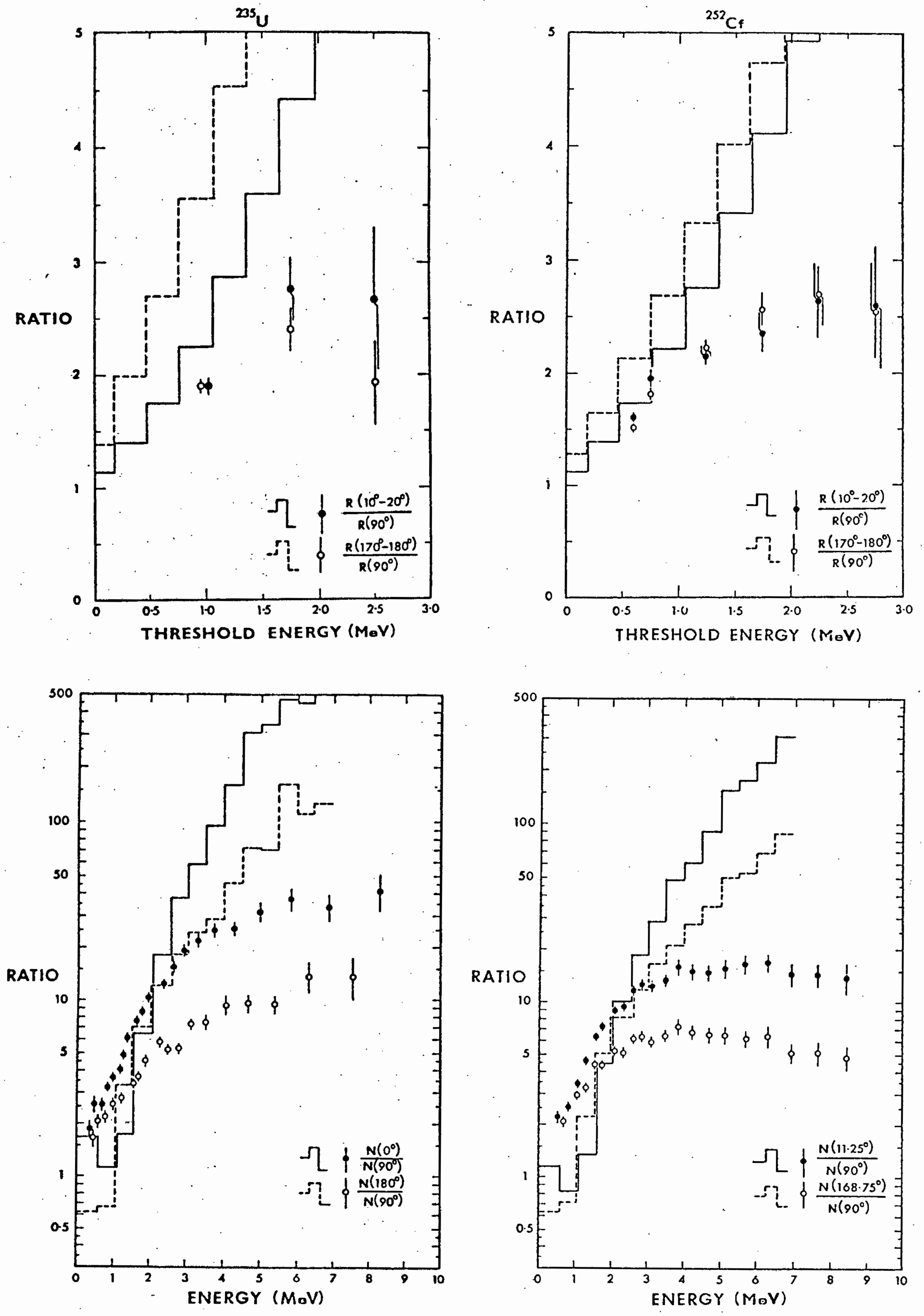

Figure 6.6 The threshold energy dependence of the n-n angular correlation (upper figures), showing measurements (points) and Monte Carlo predictions (histograms) for a model which assumed enhanced polar emission of neutrons from the fragments of the form $1 + \cos^2\theta$, and no scission component. In the lower figures, measurements (Bo62a,Sk63) of the neutron angular distribution for fission of ^{235}U (left) and ^{252}Cf (right) are compared with the predictions of this model.

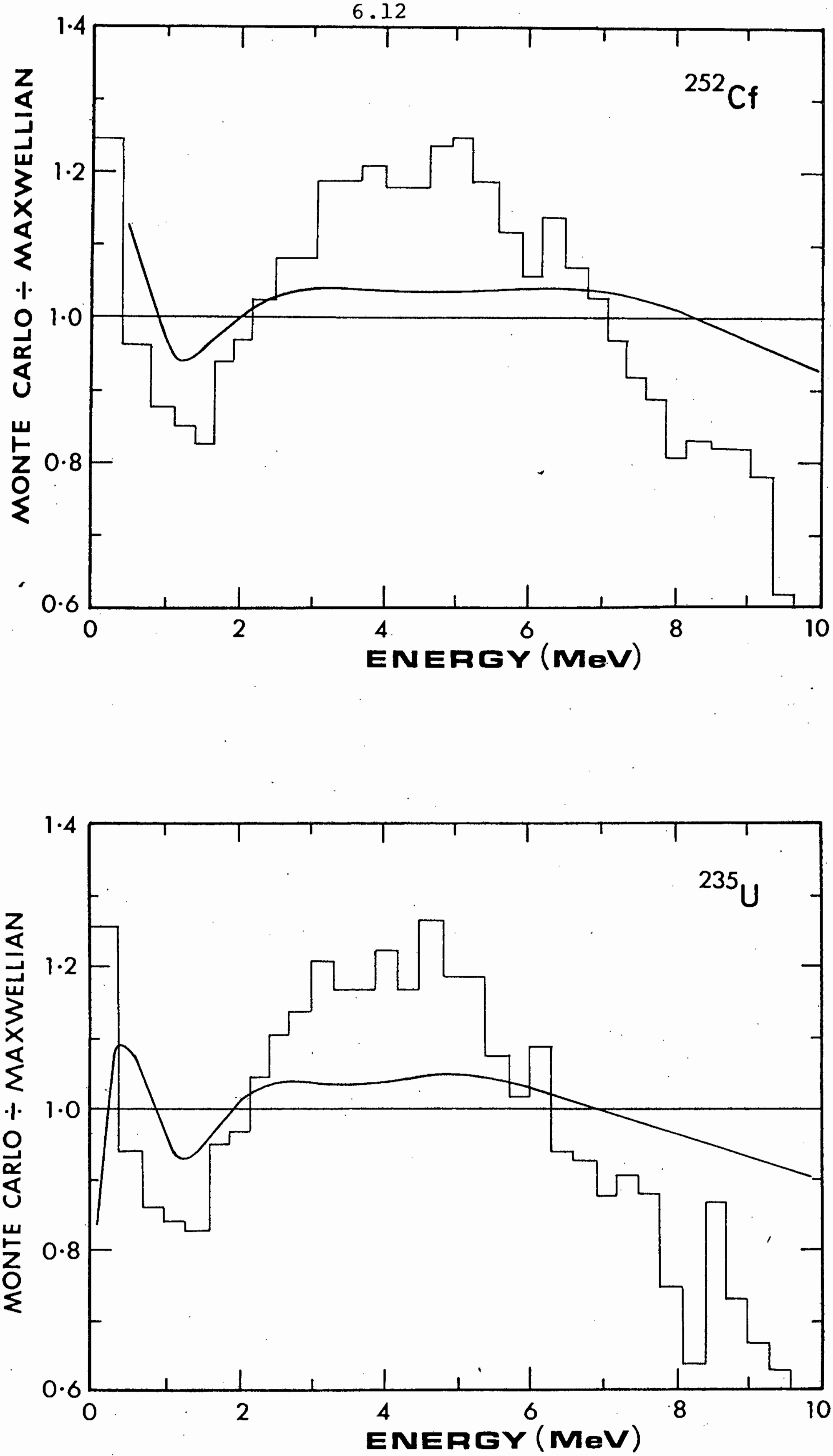

Figure 6.7 Calculated energy spectra (histograms) for a model which assumed enhanced polar emission of neutrons from the fragments according to $1 + \cos^2\theta$, and no scission component. The curves represent measurements of the spectra for fission of ^{235}U (We72) and ^{252}Cf (Gr73).

in Figures 6.8 and 6.9. The n-n angular correlation is seen to be peaked at small angles for all threshold energies, but the discrepancy with experimental results is considerably greater than for the pure evaporation model (Figure 6.3). Agreement between the predicted and measured angular distributions is improved at all energies. The neutron energy spectra predicted by this model for neutron emission are markedly different from those for other models considered, showing even greater deviations from the measured spectra.

The differences between the Monte Carlo predictions and the calculations of Green *et al* in which the same neutron emission parameters were used are attributed to the different methods of calculation. In the present model the fragment mass dependence of the nuclear temperatures and neutron yields were taken into account, while the analytical model of Green *et al* assumed mass independent quantities.

NEUTRON EMISSION DURING FRAGMENT ACCELERATION

The possibility of evaporation of a fraction of the fission neutrons during the fragment acceleration period was investigated by Skarsvåg (Sk73). Clearly, the laboratory neutron angular distribution from such a model is more isotropic than that which results if all neutrons are assumed to be emitted from fully accelerated fragments. The model leads to results intermediate between those with and without an isotropic scission component. The present analysis therefore disfavours such early neutron emission, on the basis of the increased discrepancies observed for models which include an isotropic scission component.

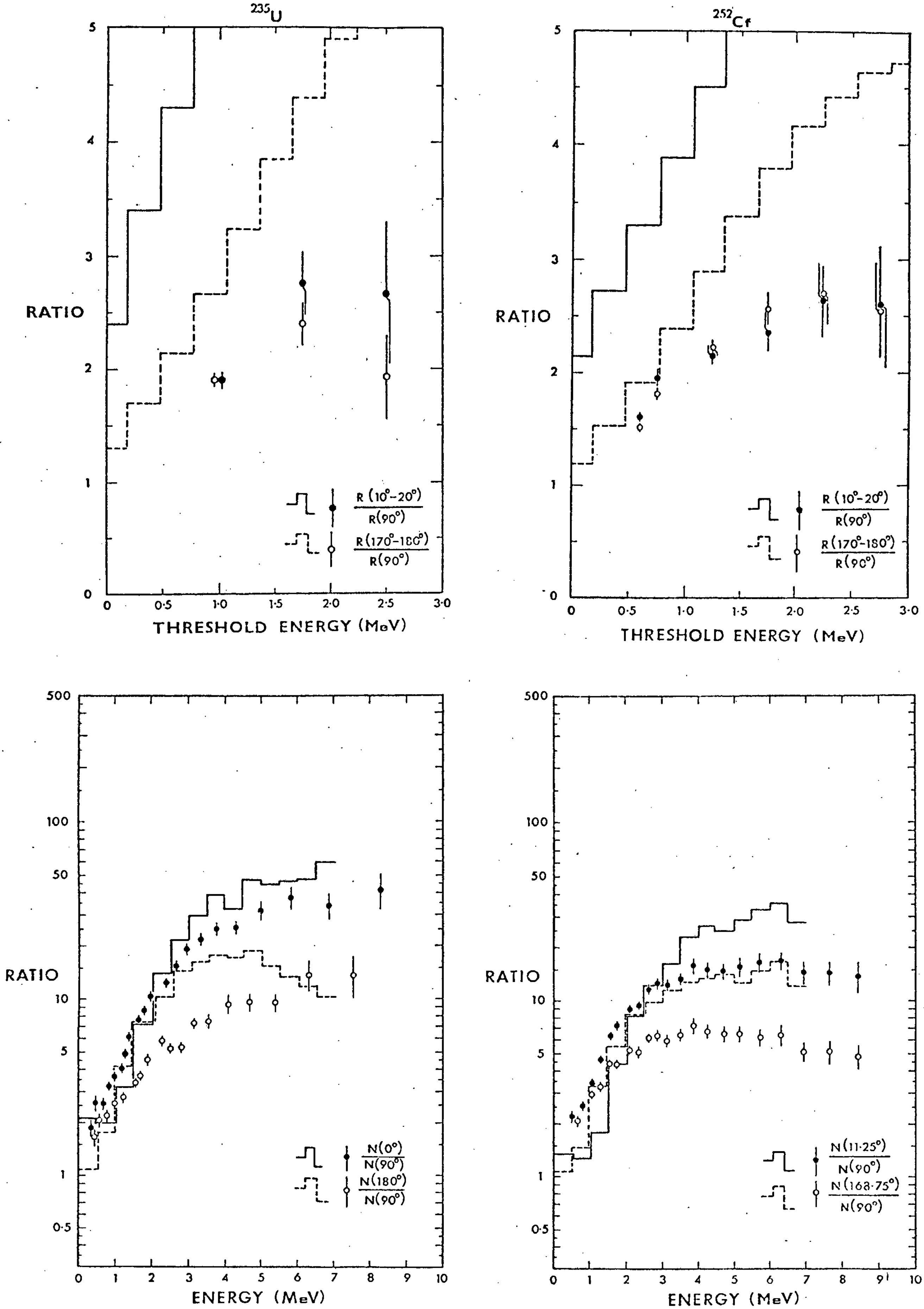

Figure 6.8 The threshold energy dependence of the n-n angular correlation (upper figures), showing measurements (points) and Monte Carlo predictions (histograms) for a model which assumed a 25% scission component with angular distribution $1-0.368\ \mathrm{Cos}^2\theta$, and emission of the remaining 75% of the neutrons from the fragments according to $1 + 1.54\ \mathrm{Cos}^2\theta$. In the lower figures, measurements (Bo62a,Sk63) of the neutron angular distribution for fission of ^{235}U (left) and ^{252}Cf (right) are compared with the predictions of this model.

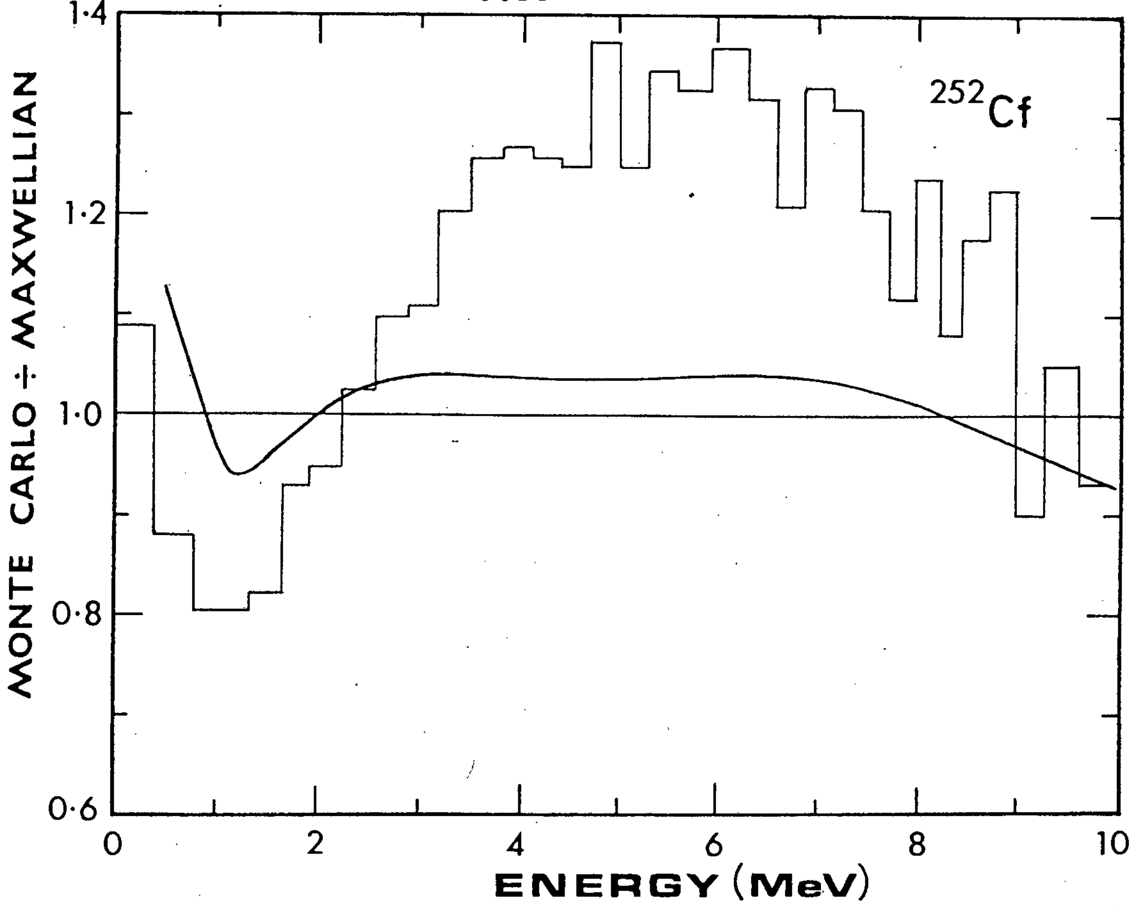

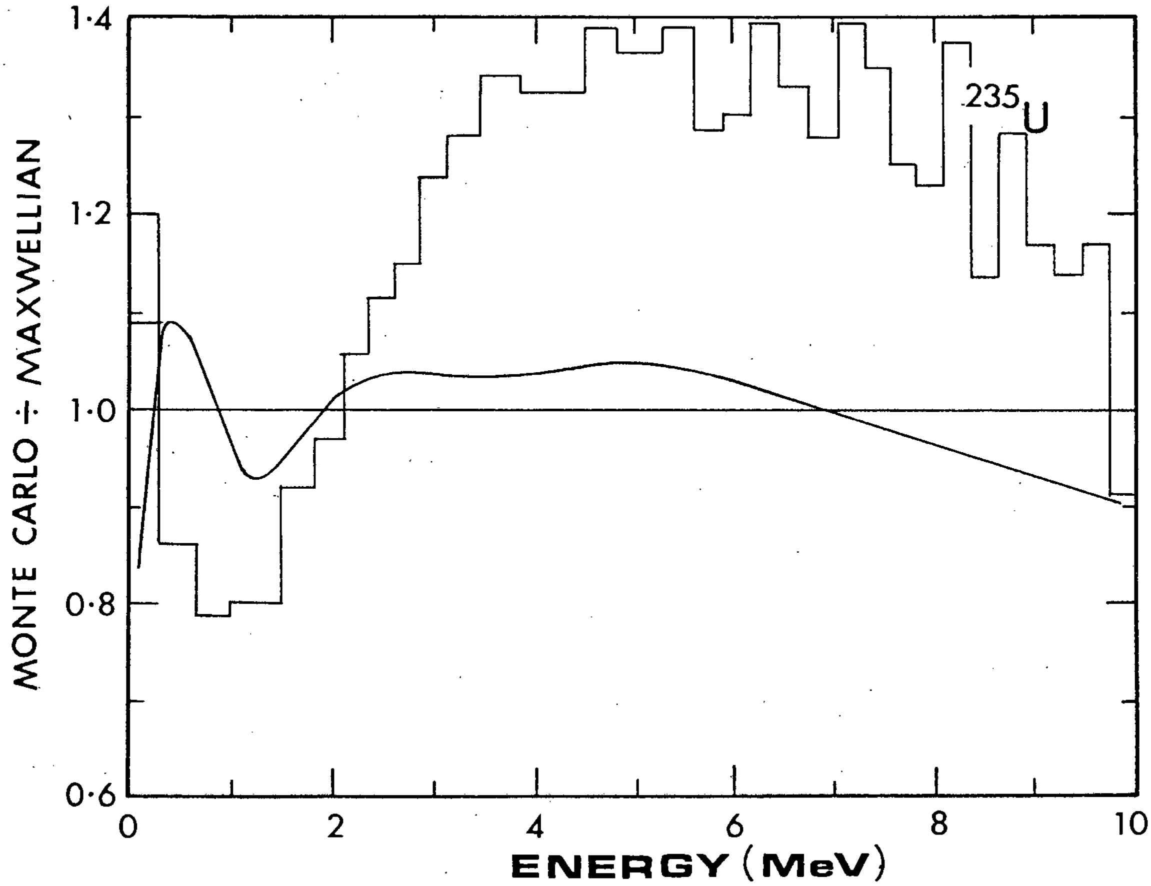

Figure 6.9 Calculated energy spectra (histograms) for a model which assumed a 25% scission component with angular distribution $1 - 0.368\ \mathrm{Cos}^2\theta$, and emission of the remaining 75% of the neutrons from the fragments according to $1 + 1.54\ \mathrm{Cos}^2\theta$. The curves represent measurements of the spectra for fission of ^{235}U (We72) and ^{252}Cf (Gr73).

6.2 CONCLUSIONS

In view of the complexity of the fission process it is not surprising that the simple models used to describe neutron emission are unable to predict the observed distributions accurately. The models which were considered were used to indicate the effects of various modifications to the evaporation model, rather than to attempt to achieve good agreement with experiment. Even if, after elaborate searching, a fit is achieved between the model predictions and the distributions measured experimentally, this approach would not verify the emission hypothesis (or explain the mechanisms involved), since different models may give rise to similar predictions. Several conclusions regarding neutron emission may however be drawn from this analysis.

The predictions of a model which assumes isotropic evaporation from the fully accelerated fission fragments cannot adequately describe the measured neutron spectrum, angular distribution or the n-n angular correlation.

The measurements of the angular correlation of neutrons from fission of ^{235}U and ^{252}Cf indicate that the yield of coincident neutrons at small angles relative to one another exceeds that predicted by the evaporation model.

Comparison of evaporation model predictions and measurements of the neutron angular distribution as a function of energy indicate that some mechanism is needed to increase the yield of low energy ($\lesssim$2 MeV) neutrons emitted at small angles to the fission axis. This evidence is supported by discrepancies observed in the calculated fission spectrum, which show that the evaporation model leads to a deficient yield of neutrons in this energy region.

Discrepancies in the calculated energy and angular spectra also indicate that a mechanism is required to reduce the neutron yield at energies $1.5 \lesssim E \lesssim 5.5$ MeV, and to distribute these neutrons more isotropically in the laboratory frame than would result from an evaporation model.

Comparison of the Monte Carlo predictions and the results of analytical calculations has demonstrated the importance of including the dependence of the neutron emission parameters on the masses of fission fragments. Whereas the neutron angular distribution calculated from an analytical model (Bo62a) is more anisotropic than that observed, the Monte Carlo predicted distribution is more isotropic. As a consequence, the results of the present calculations do not support the existence of an isotropic scission neutron component.

Inclusion of an anisotropic low energy scission neutron component directed preferentially along the fission axis is found to reduce the discrepancies between calculated and measured distributions. It seems likely that by suitably adjusting the magnitude, energy spectrum and angular distribution of a polar scission neutron component, good agreement could be reached between measurements and predictions for low energy neutrons. However, discrepancies would remain at higher energies, and these would not be reduced by increasing the mean energy of the polar scission component, since the experimental measurements call for fewer high energy axial neutrons.

The effects of fragment angular momentum on the angular emission of neutrons appear to be small. Increasing the anisotropy of emission ($1+b\ \mathrm{Sin}^2\Psi$) by reduction of the fragment moment of inertia appears to increase the discrepancies between predictions and measurements. This suggests that the fragment moment of inertia is not reduced below 50% of the rigid body value.

6.3 FURTHER WORK

There is considerable scope for further experimental investigation of the nature of the small angle enhancement of the n-n angular correlation and the enhanced axial emission of low energy neutrons.

Further measurements could be made to establish the energy dependence of the n-n angular correlation from $^{235}U(n_{th},f)$ and ^{252}Cf (sf) to higher precision. The standard deviations of the experimental measurements are seen to increase rapidly with increasing detector threshold energy, and the scatter in the measured distributions increases. This is a consequence of the Maxwellian form of the fission spectrum, which results in a sharp drop-off in the neutron yield at high energies, and the method of using proton recoils to indicate neutron energies. Further measurements to reduce the standard deviations of high energy measurements, or to obtain data for detector thresholds $\gtrsim$3 MeV would require considerably longer running times. Measurements using the time-of-flight technique provide relatively more data at higher neutron energies (since the energies are measured directly and not by way of proton recoils), but the method requires a triple coincidence (n-n-γ) and larger detector -

source distances in order to achieve n-γ discrimination and reasonable energy resolution. For these reasons, time-of-flight measurements also require long running times. There is also the possibility of introducing an additional correlation into the measurements by requiring the detection of a fission γ-ray.

It is considered that further experimental work should rather be aimed at the collection of information on the fission fragments in coincidence with neutrons or γ-rays. As an extension of this work, measurements could be made of the n-n angular correlation as a function of the mass ratio of the fission fragments in order to determine whether the enhanced small angle n-n correlation is associated with a particular region of the fragment mass distribution. For small angle n-n coincidence events an enhancement is expected to be observed in the heavy regions of the mass distributions of light and heavy fragments, as a result of the sawtooth neutron yield distribution. The flexibility of the Monte Carlo method permits easy prediction of the mass distributions expected to be observed in coincidence with n-n pairs at various correlation angles - taking account of the enhancements of particular mass regions resulting from the sawtooth neutron yield curve. The experiment would involve measurement of the angular correlation at, say, $\theta_{nn} = 10^0$, 90^0 and 180^0, recording the fragment mass ratio for each event.

Measurements of the neutron angular distribution are of basic importance to the understanding of neutron emission. Because of their importance, it would be useful to obtain additional, higher precision measurements of these distributions than were obtained in the excellent experiments carried out by Bowman *et al* (Bo62a) and Skarsvåg and Bergheim (Sk63). As noted by Bowman *et al*, such measurements would have to aim at a precision of the order of 1 or 2%, and should be concentrated on the interesting angular region close to the fission axis. Measurements for ^{252}Cf have not been performed at 0^0 or 180^0 to the light fragment direction and it is important to obtain data at these angles to clarify the suggested enhanced axial emission. A comprehensive experiment involving the measurement of both the neutron angular distribution and the n-n angular correlation - using the same apparatus - would be well worthwhile.

The possibility was considered of measuring the triple n-n-n coincidence rate for two neutron detectors mounted at 180^0 relative to one another on either side of the fission source, and a third neutron detector at angle θ to the axis defined by the source and detector pair. Because of the anisotropy introduced into the neutron angular distribution by the fragment motion, detection of an n-n pair at 180^0 would preferentially select neutrons emitted in the direction of the fission axis. The observation of a third neutron at angle θ relative to this pair should give a measurement similar to the neutron angular distribution measured conventionally with respect to the fragment flight directions. The predictions of Monte Carlo calculations would provide the basis for interpretation of the results of an experiment of this nature. The experiment was not performed, since calculations showed that for the existing sources and detector-source distances, the coincidence count rate is expected to be reduced to an unreasonable figure of the order of 1 true n-n-n coincidence per 60 hours of running time.

Additional information on particle emission mechanisms may be obtained from coincident fission gammas. Measurements could be made of the n-γ angular correlation or even n-n-γ (with a much reduced count rate), although experimental difficulties may arise from the high γ-background.

Measurements of the n-n angular correlation for thermal neutron fission of ^{233}U and ^{239}Pu would provide an interesting comparison with the present results. However a difficulty would arise in interpreting such measurements. The Monte Carlo model requires good experimental data on the neutron emission parameters for use as input in the calculation, and these are not readily available for nucleides other than ^{235}U and ^{252}Cf. Even for $^{235}U(n_{th},f)$, there appear to be no published measurements of the neutron yield variance distribution $\sigma_{\nu}^{2}(A)$, and there are generally fewer independent measurements (and showing larger discrepancies) than for ^{252}Cf (sf). The situation is worse for $^{233}U(n_{th},f)$ and $^{239}Pu(n_{th},f)$.

APPENDIX A

ANGULAR CORRELATION OF NEUTRONS FROM SPONTANEOUS FISSION OF ^{252}Cf

BY

J.S. PRINGLE AND F.D. BROOKS

(Reprinted from Physical Review Letters, 35 (1975) 1563)

Angular Correlation of Neutrons from Spontaneous Fission of ^{252}Cf

J. S. Pringle and F. D. Brooks
Physics Department, University of Cape Town, Rondebosch, 7700, South Africa
(Received 18 August 1975)

The n-n angular correlation for neutrons emitted in spontaneous fission of ^{252}Cf has been measured. Discrepancies are observed when these and other experimental observations are compared with Monte Carlo calculations based on the evaporation model. It is suggested that the discrepancies could be attributed to enhanced neutron emission along the fission axis.

It is well established[1,2] that a large fraction (75–90%) of the neutrons emitted promptly in spontaneous or thermal-neutron fission can be accounted for in terms of evaporation from the fully accelerated fission fragments. However the origin of the remaining 10–25% of the neutron emission remains in question and it has been suggested that these neutrons may be emitted at the instant of scission[1,2] or during the acceleration period of the fragments.[3] Models of the neutron emission rest mainly on experimental observations of the velocity and angular distributions of the prompt neutrons, the angular distributions being referred to the axis defined by the direction of the light fragment.

Another observable in the neutron emission process is the neutron-neutron angular correlation, that is the n-n coincidence rate as a function of angle between emitted neutrons. Such a measurement was reported for thermal-neutron fission of ^{235}U by De Benedetti *et al.*[4] in 1948. However no further measurement of this observable appears to have been reported since then. The n-n angular correlation experiment does not require the detection of fission fragments, and hence stronger and thicker sources may be used than in angular distribution measurements. On the other hand, the observations are automatically averaged over all orientations of the fission axis, which implies some loss of detail. The correlation is nevertheless sensitive to the characteristics of neutron emission and provides a useful additional method for testing models of emission process. We have measured the n-n angular correlation of prompt neutrons from the spontaneous fission of ^{252}Cf. In order to compare results with predictions based on the evaporation model we have also made Monte Carlo calculations simulating our experiment and the measurement of the neutron angular distribution.[1]

The n-n angular correlation was measured using a source consisting of 2 μg of ^{252}Cf in the form of four 15-mm-long rods, each sealed in a 1-mm-diam platinum-iridium container. The neutron detectors were an NE213 liquid scintillator (38 mm diam × 25 mm length) and an anthracene crystal (25 mm diam × 25 mm length) each mounted on a magnetically shielded photomultiplier tube. Pulse-shape discrimination was used to reject γ events and the detectors were operated at a proton detection threshold of 0.7 MeV. The pulse-shape discrimination rejection efficiencies of both detectors, as measured for Compton electrons from ^{60}Co γ rays, were better than 99.9%. The proton detection thresholds were calibrated using monoenergetic neutron beams obtained from the reaction ^{7}Li$(p,n)^7$Be. One detector and the source were fixed in the horizontal plane and the other detector was rotated about a vertical axis through the source to vary the n-n correlation angle θ. The time-delay spectrum was recorded and the true coincidence rate was determined from the peak in this spectrum. The accidental coincidence rate, estimated from the remainder of the time spectrum, never exceeded 10% of the true rate.

The distances from the source to the two scintillators were 30 cm for the measurements made at $\theta \geq 45°$. For $\theta < 45°$ one detector was moved back to 40–50 cm and a shadow shield was inserted between the two detectors to attenuate spurious coincidences arising from neutron scattering from one detector to the other. This scattering background was carefully investigated and the geometry and length of the shield were chosen to limit it to a negligible level.

The singles count rates N_1 and N_2 of the two detectors and the coincidence rate $N_c(\theta)$ at angle θ were determined in the experiment. Let N_f be the fission rate of the source, $\bar{\nu}$ the average neutron yield per fission, and Ω_1 and Ω_2 the solid angles subtended by the two detectors. Then, since Ω_1 and Ω_2 are small,

$$N_1 = \Omega_1 \epsilon_1 \bar{\nu} N_f / 4\pi \text{ and } N_2 = \Omega_2 \epsilon_2 \bar{\nu} N_f / 4\pi,$$

where ϵ_1 and ϵ_2 are the average efficiencies of the detectors for detecting a fission neutron. The coincidence rate is given by

$$N_c(\theta) = \Omega_1 \Omega_2 \epsilon_1 \epsilon_2 \bar{\nu} N_f P(\theta)/4\pi,$$

where $P(\theta)$ represents the number of fission neutrons emitted per unit solid angle at angle θ to, and in coincidence with, the νth fission neutron.

We define a ratio

$$R(\theta) = N_c(\theta)/N_1 N_2 = 4\pi P(\theta)/\bar{\nu} N_f.$$

Thus $R(\theta)$ is proportional to the angular correlation $P(\theta)$, independent of the experimental geometry (Ω_1 and Ω_2), and insensitive to small variations in instrumental stability insofar as these affect ϵ_1 and ϵ_2.

The experimental results are plotted in Fig. 1 together with a prediction of $R(\theta)$ based on an evaporation model including a 10% scission neutron component. The prediction was generated by a Monte Carlo calculation for 4×10^4 simulated fissions. The first stage of the calculation simulated the neutron emission from the source as follows. In each fission, pre-emission fragment masses were selected by sampling a mass distribution based on two sets of experimental data.[5,6] The (fully accelerated) velocities of the fragments in the laboratory frame were determined from the data of Whetstone.[6] For each fragment, the average neutron yield $\bar{\nu}$ and the variance σ_ν^2 were determined from the data of Signarbieux *et al.*[7] The actual number of neutrons emitted by each fragment was chosen by sampling a Gaussian $(\bar{\nu}, \sigma_\nu^2)$ distribution. A fraction[1] (10%) of the neutrons, randomly chosen, was designated as scission neutrons. It was assumed[1] that this component was emitted isotropically from a source stationary in the laboratory frame, while the remaining 90% of the fission neutrons were emitted isotropically in the frames of the fully accelerated fragments. The angles of emission of both scission and fragment neutrons in the respective emitting frames were assumed to be uncorrelated. Neutron emission energies were sam-

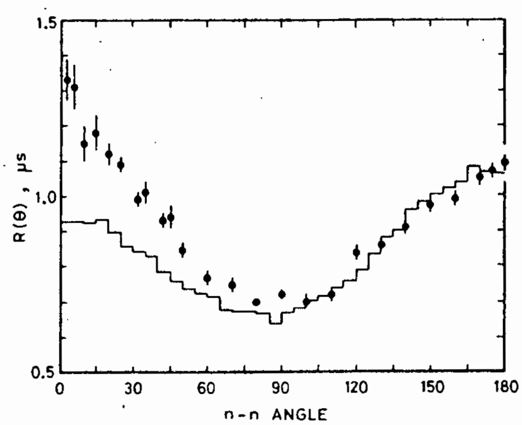

FIG. 1. The n-n angular correlation $R(\theta)$ for ^{252}Cf fission, showing experimental measurements (points) and Monte Carlo simulation (histogram).

pled from evaporation spectra of the form

$$N(E)=(E/T^2)\exp(-E/T),$$

where T is the nuclear temperature of the fragment emitting the neutron and E is the neutron energy in the appropriate frame. Fragment temperatures were determined from the data of Kluge and Lajtai.[8] An evaporation temperature $T=1.3$ MeV was used in the case of scission neutrons.[1] In accordance with recent experimental evidence,[9] energies of evaporation neutrons were assumed to be uncorrelated. The Monte Carlo calculation was checked by computing various parameters of the simulated fission source. For example, the simulation gave $\bar{\nu}=3.73$, and a ratio $\bar{\nu}_L/\bar{\nu}_H$, for the light and heavy fragments, of 1.15. Both values are in good agreement with experiment. The simulated neutron spectrum was also consistent with an experimental measurement.[10]

The final stages of the Monte Carlo calculation simulated the present experiment and the angular distribution measurement of Bowman *et al.*[1] The simulated angular correlation was normalized to the experimental data in the range $\theta=80°-180°$ and is plotted in Fig. 1. The sensitivity of the simulation to the proton detection threshold was investigated by repeating the Monte Carlo calculation using thresholds 0.2 MeV lower and higher than the experimental value of 0.7 MeV. No significant change was observed in the form of the correlation. From Fig. 1 it may be seen that the simulation reproduces the form of the experimental data reasonably well at angles in the range $\theta=100°-180°$ but not smaller angles.

The angular distribution measurement of Bowman *et al.*[1] was simulated using a *neutron* detection threshold of 0.55 MeV (velocity 1.025 cm/nsec) as used in their experiment. The simulated distribution was normalized to their data in the angle range $\theta=40°-140°$ and is shown (histogram) together with the data in Fig. 2. A curve by Bowman *et al.*[1] based on an analytical formula in which average values, independent of the fragment mass ratio, were used for the velocities, temperatures, and neutron yields of the fission fragments is also shown in Fig. 2. Whereas the curve fits the data well, the prediction of the Monte Carlo calculation is too low both at small angles, $\theta \lesssim 30°$, and large angles, $\theta \gtrsim 150°$. This discrepancy between the two calculations was investigated by modifying the Monte Carlo calculation so as to use the fixed values used by Bowman *et al.*[1] for the fragment velocities, temperatures, and neutron yields. The modified calculation gave results in close agreement with the curve shown in Fig. 2, indicating that the discrepancy between curve and histogram may be attributed to the different assumptions made in the two calculations. The present simulation (histogram) is more realistic insofar as it takes account of the dependence of neutron emission characteristics on the fragment masses. For this reason and notwithstanding the poorer agreement with experiment, we consider it a better representation of the angular distribution of the evaporation model.

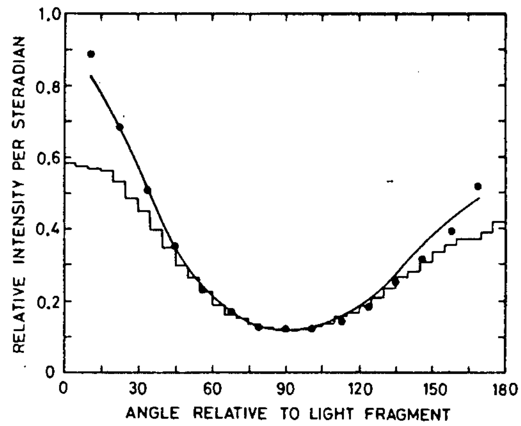

FIG. 2. Simulated angular distribution of neutrons from ^{252}Cf fission (histogram). The points show experimental data (Ref. 1) and the curve shows the fit obtained by using an analytical model (Ref. 1). The standard deviations of the data are smaller than the point size.

Further calculations were made to test the sensitivity of the simulations to the scission neutron fraction. For fractions less than 10% there is little change in the distributions, while larger fractions increase the discrepancies between experiment and theory. It is also evident that the fits would not be improved by attributing[3] a fraction of the neutron emission to evaporation during the fragment acceleration period. Such a model leads to results intermediate between those with and without a scission component.

We therefore conclude that the evaporation model in the form considered here cannot explain the results of the neutron angular correlation and angular distribution measurements, and that some mechanism must operate which enhances neutron emission along the fission axis. Ericson and Strutinski[11] have considered the effect of fragment angular momentum and have shown that this might cause such an enhancement. However Gavron and Fraenkel[9] consider that this effect must be small for the case of ^{252}Cf fission. Another possibility is that neutrons emitted at the scission stage may be directed preferentially along the fission axis. Recent studies[12] of the analogous[13] process of light charged particle emission in ternary fission have indicated an unexpectedly large axial component and it would therefore not be surprising if the same were true for scission neutrons. On the evidence now available however it is not possible to do more than speculate as to the origin of the enhanced axial emission of neutrons.

We thank the International Atomic Energy Agency, Vienna, for the loan of the ^{252}Cf source and the South African Council for Scientific and Industrial Research for financial support and a bursary to one of us (J.S.P.).

[1]H. R. Bowman, S. G. Thompson, J. C. D. Milton, and W. J. Swiatecki, Phys. Rev. 126, 2120 (1962), and 129, 2133 (1963).

[2]K. Skarsvåg and K. Bergheim, Nucl. Phys. 45, 72 (1963); S. S. Kapoor, R. Ramanna, and P. N. Rama Rao, Phys. Rev. 131, 283 (1963); M. V. Blinov, N. M. Kazarinov, and I. T. Krisyuk, Yad. Fiz. 16, 1155 (1973) [Sov. J. Nucl. Phys. 16, 634 (1973)].

[3]K. Skarsvåg, Phys. Scr. 7, 160 (1973); G. A. Pik-Pichak, Yad. Fiz. 10, 321 (1970) [Sov. J. Nucl. Phys. 10, 185 (1970)].

[4]S. De Benedetti, J. E. Francis, W. M. Preston, and T. W. Bonner, Phys. Rev. 74, 1645 (1948).

[5]H. W. Schmitt, J. H. Neiler, and F. J. Walter, Phys. Rev. 141, 1146 (1966).

[6]S. L. Whetstone, Phys. Rev. 131, 1232 (1963).

[7]C. Signarbieux, J. Poitou, M. Ribrag, and J. Matuszek, Phys. Lett. 39B, 503 (1972).

[8]Gy. Kluge and A. Lajtai, Phys. Lett. 27B, 65 (1968).

[9]A. Gavron and Z. Fraenkel, Phys. Rev. C 9, 632 (1974).

[10]J. W. Meadows, Phys. Rev. 157, 1076 (1967).

[11]T. Ericson and V. Strutinski, Nucl. Phys. 8, 284 (1958), and 9, 689 (1959).

[12]E. Piasecki, M. Dakowski, and A. Kordyasz, in *Proceedings of the Symposium on the Physics and Chemistry of Fission, Rochester, New York, 1973* (International Atomic Energy Agency, Vienna, Austria, 1974), p. 383; V. M. Adamov, L. V. Drapchinsky, S. S. Kovalenko, K. A. Petrzhak, L. A. Pleskachevsky, and I. T. Tyutyugin, Phys. Lett. 48B, 311 (1974).

[13]N. Feather, in *Proceedings of the Symposium on the Physics and Chemistry of Fission, Vienna, Austria, 1969* (International Atomic Energy Agency, Vienna, Austria, 1969), p. 83.

R E F E R E N C E S

Ad74 V.M. Adamov, L.V. Drapchinsky, S.S. Kovalenko, K.A. Petrzhak, L.A. Pleskachevsky, and I.I. Tyutyugin, Phys. Lett. 48B (1974) 311

Aℓ61 T.K. Alexander and F.S. Goulding, Nucl. Instrum. Methods 13 (1961) 244

Am65 S. Amiel, in Physics and Chemistry of Fission (Proc. Symp. Salzburg, 1965) 2, IAEA, Vienna (1965) 171

An73 L.L. Anderson, Phys. Med. Biol. 18 (1973) 779

Ap64 V.F. Apalin, Y.N. Gritsyuk, I.E. Kutikov, V.I. Lebedev and L.A. Mikaelyan, Nucl. Phys. 55 (1964) 249

Ar71 A. Artna-Cohen, Nuclear Data Sheets B6 (1971) 287

Av72 V.Y. Averchenkov, Y.Y. Nefedov and Y.V. Khilov, Sov. J. Nucl. Phys. 14 (1972) 632

Bj69 S. Bjornholm and V.M. Strutinsky, Nucl. Phys. A136 (1969) 1

Bℓ73 M.V. Blinov, N.M. Kazarinov and I.T. Krisyuk, Sov. J. Nucl. Phys. 16 (1973) 634

Bℓ76 M.V. Blinov, V.A. Vitenko and I.T. Krisyuk, INDC(CCP) - 66/U, IAEA, February 1976

Bo39 N. Bohr and J.A. Wheeler, Phys. Rev. 56 (1939) 426

Bo56 A. Bohr, Int. Conf. Peaceful Uses of Atomic Energy, (Proc. Conf. Geneva, 1955) 2, United Nations, New York (1956) 151

Bo62a H.R. Bowman, S.G. Thompson, J.C.D. Milton and W.J. Swiatecki, Phys. Rev. 126 (1962) 2120

Bo62b D. Bodansky, Ann. Rev. Nucl. Sci. 12 (1962) 79

Bo63 H.R. Bowman, J.C.D. Milton, S.G. Thompson and W.J. Swiatecki, Phys. Rev. 129 (1963) 2133

Bo67 J.W. Boldeman and A.W. Dalton, AAEC/E172, Australian Atomic Energy Commission, Lucas Heights (1967)

Bo71 J.W. Boldeman, A.R. De L. Musgrove and R.L. Walsh, Aust. J. Phys. 24 (1971) 821

Bo74a Y. Boneh and Z. Fraenkel, Phys. Rev. C10 (1974) 893

Bo74b J.W. Boldeman, Nucl. Sci. Eng. 55 (1974) 188

Br56 F.D. Brooks, Prog. Nucl. Phys. 5 (1956) 252; and unpublished data

Br59 F.D. Brooks, Nucl. Instrum. Methods. 4 (1959) 151

Ca59 E.D. Cashwell and C.J. Everett, A Practical Manual on the Monte Carlo Method for Random Walk Problems, Pergamon Press, (1959) New York

Ca72 G.C. Campbell and J.L. Rowlands, in Prompt Fission Neutron Spectra (Proc. Cons. Meeting, Vienna, 1971) IAEA, Vienna (1972) 33

Ch68 E. Cheifetz and Z. Fraenkel, Phys. Rev. Lett. 21 (1968) 36

Ch70 E. Cheifetz, Z. Fraenkel, J. Galin, M. Lefort, J. Peter and X. Tarrago, Phys. Rev. C2 (1970) 256

Co67 S.W. Cosper, J. Cerny and R.C. Gatti, Phys. Rev. 154 (1967) 1193

De48 S. De Benedetti, J.E. Francis, W.M. Preston and T.W. Bonner, Phys. Rev. 74 (1948) 1645

Di73 K. Dietrich, in Physics and Chemistry of Fission (Proc. Symp. Rochester, 1973), 2, IAEA, Vienna (1974) 461

Di76 K. Dietrich, private communication (Cape Town, August 1976)

Dy74 P.P. D'yachenko, V.M. Piksajkin and A. Lajtai, Sov. J. Nucl. Phys. 19 (1974) 619

Eℓ70 Y.A. Ellis, Nuclear Data Sheets, B4 (1970) 635

Er58 T. Ericson and V.M. Strutinsky, Nucl. Phys. 8 (1958) 284

Er59 T. Ericson and V.M. Strutinsky, Nucl. Phys. 9 (1958/59) 689

Fe69 N. Feather, in Physics and Chemistry of Fission (Proc. Symp. Vienna, 1969), IAEA, Vienna (1969) 83

Fo56 P. Fong, Phys. Rev. 102 (1956) 434

Fo74 P. Fong, Phys. Rev. C10 (1974) 1122

Fr52 J.S. Fraser, Phys. Rev. 88 (1952) 536

Fr66 J.S. Fraser and J.C.D. Milton, Ann. Rev. Nucl. Sci. 16 (1966) 379

Fu62 R.W. Fuller, Phys. Rev. 126 (1962) 684

Ga71 A. Gavron and Z. Fraenkel, Phys. Rev. Lett. 27 (1971) 1148

Ga74 A. Gavron and Z. Fraenkel, Phys. Rev. C9 (1974) 632

Ga76a A. Gavron, H.C. Britt and J.B. Wilhelmy, Phys. Rev. C13 (1976) 2577

Ga76b A. Gavron, Phys. Rev. C13 (1976) 2562

Gr67 J.R. Grover and J. Gilat, Phys. Rev. 157 (1967) 802, 814, 823, 832

Gr73 L. Green, J.A. Mitchell and N.M. Steen, Nucl. Sci. Eng. 50 (1973) 257

Gr76 I.S. Grant, Rep. Prog. Phys. 39 (1976) 955

Ha59 I. Halpern, Ann. Rev. Nucl. Sci. 9 (1959) 245

Ha71 I. Halpern, Ann. Rev. Nucl. Sci. 21 (1971) 245

Hi53 D.L. Hill and J.A. Wheeler, Phys. Rev. 89 (1953) 1102

Ho74 D.C. Hoffmann and M.M. Hoffmann, Ann. Rev. Nucl.Sci. 24 (1974) 151

Hy64 E.K. Hyde, The Nuclear Properties of the Heavy Elements, Vol. 3 (Prentice-Hall, New York, 1964)

Is73 M.M. Islam and H.H. Knitter, Nucl. Sci. Eng. 50 (1973) 108

Je72 L. Jeki, Gy. Kluge, A. Lajtai, P.P. D'yachenko and B.D. Kuzminov, in Prompt Fission Neutron Spectra (Proc. Cons. Meeting, Vienna, 1971) IAEA, Vienna (1972) 81

Jo64 S.A.E. Johansson, Nucl. Phys. 60 (1964) 378

Jo69 W. John, J.J. Wesolowski and F. Guy, Phys. Lett. 30B (1969) 340

Jo77 P.I. Johansson and B. Holmqvist, Nucl. Sci. Eng. 62 (1977) 695

Ka63 S.S. Kapoor, R. Ramanna and P.N. Rama Rao, Phys. Rev. 131 (1963) 283

Ke68 I. Kelson, Phys. Rev. Lett. 20 (1968) 867

Kℓ69 Gy. Kluge and A. Lajtai, Phys. Lett. 30B (1969) 311

Kℓ71 Gy. Kluge, Phys. Lett. 37B (1971) 217

Ko76 G.V. Kotel'nikova, B.D. Kuz'minov, G.N. Lovchikova, O.A. Sal'nikov, N.N. Semenova, V.S. Nesterenko, A.M. Trufanov and N.I. Fetisov, INDC (CCP) - 81/U, IAEA, May 1976

Lu76 B. Lucas, C. Mazur, M. Ribrag and C. Signarbieux, in Progress Report of CEA Department de Physique Nucleaire CEN Saclay, 1975/76, p 96

Ma65 H. Maier-Leibnitz, P. Armbruster and H.J. Specht, in Physics and Chemistry of Fission (Proc. Symp. Salzburg, 1965) 2, IAEA, Vienna (1965) 113

Ma67 E.E. Maslin, A.L. Rodgers and W.G.F. Core, Phys. Rev. 164 (1967) 1520

Ma74 J. Maruhn and W. Greiner, Phys. Rev. Lett. 32 (1974) 548

Me67 J.W. Meadows, Phys. Rev. 157 (1967) 1076

Mi62 J.C.D. Milton and J.S. Fraser, Can. J. Phys. 40 (1962) 1626

Mi65 J.C.D. Milton and J.S. Fraser, in Physics and Chemistry of Fission (Proc. Symp. Salzburg, 1965) 2, IAEA, Vienna (1965) 39

Mi69 J.C.D. Milton, in Physics and Chemistry of Fission (Proc. Symp. Vienna, 1969), IAEA, Vienna (1969) 879

Mi73 A. Michaudon, Adv. in Nucl. Phys. 6 (1973) 1

Mo71 U. Mosel and H.W. Schmitt, Nucl. Phys. A165 (1971) 73

Na71 D.M. Nadkarni, in Proc. Conf. Neutron Induced Fission, INDC, Bombay (1971) 89

Na74 S. Nair and D.B. Gayther, in U.K. Nuclear Data Progress Report 1973/74, AERE Harwell (1974) 38

Na75 S. Nair and D.B. Gayther, in U.K. Nuclear Data Progress Report 1974/75, AERE Harwell (1975) 24

Na76 S. Nair, D.B. Gayther, B.H. Patrick and E.M. Bowey, in U.K. Nuclear Data Progress Report 1975/76, AERE Harwell (1976) 18

Ne72 V.N. Nefedov, A.K. Melnikov and B.I. Starostov, in Prompt Fission Neutron Spectra (Proc. Cons. Meeting, Vienna, 1971) IAEA, Vienna (1972) 89

Ni61 J. Niday, Phys. Rev. 121 (1961) 1471

Ni72a J.R. Nix, Ann. Rev. Nucl. Sci. 22 (1972) 65

Ni72b H. Nifenecker, C. Signarbieux, M. Ribrag, J. Poitou and J. Matuszek, Nucl. Phys. A189 (1972) 285

Ni74 H. Nifenecker, C. Signarbieux, R. Babinet and J. Poitou, in Physics and Chemistry of Fission (Proc. Symp. Rochester, 1973), 2, IAEA, Vienna (1974) 117

No70 L.C. Northcliffe and R.F. Schilling, Nuclear Data Tables A7 (1970) 233

Ow60 G.E. Owen and C.D. Swartz, in Fast Neutron Physics, part 1, eds. J.B. Marion and J.L. Fowler (Interscience, New York, 1960), 211

Pi70a H. Piekarz, J. Blocki, T. Krogulski and E. Piasecki, Nucl. Phys. A146 (1970) 273

Pi70b G.A. Pik-Pichak, Sov. J. Nucl. Phys. 10 (1970) 185

Pi70c E. Piasecki, M. Dakowski, T. Krogulski, J. Tys and J. Chwaszczewska, Phys. Lett. 33B (1970) 568

Pi74a E. Piasecki and J. Blocki, Acta Physica Polonica B5 (1974) 247

Pi74b E. Piasecki, M. Dakowski and A. Kordyasz, in Physics and Chemistry of Fission (Proc. Symp. Rochester, 1973), 2, IAEA, Vienna (1974) 383

Pi75 E. Piasecki, M. Sowinski, L. Nowicki, A. Kordyasz, E. Cieslak and W. Czarnacki, Nucl. Phys. A255 (1975) 387

Pi77 V.M. Piksajkin, P.P. D'yachenko, A. Lajtai, N.N. Semenova, E.A. Seregina and L.S. Kutsaeva, INDC (CCP) - 100/U, IAEA, February 1977

Pℓ72 F. Pleasonton, R.L. Ferguson and H.W. Schmitt, Phys. Rev. C6 (1972) 1023

Pr75 J.S. Pringle and F.D. Brooks, Phys. Rev. Lett. 35 (1975) 1563 - see Appendix A

Ra61 R. Ramanna, R. Chaudhry, S.S. Kapoor, K. Mikke, S.R.S. Murthy and P.N. Rama Rao, Nucl. Phys. 25 (1961) 136

Ra68 G.M. Raisbeck and T.D. Thomas, Phys. Rev. 172 (1968) 1272

Re73 W.N. Reisdorf, J.P. Unik and L.E. Glendenin, Nucl. Phys. A205 (1973) 348

Ri72 M. Ribrag, J. Poitou, J. Matuszek and C. Signarbieux, Revue De Physique Appliquée 7 (1972) 197

Sa65 C.P. Sargent, W. Bertozzi, P.T. Demos, J.L. Matthews and W. Turchinetz, Phys. Rev. 137B (1965) 89

Sa76 A.E. Savel'ev, V.P. Gorelov and B.M. Dzyuba, Sov. J. Nucl. Phys. 24 (1976) 135

Sc66 H.W. Schmitt, J.H. Neiler and F.J. Walter, Phys. Rev. 141 (1966) 1146

Sc75 J. Scobie, R.D. Scott and D.G. Vass, in U.K. Nuclear Data Progress Report 1974/5, AERE Harwell (1975) 89

Si72 C. Signarbieux, J. Poitou, M. Ribrag and J. Matuszek, Phys. Lett. 39B (1972) 503

Si74 C. Signarbieux, R. Babinet, H. Nifenecker and J. Poitou, in Physics and Chemistry of Fission (Proc. Symp. Rochester, 1973), 2, IAEA, Vienna (1974) 179.

Sk63 K. Skarsvåg and K. Bergheim, Nucl. Phys. 45 (1963) 72

Sk70 K. Skarsvåg, Nucl. Phys. A153 (1970) 82

Sk73 K. Skarsvåg, Phys. Scr. 7 (1973) 160

Sk75 K. Skarsvåg, Nucl. Phys. A253 (1975) 274

Sm71 A.B. Smith, Nucl. Sci. Eng. 44 (1971) 439

Sm72 A.B. Smith, in Prompt Fission Neutron Spectra (Proc. Cons. Meeting, Vienna, 1971) IAEA, Vienna (1972) 3

Sm77 A.B. Smith, P. Guenther and R. Sjoblom, Nucl. Instrum. Methods 140 (1977) 397

Sp66 D. Sperber, Phys. Rev. 141 (1966) 927

Sp74a V. Spiegel, Nucl. Sci. Eng. 53 (1974) 326

Sp74b H.J. Specht, Rev. Mod. Phys. 46 (1974) 773

St65 J.R. Stehn, M.D. Goldberg, R. Weiner-Chasman, S.F. Mughabghab, B.A. Magurno and V.M. May, Neutron Cross Sections, BNL 325, 2nd edition, Suppl. No. 2 III (1965)

St67 V.M. Strutinsky, Nucl. Phys. A95 (1967) 420

St68 V.M. Strutinsky, Nucl. Phys. A122 (1968) 1

St73 R.W. Stoughton, J. Halperin, C.E. Bemis and H.W. Schmitt, Nucl. Sci. Eng. 50 (1973) 169

Te59 J. Terrell, Phys. Rev. 113 (1959) 527

Te65 J. Terrell, in Physics and Chemistry of Fission (Proc. Symp. Salzburg, 1965), 2, IAEA, Vienna (1965) 3

Th64 T.D. Thomas and R. Vandenbosch, Phys. Rev. 133B (1964) 976

Th67 T.D. Thomas and J.R. Grover, Phys. Rev. 159 (1967) 980

Th68 T.D. Thomas, Ann. Rev. Nucl. Sci. 18 (1968) 343

Va73 R. Vandenbosch and J.R. Huizenga, Nuclear Fission (Academic Press, New York and London, 1973)

Va76 G.V. Val'skii, Sov. J. Nucl. Phys. 24 (1976) 140

Wa52 B.E. Watt, Phys. Rev. 87 (1952) 1037

Wa75 C. Wagemans and A.J. Deruytter, Z. Physik A275 (1975) 149

Wa77 R.L. Walsh and J.W. Boldeman, Nucl. Phys. A276 (1977) 189

We37 V.F. Weisskopf, Phys. Rev. 52 (1937) 295

We72 H. Werle and H. Bluhm, in Prompt Fission Neutron Spectra (Proc. Cons. Meeting, Vienna 1971) IAEA, Vienna (1972) 65

Wh52 W.J. Whitehouse, Prog. Nucl. Phys. 2 (1952) 120

Wh63 S.L. Whetstone, Phys. Rev. 131 (1963) 1232

Wh67 S.L. Whetstone and T.D. Thomas, Phys. Rev. 154 (1967) 1174

Wi47 R.R. Wilson, Phys. Rev. 72 (1947) 189

Wi72 J.B. Wilhelmy, E. Cheifetz, R.C. Jared, S.G. Thompson, H.R. Bowman and J.O. Rasmussen, Phys. Rev. C5 (1972) 2041

Wi76 B.D. Wilkins, E.P. Steinberg and R.R. Chasman, Phys. Rev. C14 (1976) 1832

Wi76a I. Wilhelm, R. Bayer, J. Cvanda and Z. Dlouhy, Nucl. Phys. A262 (1976) 301

Wo76a H. Wohlfarth, W. Lang, H.G. Clerc, H. Schrader, K.H. Schmidt and H. Dann, Phys. Lett. 63B (1976) 275

Wo76b A. Wolf and E. Cheifetz, Phys. Rev. C13 (1976) 1952

Zi74 M. Zielinska-Pfabe and K. Dietrich, Phys. Lett. 49B (1974) 123